INTERACTION STUDIES OF HUMAN DEAD-BOX HELICASES WITH VIRAL NON-CODING RNA

Corey Nelson
Bachelor of Science, University of Lethbridge, 2019

A thesis submitted
in partial fulfilment of the requirements for the degree of

Master of Science

in

Biochemistry

Department of Chemistry and Biochemistry
University of Lethbridge
LETHBRIDGE, ALBERTA, CANADA

INTERACTION STUDIES OF HUMAN DEAD-BOX HELICASES WITH VIRAL NON-CODING RNA

COREY NELSON

Date of Defense: April 23, 2021

Dr. T. Patel Thesis Supervisor	Associate Professor	Ph.D.
Dr. A. Zovoilis Thesis Examination Committee Member	Assistant Professor	Ph.D.
Dr. S. Wiseman Thesis Examination Committee Member	Associate Professor	Ph.D.
Dr. J. Lemieux External Examiner University of Alberta Edmonton, Alberta	Professor	Ph.D.
Dr. M. Gerken Chair, Thesis Examination Committee	Professor	Ph.D.

Abstract

Mosquito-borne illnesses are responsible for millions of deaths every year. Some of the most common diseases spread include Japanese Encephalitis, Zika, and Rift Valley Fever Virus. This thesis seeks to describe the interactions between the non-coding regions of the RNA genomes of the viruses above and DEAD-box RNA helicases DDX3X and DDX17. Microscale thermophoresis indicated that DDX3X binds the JEV 5′ RNA with a lower dissociation constant than the ZIKV 5′ but could unwind both RNAs. DDX17 binds both the intergenic non-coding and 5′ terminal RNAs from the S segment of the genome, also unwinding both. Small-angle X-ray scattering generated low-resolution 3D structures of DDX17 and the non-coding RNAs. Finally, using a baculovirus expression system has shown the potential to express full-length DDX3X but requires optimization before it is ready for downstream experimentation.

Acknowledgements

Firstly, I would like to thank the members of the Patel lab, past and present. There are many special people I have had the pleasure of working with. I have grown as a person and an academic because of you all. To Dr. Trushar Patel, thank you for supporting and becoming a mentor to me. I am incredibly grateful for all you have done. To Tyler Mrozowich, thanks for ordering stuff for me and guiding my research in a meaningful capacity; it has been a pleasure to be your colleague and friend.

Thank you to Dr. Steve Wiseman and Dr. Athan Zovoilis for participating on my committee and Dr. Joanne Lemieux for participating in my defence. Thank you to Alberta Innovates and the University of Lethbridge for funding this work.

I would be remiss if I didn't acknowledge my family. Their support has enabled me to overcome countless challenges. I am incredibly fortunate and privileged to have parents that have helped me succeed at every possible turn. To my sisters, whose annoyances know no end, thanks for that, I appreciate you both nonetheless. To Taylor, thank you for being there for me through the best and the worst times.

Table of Contents

Chapter 3: Human DDX17 Unwinds Rift Valley Fever Virus Non-Coding RNAs

Chapter 4: Development Towards a Baculovirus Proteins Expression System

Chapter 5: Conclusions

List of Tables

List of Figures

Abbreviations

2DSA	Two-Dimensional Spectrum Analysis
5′ NCR	5′ Non-Coding RNA
ATP	Adenosine Triphosphate
AUC	Analytical Ultracentrifugation
BME	2-Mercaptoethanol
BSA	Bovine Serum Albumin
DENV	Dengue Virus
DNA	Deoxyribonucleic Acid
FITC	Fluorescein Isothiocyanate
FPLC	Fast Protein Liquid Chromatography
GBS	Guillain-Barré syndrome
GFP	Green Fluorescent Protein
HBV	Hepatitis B Virus
HCV	Hepatitis C Virus
HIV	Human Immunodeficiency Virus
HPLC	High-Performance Liquid Chromatography
IFN	Interferon
IGR	Intergenic region
JEV	Japanese Encephalitis Virus
LB	Luria's Broth
mRNA	Messenger RNA
ncRNA	Non-Coding RNA
PAGE	Polyacrylamide Gel
PMSF	Phenylmethylsulfonyl Fluoride

POWV	Powassan Virus
RDRP	RNA dependent RNA Polymerase
RNA	Ribonucleic Acid
rRNA	Ribosomal RNA
RVFV	Rift Valley Fever Virus
SAXS	Small-Angle X-ray Scattering
SDS	Sodium Dodecyl Sulfate
SEC	Size-Exclusion Chromatography
SF9	Spodoptera frugiperda 9
siRNA	Small Interfering RNA
SLEV	St. Louis Encephalitis Virus
SV	Sedimentation Velocity
TBE	Tick-Borne Encephalitis Virus
TR	Terminal Regions
UTR	Untranslated Region
WNV	West Nile Virus
YFV	Yellow Fever Virus
ZIKV	Zika Virus

Chapter 1: Introduction

1.0 Overview

Mosquitoes are at the forefront when discussing humanity's most deadly predator [1, 2]. The myriad of diseases spread by the proboscis-wielding insect is estimated to have resulted in 52 billion human casualties in total [3], with annual deaths ranging between 1 to 2 million. Mosquitoes have played a significant role in shaping the world as we know it. The Roman empire's industrial expansion led to deforestation in regions that eventually led to a large area covered by standing water, forming what would be known as the Pontine Marshes [4, 5]. The marshes became a hotbed for mosquitoes and the diseases that they carried. The Romans assumed that the swamps were giving off noxious gasses that caused both invading armies and the Roman populous to become deathly ill. The mosquitoes weakened the empire and eventually contributed to its demise. The alleged fumes killing the Romans are now presumed to be a combination of what we now know to be malaria and arboviruses [5]. The idea to implement preventative measures occurred to Julius Caesar. He was the first to create plans to remove the stagnant water that had plagued Rome [3]. This was later realized by Benito Mussolini while he looked to develop Italy's agriculture and industry [6]. Draining the marshes was directly effective in preventing the spread of mosquito-borne illness in Italy. Developing ways to prevent the spread of mosquito-borne diseases has been ongoing for thousands of years, likely continuing into the foreseeable future.

Humans have known about viruses since the late 1800s, but the first human virus to be described was the Yellow Fever Virus in 1901 [7]. Once researchers developed identification methods for viruses, viral discoveries occurred frequently. Even now, three new viruses are discovered annually [7]. Mosquitoes are the premier vector for a large selection of virus families, including *Flaviviridae* and *Bunyavirales* [8, 9]. The World Health Organization lists concerns for numerous potential viral outbreaks, primarily spread via mosquito vectors, such as Zika virus (ZIKV), which has seen 42 reported outbreaks since 2015 [10]. Increasing urbanization and population density have promoted these viruses' spread, while climate change has broadened the mosquitoes' habitable range through flooding and favourable

temperature changes [11, 12]. Efforts to mitigate mosquito population growth through sterilization [13] or insecticide-treated nets [14] are being investigated, with the hope that they will provide an ecologically friendly solution. While there is optimism surrounding mosquitoes' genetic sterilization [15], the mitigating of mosquito-borne illness will require the development of more preventative measures and treatment options.

1.1 Flaviviruses

RNA viruses are estimated to be responsible for up to 44% of all emerging infectious diseases [7, 16-18]. The most common family of viruses spread via mosquitoes are the *Flaviviridae* viruses. Of all the Flaviviruses, Dengue Virus (DENV) infects the most humans annually. There are an estimated 390 million infections per year, but only a quarter of infections produce moderate to severe illness [19]. DENV has four known serotypes, which has made vaccine development particularly difficult. Lifelong immunity following infection only applies to the original serotype of infection [20], and subsequent infections from other serotypes were observed to be more severe in secondary infections [21]. DENV vaccine development has been mired in controversy. Dengvaxia was first approved in the Philippines, but soon after the campaign began, there were reports that children were actually at a higher risk of infection following the vaccination [22]. The vaccine was effective in individuals who had already been infected, but many of those who had not contracted DENV previously exhibited DENV-like symptoms [23].

Despite intensive research efforts, vaccines are not available for the majority of Flaviviruses, except for Yellow fever (YFV), Japanese Encephalitis (JEV), and Tick-Borne Encephalitis (TBE) [24]. Research into these viruses cannot stop as shortages, and the costs have exposed a need for redundancy [25, 26]. For example, Hepatitis B vaccines have been available for 20 years [27], but nearly one million people still die annually [28]. JEV infections are predicted to pose a threat to fifty percent of the world's population, similar to DENV, which threatens an estimated forty percent [29, 30]. Flaviviruses in North America include West Nile (WNV), St. Louis Encephalitis (SLEV), and Powassan Virus (POWV) [31-33]. Every continent, except Antarctica, faces a threat from flaviviruses (Figure 1.1), making vaccination and treatment options increasingly necessary [34].

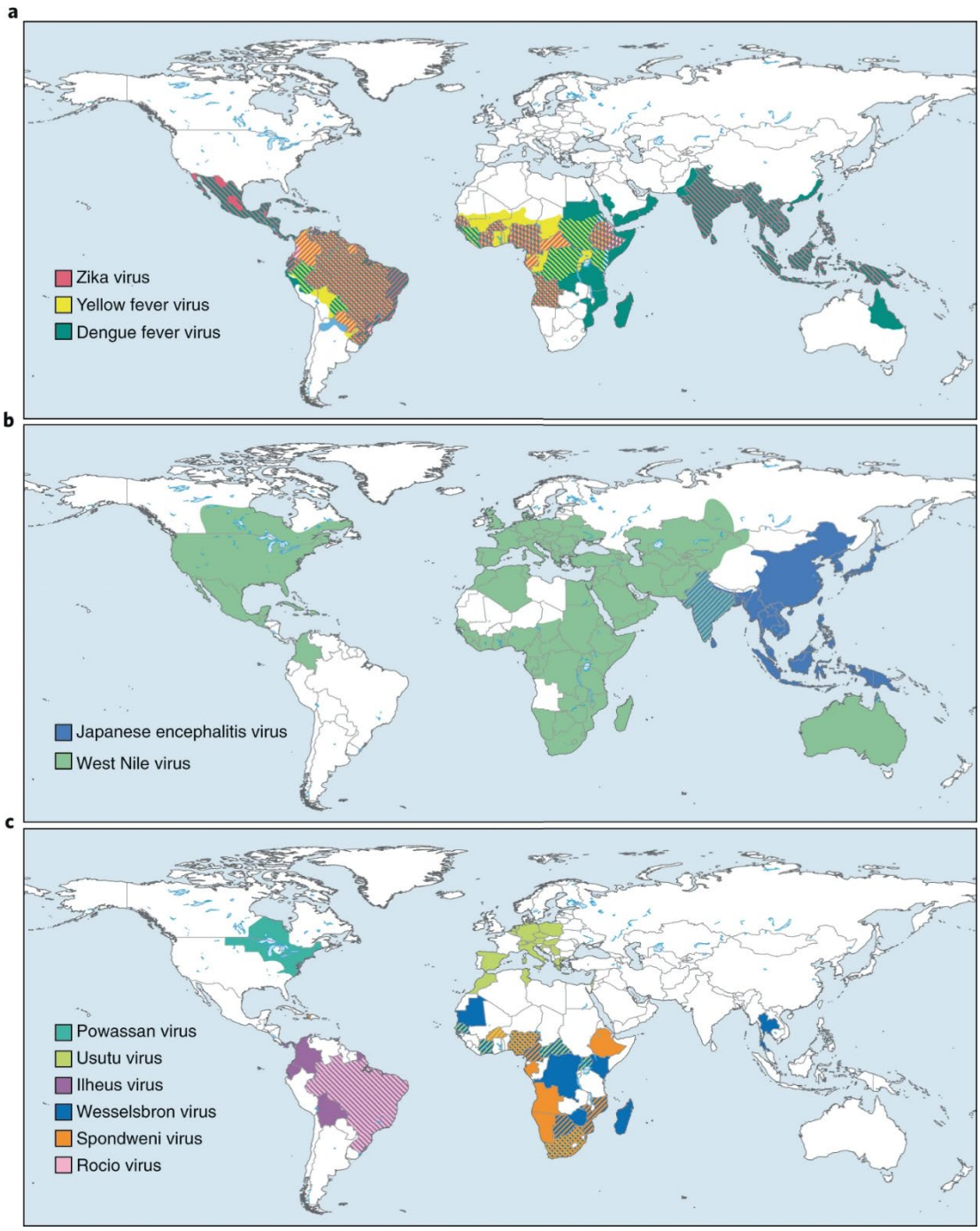

Figure 1.1. Global distribution for significant (A and B) and emerging flaviviruses (C). Demonstrating potential the geographical range of the flaviviruses. Reprinted with permission from Springer Nature [34].

Flaviviruses are positive-sense, single-stranded RNA viruses, typically with ~11 kilobase genomes [35]. Cell entry is achieved through clathrin-mediated endocytosis [36], followed by shuttling to the endosome, where the change in pH allows the viral membrane to fuse with the endosome [37]. Following

fusion, the genome is released into the cytosol, producing negative sense "mother" genomes and translating the viral proteins [38]. The genome is complete with a 5' Cap, which promotes the RNA molecule's stability via an unusual 5' to 5' triphosphate linkage terminating in a guanine base [39]. Translation occurs as a single polypeptide that depends on a combination of host and viral proteases to process the ten individual proteins, three of which are structural and seven non-structural [40-42]. Another feature of the Flavivirus genome is the ability to cyclize to recruit proteins required for replication [43]. There is a conserved 10-11 nucleotide sequence within the terminal regions (TRs) responsible for the cyclization, and they perfectly complement their target sequence.

Terminal regions are the viral RNA genome sections that do not encode for proteins, like non-coding RNA but with the added stipulation that they are flanking the whole coding region (figure 1.2A). Occasionally viruses have non-coding sequences central in the genome and flanked by two coding regions [44]. Non-coding regions are often essential regulators of replication, critical in recruiting host factors [45]. Flavivirus TRs are mostly structured and conserved between members [46]. This overlap suggests that exploiting interactions with host elements could elucidate a versatile treatment option for multiple Flaviviruses.

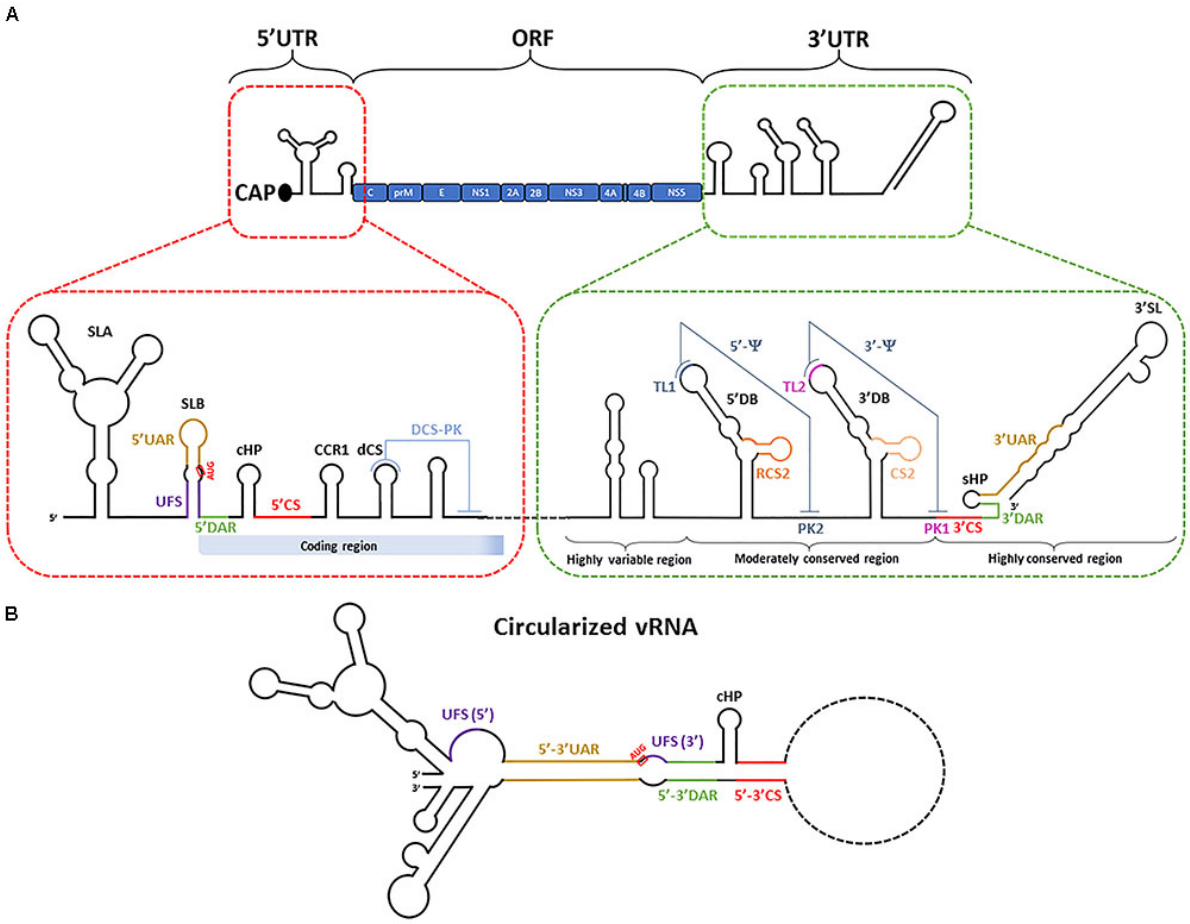

Figure 1.2. Schematic representation of a typical flavivirus genome's secondary structure. A) 5' and 3' terminal regions flanking the coding region. Indicates the complex secondary structure as well as several interactions that occur within the terminal regions. B) Circularized RNA predicted structure. Panhandle structure forms to promote viral replication. Reprinted with permission from Frontiers in Genetics [47].

1.1.1 Japanese Encephalitis Virus

JEV infections constitute some of the most severe Flavivirus infections, with up to one in four cases resulting in death and half of the cases resulting in psychiatric sequelae [48]. JEV infection symptoms can range from none to severe disease, including headaches, nausea, vomiting, and brain tissue inflammation [48, 49]. In extreme cases, JEV infection can induce Parkinson's like disorder, where patients exhibit tremors and similar movement disorders [50]. JEV promotes neuronal death and activates microglia, the central nervous system's primary immune response [51]. The infection is not restricted to the brain, though, with tissue damage occurring in the myocardium, spleen, liver, and lymph nodes [52].

Detecting JEV infections has also proved difficult; the most accurate test requires cerebrospinal fluid to test for JEV antibodies [53]. In conjunction with the fact that many countries with endemic JEV struggle to provide comprehensive health care, the difficulties associated with testing suggest that the number of cases is likely underreported. The majority of JEV infections occur in children, and it is the leading cause of encephalitis in Asian children [54]. Developing novel therapeutics for JEV is essential for developing countries with limited treatment and prevention options.

JEV's genome is consistent with other Flaviviruses, 11kB long genome with structured terminal regions. Some of the structures within the 3' TR of JEV are critical regulators of the host immune system, enabling the formation of subgenomic RNA, capable of preventing interferon activation, avoiding siRNA, and promoting cell death [55-57]. It appears that subgenomic RNA's most critical role is the coordination of translation and replication of the genome itself. Ribosomes and NS5 (RNA-dependent RNA polymerase) work in opposite directions, so there must be a way to get both tasks completed efficiently. Subgenomic RNA appears to repress negative-sense RNA generation to allow for translation, but subgenomic RNA only begins forming after ~36 hours [58, 59]. Allowing the negative-sense RNA to be developed before the translation is fully engaged means more copies of the positive sense genome are ready for translation and eventually packaging. The implication of these findings shows that the TR structure is capable of coordinating the timing behind replication.

The TRs of JEV recruit host proteins to promote viral replication, one of which is DDX5, an RNA helicase. DDX5 was first identified as an interacting partner of the 3' of JEV in an RNA pull-down experiment, and in follow-up experiments, it was determined to be an essential component for viral replication [60]. Another RNA helicase, DDX3X, was also observed in multiple stages of the JEV life cycle [61]. These interactions are essential to examine. The interface between host and pathogen can be a potent target for therapeutics.

1.1.2 Zika Virus

ZIKV's discovery was in 1947 but went largely ignored until the 2007 outbreak in Asia [62]. Predominantly spread via mosquito, like JEV, the 2007 outbreak infected 73% of individuals three and

older on Yap island in Micronesia, demonstrating the risk that ZIKV could pose [63]. ZIKV Infections typically have humans placed as dead-end hosts [64]; however, ZIKV appears to have sexual transmission and vertical transmission, as well [65]. Since many people are unlikely to exhibit symptoms, the virus spreads horizontally through unsuspecting individuals. ZIKV infections can present symptoms that can be easily mistaken for DENV [66], which makes the situation more complicated. People in regions where DENV and ZIKV are both endemic should take caution concerning horizontal transmission, particularly when pregnant women are involved, as the virus is suspected of causing microencephaly [67].

Outbreaks in Brazil and French Polynesia raised concerns about ZIKV vertically transmitting from mother to fetus, causing retardation in the form of significantly reduced brain size [67, 68]. The teratogenic nature of ZIKV makes the virus particularly devastating compared to other Flaviviruses, like DENV. Several Guillain-Barré syndrome (GBS) cases manifested in ZIKV infected individuals during the French Polynesia outbreak, causing muscle weakness, difficulty with breathing and a loss of coordination [69]. Many GBS patients had persisting issues lasting longer than three months. The potential severity of ZIKV, and its debated ability to spread through North America [70], makes developing treatment and prevention options essential.

Like JEV, ZIKV also produces subgenomic RNA that provides similar interferon suppressing function [71]. Since the TRs of all Flaviviruses are highly conserved, these similarities are unsurprising, but there is still a sizeable gap in knowledge regarding the host interacting partners of ZIKV. The terminal regions of ZIKV are somewhat unique due to the likely internal ribosomal entry site in the 5′ TR [72]. There is a need to identify the interactions between ZIKV TRs and host proteins to uncover targets for the therapeutics we require. Testing previously identified interactions from other Flaviviruses, like JEV, will provide a jumping-off point to characterize ZIKV better.

1.2 Rift Valley Fever Virus

There is concern surrounding another group of highly infectious viruses that can cause severe illness in humans and livestock [73]. Order *Bunyavirales* consists of negative or ambisense (simultaneous positive and negative sense) RNA viruses. Typically, the genomes comprise three separate segments,

small (S), medium (M), and large (L), named based on the segment's length [74]. The S segment being ambisense, while the M and L are negative-sense. Like flaviviruses, bunyaviruses spread predominantly via arthropod vectors, but there are unique exceptions, like Hantavirus, which entirely relies on rodent vectors [74, 75]. Gaining entry to the target cells occurs via dynamin-dependent caveola mediated endocytosis, a slightly different mechanism than the Flaviviruses [76].

One Bunyavirus that has seen multiple outbreaks, the first occurring in Eastern Africa, 1931, is the Rift Valley Fever Virus (RVFV) [77]. This virus has decimated livestock during outbreaks, causing mass deaths of cattle and sheep neonates [78]. Symptoms of RVFV infection in humans include fever, dizziness, muscle fatigue and soreness [79]. One-tenth of infected individuals will experience more severe symptoms. Rarely, people experience ocular disease that can occasionally result in blindness [80]. Encephalitis also occurs infrequently but can have lasting consequences [81]. Finally, RVFV can lead to hemorrhagic fever, a deadly symptom, causing half of the afflicted individuals to die. In livestock, the virus is particularly deadly to young and pregnant animals, leading to pregnancy termination [82]. A vaccine is available for veterinarian practices, but human vaccinations proved costly and required many booster doses to maintain immunity [83, 84].

Once in the cytosol, the genome begins making copies of the complementary RNA for each segment, done via an RNA-dependent RNA polymerase (RDRP) packaged in the virus [85, 86]. The genome lacks a 5' cap but "snatches" one from a host mRNA to promote the RNA transcription [87]. The M and L segments begin producing protein from the complementary strand, while the S segment translates protein from both the original genome and the complimentary one. Replication occurs through circularization, which relies on the complimentary TRs to form a pan-handle structure (figure 1.2B), where the RDRP remains attached, producing new copies of the genome [85, 88].

RVFV's S segment genome is an ambisense RNA that contains both terminal regions and a non-coding region that divides the positive and negative sense portions of the genome. These non-coding portions exhibit significant secondary structure, suggesting their role is regulatory in a similar manner to

the TRs of Flaviviruses [44]. RVFV interactions with host RNA helicases have been reported, specifically DDX17 [89].

1.3 DEAD-Box Helicases

DEAD-Box helicases belong to superfamily 2 of helicases [90]; RNA helicases depend on ATP to restructure double-stranded RNA molecules [91]. The name DEAD-box stems from the conserved motif of Asp-Glu-Ala-Asp and is essential in the ATP-binding domain [92]. In humans, these proteins are involved in many biological processes, such as ribosomal RNA processing, micro-RNA processing, spermatogenesis, cell proliferation, and translation regulation, to name a few [93-96]. In total, nine conserved motifs make up the biologically active ATP binding and RNA binding domain while being flanked by disordered terminals that make full-length protein constructs challenging to express [92, 97].

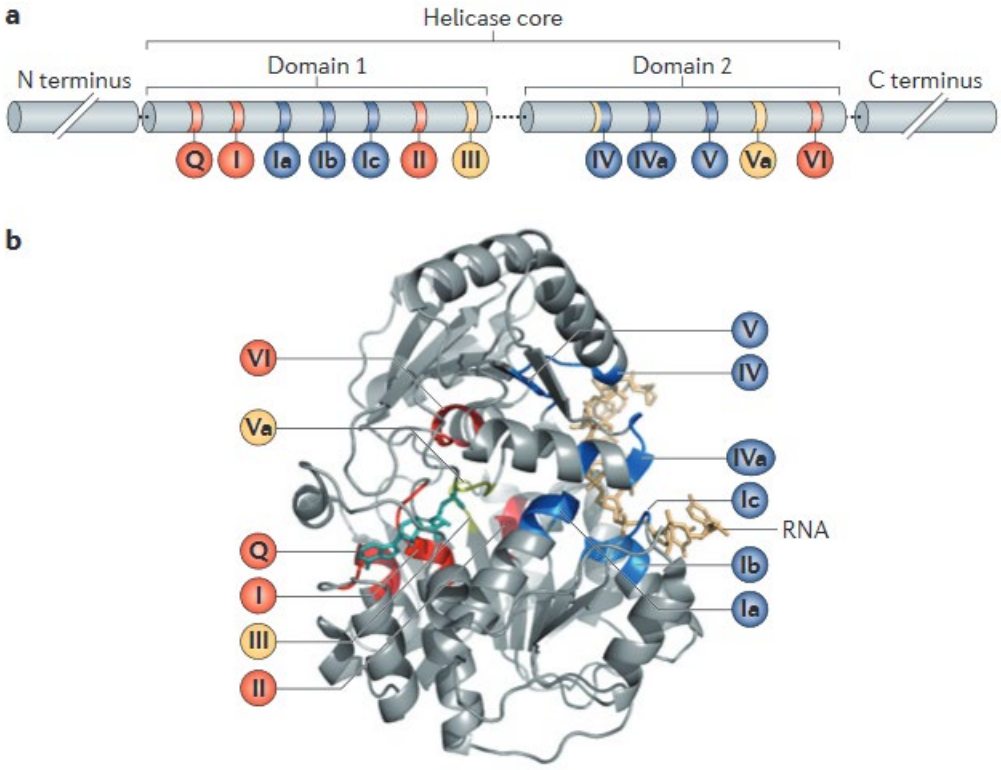

Figure 1.3. Schematic of DEAD-Box helicase, highlighting the organization of domains and folded structure. A) Linear schematic of DEAD-Box helicase, bands indicate the general position of conserved motifs. B) Structure of DEAD-Box helicase "Vasa" from *Drosophila melanogaster* bound to an RNA molecule. Reprinted with permission from Nature Reviews Molecular Cell Biology [98].

1.3.1 DDX3X

DDX3X is a member of the DEAD-Box helicase family and is located on the human X chromosome. It also has a Y-chromosome homolog expressed predominantly in male germ cells but can rescue non-functional DDX3X mutants [99]. DDX3X is approximately 73kDa, and like most DEAD-Box helicases, it has significant cell metabolism roles. The RNA helicase has demonstrated the ability to suppress translation during stress conditions [100]. It does this by interacting with initiation factors and preventing translation [101]. Pull-downs identified spliced mRNAs bound to DDX3X immediately following splicing, suggesting that the helicase plays a role during splicing [102]. Assembly of the 80S ribosome also depends on DDX3X for formation [103]. Additionally, the protein has to have sequence similarities to common splicing factors, indicating a potential role in splicing RNAs [104]. In a cancer-related context, DDX3X modulates transcription of cell cycle regulator p21, suggesting DDX3X has a position as a tumour suppressor [105, 106]. Another group observed that DDX3X upregulation in breast cancer correlates with more aggressive and invasive tumours [107].

DDX3X's dual nature is not exclusive to cancer; some viruses exploit DDX3X for replication, suggesting that the protein is integral in the viral life cycle. However, DDX3X can obstruct the replication of other viruses, often through signalling the immune system. DDX3X has been described as indispensable for Human Immunodeficiency virus 1 (HIV-1) via DDX3X's ability to export the unspliced HIV RNA [108]. Using indirect inhibitors against viral infections that target host proteins is essential, particularly as viruses become resistant to direct therapies when used alone [109]. The need for indirect therapies has driven developments into DDX3X inhibitors as antivirals. This has shown promise for the treatment of HIV-1, at least in mice thus far [110]. Hepatitis C virus (HCV) protein interactions with DDX3X were the first identified viral protein interaction for DDX3X; more specifically, the HCV core protein was co-localized with DDX3X. HCV replication rate decreased when DDX3X expression was knocked down, demonstrating that HCV replication requires DDX3X [111].

Comparing DENV infected cells with and without DDX3X present, it is clear that the virus' replication is inhibited by DDX3X [112]. DDX3X is an essential modulator of the type one interferon (IFN)

pathway, promoting the innate immune response against DENV [112, 113]. Hepatitis B virus (HBV) is another virus that DDX3X impedes. HBV is also targeted via the IFN immune response, and to overcome the immune system, HBV suppresses the interactions DDX3X makes as part of the IFN response [114]. Exploiting DDX3X for a one-size-fits-all approach will not work, it is a keystone in both viral and antiviral systems. Using inhibitors can be effective, so long as the risk of vulnerability to other viruses, like DENV and HBV, is considered.

1.3.2 DDX17

Like DDX3X, DDX17 is an RNA helicase capable of unwinding RNA in an ATP-dependent fashion [115]. It has a molecular weight of 80.3 kDa, making it larger than its aforementioned paralog. DDX17 is an essential regulator of transcription, splicing and miRNAs through its interaction with another DEAD-box helicase, DDX5 [116]. Like DDX3X, DDX17 also exerts control over cell cycle processes. DDX5 and 17 are both essential in development, but their ability to promote cell proliferation and prevent apoptosis indicates a potential role as oncogenes [96]. Despite DDX17 and DDX3X's similarities functionally, only a 45% identity overlap exists between the two, with the overlap region consisting of the ATP and RNA binding domains forming the minimal helicase domain [117].

DDX17 is involved with numerous viruses, and much like DDX3X, its role is varied from virus to virus. Some Influenza strains appear to depend on DDX17 to assist with viral replication, specifically H1N1 [118]. DDX17-like RH30 relocates from the nucleus during Tombusvirus infection, where it blocks replication by interfering with host and viral machinery [119]. The ability of DDX17 to migrate from the nucleus to the cytoplasm suggests a pathway where the RNA helicase acts as an early detector of viral invaders.

1.4 Objectives of Thesis

The host protein-viral nucleic acid interaction is a critical component of viral replication. My thesis work seeks to highlight interactions between a pair of DEAD-box helicases and viral non-coding RNAs that can provide targets for indirect antivirals. DDX3X was shown to interact with the 5' terminal region of JEV

[61], therefore I hypothesize that the interaction is direct and DDX3X will also unwind the RNA. Additionally, since terminal regions are highly conserved, DDX3X should directly interact and unwind the ZIKV 5' terminal region as well. DDX17 was demonstrated to limit RVFV infection through it's interaction with non-coding RNAs from the S-segment [89], therefore it is reasonable to hypothesize that DDX17 will both recognize the RVFV 5' NCR and IGR directly in isolation and unwind them.

Expression of recombinant proteins is typically done using bacterial systems, but these often come with a set of compromises. Bacteria lack the post translational modifications of eukaryotic protein expression and some proteins fail to be expressed in bacteria entirely. Using insect cell culture to produce recombinant proteins provides a eukaryotic expression system that will produce proteins that otherwise wouldn't be expressed in Bacteria, like many full length DEAD-box proteins.

My first objective is to characterize the direct interaction of $DDX3X_{132-607}$ with the 5' terminal regions of both Japanese Encephalitis and additionally, characterize the helicase activity of $DDX3X_{132-607}$. Secondly, I sought to determine if $DDX17_{135-555}$ was capable of directly interacting with the intergenic and 5' non-coding regions of the S segment from the Rift Valley Fever Virus and determine if the protein is capable of unwinding the RNAs. The final objective is to develop a method towards expression of recombinant proteins using genetically engineered viruses to exploit insect cells.

1.5 References

1. Kamerow, D., The world's deadliest animal. *Bmj* **2014,** 348.
2. Spielman, A., *Mosquito: The story of man's deadliest foe*. Hachette Books: 2001.
3. Winegard, T. C., *The mosquito: a human history of our deadliest predator*. Text Publishing: 2019.
4. O'Sullivan, L.; Jardine, A.; Cook, A.; Weinstein, P., Deforestation, mosquitoes, and ancient Rome: lessons for today. *BioScience* **2008,** 58, (8), 756-760.
5. Hempelmann, E.; Krafts, K., Bad air, amulets and mosquitoes: 2,000 years of changing perspectives on malaria. *Malaria journal* **2013,** 12, (1), 232.
6. Bo Frandsen, S., 'The war that we prefer': The Reclamation of the Pontine Marshes and Fascist Expansion. *Totalitarian Movements and Political Religions* **2001,** 2, (3), 69-82.
7. Woolhouse, M.; Scott, F.; Hudson, Z.; Howey, R.; Chase-Topping, M., Human viruses: discovery and emergence. *Philosophical Transactions of the Royal Society B: Biological Sciences* **2012,** 367, (1604), 2864-2871.
8. Huang, Y.-J. S.; Higgs, S.; Horne, K. M.; Vanlandingham, D. L., Flavivirus-mosquito interactions. *Viruses* **2014,** 6, (11), 4703-4730.
9. Elliott, R. M., Emerging viruses: the Bunyaviridae. *Molecular medicine* **1997,** 3, (9), 572-577.
10. Organization, W. H. Emergencies preparedness, response: Epidemic focus. https://www.who.int/csr/disease/epidemic-focus/flavivirus-epidemics/en/ (01-06),
11. Mackenzie, J.; Williams, D., The zoonotic flaviviruses of Southern, South-Eastern and Eastern Asia, and australasia: the potential for emergent viruses. *Zoonoses and public health* **2009,** 56, (6-7), 338-356.
12. Tabachnick, W. J., Climate change and the arboviruses: lessons from the evolution of the dengue and yellow fever viruses. *Annual review of virology* **2016,** 3, 125-145.
13. Mbare, O.; Lindsay, S. W.; Fillinger, U., Pyriproxyfen for mosquito control: female sterilization or horizontal transfer to oviposition substrates by Anopheles gambiae sensu stricto and Culex quinquefasciatus. *Parasites & vectors* **2014,** 7, (1), 280.
14. Guillet, P.; Alnwick, D.; Cham, M. K.; Neira, M.; Zaim, M.; Heymann, D.; Mukelabai, K., Long-lasting treated mosquito nets: a breakthrough in malaria prevention. *Bulletin of the World Health Organization* **2001,** 79.
15. Zhang, D.; Zheng, X.; Xi, Z.; Bourtzis, K.; Gilles, J. R., Combining the sterile insect technique with the incompatible insect technique: I-impact of Wolbachia infection on the fitness of triple-and double-infected strains of Aedes albopictus. *PLoS One* **2015,** 10, (4), e0121126.
16. Binder, S.; Levitt, A. M.; Sacks, J. J.; Hughes, J. M., Emerging infectious diseases: public health issues for the 21st century. *Science* **1999,** 284, (5418), 1311-1313.
17. Jones, K. E.; Patel, N. G.; Levy, M. A.; Storeygard, A.; Balk, D.; Gittleman, J. L.; Daszak, P., Global trends in emerging infectious diseases. *Nature* **2008,** 451, (7181), 990-993.
18. Morens, D. M.; Folkers, G. K.; Fauci, A. S., The challenge of emerging and re-emerging infectious diseases. *Nature* **2004,** 430, (6996), 242-249.
19. Bhatt, S.; Gething, P. W.; Brady, O. J.; Messina, J. P.; Farlow, A. W.; Moyes, C. L.; Drake, J. M.; Brownstein, J. S.; Hoen, A. G.; Sankoh, O., The global distribution and burden of dengue. *Nature* **2013,** 496, (7446), 504-507.
20. Simmons, C. P.; Farrar, J. J.; van Vinh Chau, N.; Wills, B., Dengue. *New England Journal of Medicine* **2012,** 366, (15), 1423-1432.
21. Halstead, S. B., Pathogenesis of dengue: challenges to molecular biology. *Science* **1988,** 239, (4839), 476-481.
22. Sanofi, P., Sanofi updates information on dengue vaccine. In Sanofi Paris, France: 2017.

23. Fatima, K.; Syed, N. I., Dengvaxia controversy: impact on vaccine hesitancy. *Journal of global health* **2018,** 8, (2).
24. Ishikawa, T.; Yamanaka, A.; Konishi, E., A review of successful flavivirus vaccines and the problems with those flaviviruses for which vaccines are not yet available. *Vaccine* **2014,** 32, (12), 1326-1337.
25. Lucey, D. R.; Donaldson, H., Yellow fever vaccine shortages in the United States and abroad: a critical issue. In American College of Physicians: 2017.
26. Touch, S.; Suraratdecha, C.; Samnang, C.; Heng, S.; Gazley, L.; Huch, C.; Sovann, L.; Chhay, C. S.; Soeung, S. C., A cost–effectiveness analysis of Japanese encephalitis vaccine in Cambodia. *Vaccine* **2010,** 28, (29), 4593-4599.
27. Keating, G. M.; Noble, S., Recombinant hepatitis B vaccine (Engerix-B®). *Drugs* **2003,** 63, (10), 1021-1051.
28. Organization, W. H. Hepatitis B. https://www.who.int/news-room/fact-sheets/detail/hepatitis-b (2021-02-25),
29. Connor, B.; Bunn, W. B., The changing epidemiology of Japanese encephalitis and New data: the implications for New recommendations for Japanese encephalitis vaccine. *Tropical diseases, travel medicine and vaccines* **2017,** 3, (1), 14.
30. Control, C. f. D. Dengue. https://www.cdc.gov/dengue/index.html
31. Pesko, K. N.; Torres-Perez, F.; Hjelle, B. L.; Ebel, G. D., Molecular epidemiology of Powassan virus in North America. *The Journal of general virology* **2010,** 91, (Pt 11), 2698.
32. LaDeau, S. L.; Kilpatrick, A. M.; Marra, P. P., West Nile virus emergence and large-scale declines of North American bird populations. *Nature* **2007,** 447, (7145), 710-713.
33. Diaz, A.; Coffey, L. L.; Burkett-Cadena, N.; Day, J. F., Reemergence of St. Louis encephalitis virus in the Americas. *Emerging infectious diseases* **2018,** 24, (12), 2150.
34. Pierson, T. C.; Diamond, M. S., The continued threat of emerging flaviviruses. *Nature Microbiology* **2020**, 1-17.
35. Chambers, T. J.; Hahn, C. S.; Galler, R.; Rice, C. M., Flavivirus genome organization, expression, and replication. *Annual review of microbiology* **1990,** 44, (1), 649-688.
36. Greber, U., Signalling in viral entry. *Cellular and Molecular Life Sciences CMLS* **2002,** 59, (4), 608-626.
37. Smit, J. M.; Moesker, B.; Rodenhuis-Zybert, I.; Wilschut, J., Flavivirus cell entry and membrane fusion. *Viruses* **2011,** 3, (2), 160-171.
38. Selisko, B.; Wang, C.; Harris, E.; Canard, B., Regulation of Flavivirus RNA synthesis and replication. *Current opinion in virology* **2014,** 9, 74-83.
39. Ray, D.; Shah, A.; Tilgner, M.; Guo, Y.; Zhao, Y.; Dong, H.; Deas, T. S.; Zhou, Y.; Li, H.; Shi, P.-Y., West Nile virus 5′-cap structure is formed by sequential guanine N-7 and ribose 2′-O methylations by nonstructural protein 5. *Journal of virology* **2006,** 80, (17), 8362-8370.
40. Rice, C. M.; Lenches, E. M.; Shin, S.; Sheets, R.; Strauss, J., Nucleotide sequence of yellow fever virus: implications for flavivirus gene expression and evolution. *Science* **1985,** 229, (4715), 726-733.
41. Nowak, T.; Färber, P. M.; Wengler, G.; Wengler, G., Analyses of the terminal sequences of West Nile virus structural proteins and of the in vitro translation of these proteins allow the proposal of a complete scheme of the proteolytic cleavages involved in their synthesis. *Virology* **1989,** 169, (2), 365-376.
42. Lee, I.; Bos, S.; Li, G.; Wang, S.; Gadea, G.; Desprès, P.; Zhao, R. Y., Probing molecular insights into Zika virus–host interactions. *Viruses* **2018,** 10, (5), 233.
43. Villordo, S. M.; Gamarnik, A. V., Genome cyclization as strategy for flavivirus RNA replication. *Virus research* **2009,** 139, (2), 230-239.

44. Gauliard, N.; Billecocq, A.; Flick, R.; Bouloy, M., Rift Valley fever virus noncoding regions of L, M and S segments regulate RNA synthesis. *Virology* **2006,** 351, (1), 170-179.
45. Desselberger, U.; Racaniello, V. R.; Zazra, J. J.; Palese, P., The 3'and 5'-terminal sequences of influenza A, B and C virus RNA segments are highly conserved and show partial inverted complementarity. *Gene* **1980,** 8, (3), 315-328.
46. Thurner, C.; Witwer, C.; Hofacker, I. L.; Stadler, P. F., Conserved RNA secondary structures in Flaviviridae genomes. *Journal of General Virology* **2004,** 85, (5), 1113-1124.
47. Mazeaud, C.; Freppel, W.; Chatel-Chaix, L., The multiples fates of the flavivirus RNA genome during pathogenesis. *Frontiers in genetics* **2018,** 9, 595.
48. Organization, W. H. Japanese Encephalitis. https://www.who.int/en/news-room/fact-sheets/detail/japanese-encephalitis
49. Wang, Q.; Xin, X.; Wang, T.; Wan, J.; Ou, Y.; Yang, Z.; Yu, Q.; Zhu, L.; Guo, Y.; Wu, Y., Japanese encephalitis virus induces apoptosis and encephalitis by activating the PERK pathway. *Journal of virology* **2019,** 93, (17).
50. Ogata, A.; Tashiro, K.; Nukuzuma, S.; Nagashima, K.; Hall, W. W., A rat model of Parkinson's disease induced by Japanese encephalitis virus. *Journal of neurovirology* **1997,** 3, (2), 141-147.
51. Li, Z.; Hong, S.; Gong, N., Immunohistochemical study on Japanese B encephalitis. *Chinese medical journal* **1988,** 101, (10), 768-771.
52. Miyake, M., The pathology of Japanese encephalitis: A review. *Bulletin of the World Health Organization* **1964,** 30, (2), 153.
53. Burke, D. S.; Nisalak, A.; Ussery, M. A., Antibody capture immunoassay detection of Japanese encephalitis virus immunoglobulin M and G antibodies in cerebrospinal fluid. *Journal of clinical microbiology* **1982,** 16, (6), 1034-1042.
54. Campbell, G. L.; Hills, S. L.; Fischer, M.; Jacobson, J. A.; Hoke, C. H.; Hombach, J. M.; Marfin, A. A.; Solomon, T.; Tsai, T. F.; Tsu, V. D., Estimated global incidence of Japanese encephalitis: a systematic review. *Bulletin of the World Health Organization* **2011,** 89, 766-774.
55. Pijlman, G. P.; Funk, A.; Kondratieva, N.; Leung, J.; Torres, S.; Van der Aa, L.; Liu, W. J.; Palmenberg, A. C.; Shi, P.-Y.; Hall, R. A., A highly structured, nuclease-resistant, noncoding RNA produced by flaviviruses is required for pathogenicity. *Cell host & microbe* **2008,** 4, (6), 579-591.
56. Cumberworth, S. L.; Clark, J. J.; Kohl, A.; Donald, C. L., Inhibition of type I interferon induction and signalling by mosquito-borne flaviviruses. *Cellular microbiology* **2017,** 19, (5), e12737.
57. Chang, R.-Y.; Hsu, T.-W.; Chen, Y.-L.; Liu, S.-F.; Tsai, Y.-J.; Lin, Y.-T.; Chen, Y.-S.; Fan, Y.-H., Japanese encephalitis virus non-coding RNA inhibits activation of interferon by blocking nuclear translocation of interferon regulatory factor 3. *Veterinary microbiology* **2013,** 166, (1-2), 11-21.
58. Fan, Y.-H.; Nadar, M.; Chen, C.-C.; Weng, C.-C.; Lin, Y.-T.; Chang, R.-Y., Small noncoding RNA modulates Japanese encephalitis virus replication and translation in trans. *Virology journal* **2011,** 8, (1), 1-11.
59. Fajardo Jr, T.; Sanford, T. J.; Mears, H. V.; Jasper, A.; Storrie, S.; Mansur, D. S.; Sweeney, T. R., The flavivirus polymerase NS5 regulates translation of viral genomic RNA. *Nucleic acids research* **2020,** 48, (9), 5081-5093.
60. Li, C.; Ge, L.-l.; Li, P.-p.; Wang, Y.; Sun, M.-x.; Huang, L.; Ishag, H.; Di, D.-d.; Shen, Z.-q.; Fan, W.-x., The DEAD-box RNA helicase DDX5 acts as a positive regulator of Japanese encephalitis virus replication by binding to viral 3' UTR. *Antiviral research* **2013,** 100, (2), 487-499.
61. Li, C.; Ge, L.-l.; Li, P.-p.; Wang, Y.; Dai, J.-j.; Sun, M.-x.; Huang, L.; Shen, Z.-q.; Hu, X.-c.; Ishag, H., Cellular DDX3 regulates Japanese encephalitis virus replication by interacting with viral un-translated regions. *Virology* **2014,** 449, 70-81.

62. Macnamara, F., Zika virus: a report on three cases of human infection during an epidemic of jaundice in Nigeria. *Transactions of the royal society of tropical medicine and hygiene* **1954,** 48, (2), 139-145.
63. Duffy, M. R.; Chen, T.-H.; Hancock, W. T.; Powers, A. M.; Kool, J. L.; Lanciotti, R. S.; Pretrick, M.; Marfel, M.; Holzbauer, S.; Dubray, C., Zika virus outbreak on Yap Island, federated states of Micronesia. *New England Journal of Medicine* **2009,** 360, (24), 2536-2543.
64. Weaver, S. C.; Barrett, A. D., Transmission cycles, host range, evolution and emergence of arboviral disease. *Nature Reviews Microbiology* **2004,** 2, (10), 789-801.
65. Gregory, C. J.; Oduyebo, T.; Brault, A. C.; Brooks, J. T.; Chung, K.-W.; Hills, S.; Kuehnert, M. J.; Mead, P.; Meaney-Delman, D.; Rabe, I., Modes of transmission of Zika virus. *The Journal of infectious diseases* **2017,** 216, (suppl_10), S875-S883.
66. Ginier, M.; Neumayr, A.; Günther, S.; Schmidt-Chanasit, J.; Blum, J., Zika without symptoms in returning travellers: What are the implications? *Travel medicine and infectious disease* **2016,** 14, (1), 16-20.
67. Mlakar, J.; Korva, M.; Tul, N.; Popović, M.; Poljšak-Prijatelj, M.; Mraz, J.; Kolenc, M.; Resman Rus, K.; Vesnaver Vipotnik, T.; Fabjan Vodušek, V., Zika virus associated with microcephaly. *New England Journal of Medicine* **2016,** 374, (10), 951-958.
68. Cauchemez, S.; Besnard, M.; Bompard, P.; Dub, T.; Guillemette-Artur, P.; Eyrolle-Guignot, D.; Salje, H.; Van Kerkhove, M. D.; Abadie, V.; Garel, C., Association between Zika virus and microcephaly in French Polynesia, 2013–15: a retrospective study. *The Lancet* **2016,** 387, (10033), 2125-2132.
69. Cao-Lormeau, V.-M.; Blake, A.; Mons, S.; Lastère, S.; Roche, C.; Vanhomwegen, J.; Dub, T.; Baudouin, L.; Teissier, A.; Larre, P., Guillain-Barré Syndrome outbreak associated with Zika virus infection in French Polynesia: a case-control study. *The Lancet* **2016,** 387, (10027), 1531-1539.
70. Gyawali, N.; Bradbury, R. S.; Taylor-Robinson, A. W., The global spread of Zika virus: is public and media concern justified in regions currently unaffected? *Infectious diseases of poverty* **2016,** 5, (1), 1-6.
71. Donald, C. L.; Brennan, B.; Cumberworth, S. L.; Rezelj, V. V.; Clark, J. J.; Cordeiro, M. T.; Freitas de Oliveira França, R.; Pena, L. J.; Wilkie, G. S.; Da Silva Filipe, A., Full genome sequence and sfRNA interferon antagonist activity of Zika virus from Recife, Brazil. *PLoS neglected tropical diseases* **2016,** 10, (10), e0005048.
72. Song, Y.; Mugavero, J.; Stauft, C. B.; Wimmer, E., Dengue and Zika virus 5′ untranslated regions harbor internal ribosomal entry site functions. *MBio* **2019,** 10, (2).
73. Control, C. f. D. Bunyaviridae. https://www.cdc.gov/vhf/virus-families/bunyaviridae.html
74. Schreur, P. J. W.; Kormelink, R.; Kortekaas, J., Genome packaging of the Bunyavirales. *Current opinion in virology* **2018,** 33, 151-155.
75. Mills, J. N.; Yates, T. L.; Childs, J. E.; Parmenter, R. R.; Ksiazek, T. G.; Rollin, P. E.; Peters, C., Guidelines for working with rodents potentially infected with hantavirus. *Journal of Mammalogy* **1995,** 76, (3), 716-722.
76. Harmon, B.; Schudel, B. R.; Maar, D.; Kozina, C.; Ikegami, T.; Tseng, C.-T. K.; Negrete, O. A., Rift Valley fever virus strain MP-12 enters mammalian host cells via caveola-mediated endocytosis. *Journal of virology* **2012,** 86, (23), 12954-12970.
77. Findlay, G.; Daubney, R., The Virus of Rift Valley Fever or Enzob'tic Hepatitis. *Lancet* **1931**.
78. Bird, B. H.; Ksiazek, T. G.; Nichol, S. T.; MacLachlan, N. J., Rift Valley fever virus. *Journal of the American Veterinary Medical Association* **2009,** 234, (7), 883-893.
79. Control, C. f. D. Rift Valley Fever (RVF): Signs and Symptoms. (03-02-21),

80. Newman-Gerhardt, S.; Muiruri, S.; Muchiri, E.; Peters, C. J.; Morrill, J.; Lucas, A. H.; King, C. H.; Kazura, J.; LaBeaud, A. D., Potential for autoimmune pathogenesis of Rift Valley Fever virus retinitis. *The American journal of tropical medicine and hygiene* **2013,** 89, (3), 495-497.
81. Dodd, K. A.; McElroy, A. K.; Jones, T. L.; Zaki, S. R.; Nichol, S. T.; Spiropoulou, C. F., Rift Valley fever virus encephalitis is associated with an ineffective systemic immune response and activated T cell infiltration into the CNS in an immunocompetent mouse model. *PLoS Negl Trop Dis* **2014,** 8, (6), e2874.
82. Wilson, M. L., Rift Valley fever virus ecology and the epidemiology of disease emergence a. *Annals of the New York Academy of Sciences* **1994,** 740, (1), 169-180.
83. Ikegami, T.; Makino, S., Rift valley fever vaccines. *vaccine* **2009,** 27, D69-D72.
84. Pittman, P. R.; Liu, C.; Cannon, T. L.; Makuch, R. S.; Mangiafico, J. A.; Gibbs, P. H.; Peters, C. J., Immunogenicity of an inactivated Rift Valley fever vaccine in humans: a 12-year experience. *Vaccine* **1999,** 18, (1-2), 181-189.
85. Nguyen, M.; Haenni, A.-L., Expression strategies of ambisense viruses. *Virus research* **2003,** 93, (2), 141-150.
86. Rossier, C.; Patterson, J.; Kolakofsky, D., La Crosse virus small genome mRNA is made in the cytoplasm. *Journal of Virology* **1986,** 58, (2), 647.
87. Olschewski, S.; Cusack, S.; Rosenthal, M., The Cap-Snatching mechanism of bunyaviruses. *Trends in microbiology* **2020,** 28, (4), 293-303.
88. Simons, J.; Hellman, U.; Pettersson, R., Uukuniemi virus S RNA segment: ambisense coding strategy, packaging of complementary strands into virions, and homology to members of the genus Phlebovirus. *Journal of Virology* **1990,** 64, (1), 247-255.
89. Moy, R. H.; Cole, B. S.; Yasunaga, A.; Gold, B.; Shankarling, G.; Varble, A.; Molleston, J. M.; Lynch, K. W.; Cherry, S., Stem-loop recognition by DDX17 facilitates miRNA processing and antiviral defense. *Cell* **2014,** 158, (4), 764-777.
90. Fairman-Williams, M. E.; Guenther, U.-P.; Jankowsky, E., SF1 and SF2 helicases: family matters. *Current opinion in structural biology* **2010,** 20, (3), 313-324.
91. Rozen, F.; Edery, I.; Meerovitch, K.; Dever, T. E.; Merrick, W. C.; Sonenberg, N., Bidirectional RNA helicase activity of eucaryotic translation initiation factors 4A and 4F. *Molecular and cellular biology* **1990,** 10, (3), 1134-1144.
92. Meier-Stephenson, V.; Mrozowich, T.; Pham, M.; Patel, T. R., DEAD-box helicases: the Yin and Yang roles in viral infections. *Biotechnology and Genetic Engineering Reviews* **2018,** 34, (1), 3-32.
93. Chen, C.-Y.; Chan, C.-H.; Chen, C.-M.; Tsai, Y.-S.; Tsai, T.-Y.; Wu Lee, Y.-H.; You, L.-R., Targeted inactivation of murine Ddx3x: essential roles of Ddx3x in placentation and embryogenesis. *Human molecular genetics* **2016,** 25, (14), 2905-2922.
94. Wang, X.; Zhu, Z.; Wu, X.; Li, H.; Li, T.; Li, Q.; Zhang, P.; Li, L.; Che, D.; Xiao, X., Landscape of RNA editing reveals new insights into the dynamic gene regulation of spermatogenesis based on integrated RNA-Seq. *bioRxiv* **2018**, 478206.
95. Jalal, C.; Uhlmann-Schiffler, H.; Stahl, H., Redundant role of DEAD box proteins p68 (Ddx5) and p72/p82 (Ddx17) in ribosome biogenesis and cell proliferation. *Nucleic acids research* **2007,** 35, (11), 3590-3601.
96. Janknecht, R., Multi-talented DEAD-box proteins and potential tumor promoters: p68 RNA helicase (DDX5) and its paralog, p72 RNA helicase (DDX17). *American journal of translational research* **2010,** 2, (3), 223.
97. Dutta, S.; Gupta, G.; Choi, Y.-W.; Kotaka, M.; Fielding, B. C.; Song, J.; Tan, Y.-J., The variable N-terminal region of DDX5 contains structural elements and auto-inhibits its interaction with NS5B of hepatitis C virus. *Biochemical Journal* **2012,** 446, (1), 37-46.

98. Linder, P.; Jankowsky, E., From unwinding to clamping—the DEAD box RNA helicase family. *Nature reviews Molecular cell biology* **2011,** 12, (8), 505-516.
99. Sekiguchi, T.; Iida, H.; Fukumura, J.; Nishimoto, T., Human DDX3Y, the Y-encoded isoform of RNA helicase DDX3, rescues a hamster temperature-sensitive ET24 mutant cell line with a DDX3X mutation. *Experimental cell research* **2004,** 300, (1), 213-222.
100. Shih, J.-W.; Wang, W.-T.; Tsai, T.-Y.; Kuo, C.-Y.; Li, H.-K.; Wu Lee, Y.-H., Critical roles of RNA helicase DDX3 and its interactions with eIF4E/PABP1 in stress granule assembly and stress response. *Biochemical Journal* **2012,** 441, (1), 119-129.
101. Shih, J.; Tsai, T.; Chao, C.-H.; Lee, Y. W., Candidate tumor suppressor DDX3 RNA helicase specifically represses cap-dependent translation by acting as an eIF4E inhibitory protein. *Oncogene* **2008,** 27, (5), 700-714.
102. Merz, C.; Urlaub, H.; Will, C. L.; Lührmann, R., Protein composition of human mRNPs spliced in vitro and differential requirements for mRNP protein recruitment. *Rna* **2007,** 13, (1), 116-128.
103. Geissler, R.; Golbik, R. P.; Behrens, S.-E., The DEAD-box helicase DDX3 supports the assembly of functional 80S ribosomes. *Nucleic acids research* **2012,** 40, (11), 4998-5011.
104. Ariumi, Y., Multiple functions of DDX3 RNA helicase in gene regulation, tumorigenesis, and viral infection. *Frontiers in genetics* **2014,** 5, 423.
105. Chao, C.-H.; Chen, C.-M.; Cheng, P.-L.; Shih, J.-W.; Tsou, A.-P.; Lee, Y.-H. W., DDX3, a DEAD box RNA helicase with tumor growth–suppressive property and transcriptional regulation activity of the p21waf1/cip1 promoter, is a candidate tumor suppressor. *Cancer research* **2006,** 66, (13), 6579-6588.
106. McGivern, D. R.; Lemon, S. M., Tumor suppressors, chromosomal instability, and hepatitis C virus–associated liver cancer. *Annual Review of Pathology: Mechanisms of Disease* **2009,** 4, 399-415.
107. Botlagunta, M.; Vesuna, F.; Mironchik, Y.; Raman, A.; Lisok, A.; Winnard, P.; Mukadam, S.; Van Diest, P.; Chen, J.; Farabaugh, P., Oncogenic role of DDX3 in breast cancer biogenesis. *Oncogene* **2008,** 27, (28), 3912-3922.
108. Yedavalli, V. S.; Neuveut, C.; Chi, Y.-h.; Kleiman, L.; Jeang, K.-T., Requirement of DDX3 DEAD box RNA helicase for HIV-1 Rev-RRE export function. *Cell* **2004,** 119, (3), 381-392.
109. Lou, Z.; Sun, Y.; Rao, Z., Current progress in antiviral strategies. *Trends in pharmacological sciences* **2014,** 35, (2), 86-102.
110. Brai, A.; Riva, V.; Saladini, F.; Zamperini, C.; Trivisani, C. I.; Garbelli, A.; Pennisi, C.; Giannini, A.; Boccuto, A.; Bugli, F., DDX3X inhibitors, an effective way to overcome HIV-1 resistance targeting host proteins. *European Journal of Medicinal Chemistry* **2020**, 112319.
111. Ariumi, Y.; Kuroki, M.; Abe, K.-i.; Dansako, H.; Ikeda, M.; Wakita, T.; Kato, N., DDX3 DEAD-box RNA helicase is required for hepatitis C virus RNA replication. *Journal of virology* **2007,** 81, (24), 13922-13926.
112. Li, G.; Feng, T.; Pan, W.; Shi, X.; Dai, J., DEAD-box RNA helicase DDX3X inhibits DENV replication via regulating type one interferon pathway. *Biochemical and biophysical research communications* **2015,** 456, (1), 327-332.
113. Soulat, D.; Bürckstümmer, T.; Westermayer, S.; Goncalves, A.; Bauch, A.; Stefanovic, A.; Hantschel, O.; Bennett, K. L.; Decker, T.; Superti-Furga, G., The DEAD-box helicase DDX3X is a critical component of the TANK-binding kinase 1-dependent innate immune response. *The EMBO journal* **2008,** 27, (15), 2135-2146.
114. Yu, S.; Chen, J.; Wu, M.; Chen, H.; Kato, N.; Yuan, Z., Hepatitis B virus polymerase inhibits RIG-I- and Toll-like receptor 3-mediated beta interferon induction in human hepatocytes through interference with interferon regulatory factor 3 activation and dampening of the interaction between TBK1/IKKε and DDX3. *Journal of General Virology* **2010,** 91, (8), 2080-2090.

115. Hönig, A.; Auboeuf, D.; Parker, M. M.; O'Malley, B. W.; Berget, S. M., Regulation of alternative splicing by the ATP-dependent DEAD-box RNA helicase p72. *Molecular and cellular biology* **2002,** 22, (16), 5698-5707.
116. Dardenne, E.; Espinoza, M. P.; Fattet, L.; Germann, S.; Lambert, M.-P.; Neil, H.; Zonta, E.; Mortada, H.; Gratadou, L.; Deygas, M., RNA helicases DDX5 and DDX17 dynamically orchestrate transcription, miRNA, and splicing programs in cell differentiation. *Cell reports* **2014,** 7, (6), 1900-1913.
117. Song, H.; Ji, X., The mechanism of RNA duplex recognition and unwinding by DEAD-box helicase DDX3X. *Nature communications* **2019,** 10, (1), 1-8.
118. Bortz, E.; Westera, L.; Maamary, J.; Steel, J.; Albrecht, R. A.; Manicassamy, B.; Chase, G.; Martínez-Sobrido, L.; Schwemmle, M.; García-Sastre, A., Host-and strain-specific regulation of influenza virus polymerase activity by interacting cellular proteins. *MBio* **2011,** 2, (4).
119. Wu, C.-Y.; Nagy, P. D., Blocking tombusvirus replication through the antiviral functions of DDX17-like RH30 DEAD-box helicase. *PLoS pathogens* **2019,** 15, (5), e1007771.

Chapter 2: Human DDX3X Unwinds Japanese Encephalitis and Zika Viral 5′ Terminal Regions[a]

2.0 Introduction

Infection with pathogenic viruses often leads to severe diseases that may impact, among others, the metabolic, respiratory, digestive, and central nervous systems. Among the most pathogenic family of viruses, emerging and re-emerging outbreaks of flavivirus are responsible for thousands of deaths annually [1]. Furthermore, flaviviral infections also lead to significant morbidities in survivors, which can create a substantial burden on the health system [2,3]. The Flaviviridae family includes the most prevalent arthropod-borne viruses such as dengue, Japanese encephalitis (JEV), Murray Valley, Powassan, West Nile (WNV), yellow fever, and Zika (ZIKV) viruses. Flaviviral outbreaks are becoming increasingly common, due to the ease of transmission by mosquitoes and the lack of efficient therapeutics or immunoprophylactic strategies [4–6]. As a result, flaviviruses are emerging as a global health threat. For example, the WHO reports that since 2015, ZIKV outbreaks have been reported in 42 countries [7]. The majority of flaviviruses utilize Aedes and Culex genuses of mosquitoes for transmission [8], meaning that as global temperatures increase, countries that were once protected from arboviruses are also becoming increasingly at risk [9,10].

The JEV is responsible for approximately 68,000 cases annually, with a fatality rate between 20–30% and with 30% of cases developing serious long-term disabilities [11,12]. This makes JEV one of the deadliest flaviviruses, although an approved vaccine against JEV is available [13,14]. The Zika virus (ZIKV) outbreak infected >4.5 million people in Brazil and the Americas in 2015–2016 [15,16]. ZIKV is also linked to birth defects [3,17–23] and neurological disorders [24–30]. The ZIKV has also been observed to be transmitted sexually and present symptoms in only one-fifth of cases [31,32]. Unlike JEV, there is no approved vaccine available against ZIKV. Attempts to develop vaccines have faced unexpected

---

[a] Reprinted with permission from Nelson, C., Mrozowich, T., and Patel, T. R. (2021). Human DDX3X Unwinds Japanese Encephalitis and Zika Viral 5′ Terminal Regions. *International Journal of Molecular Sciences*, 22(1), 413.

challenges due to antibody-dependent enhancement of infection with other flaviviruses [33–35]. Flaviviruses contain a positive-sense single-stranded RNA genome, comprised of 5′ and 3′ untranslated terminal regions (TRs). The 5′ TRs (~0.1 kb) contain a type 1 capped structure, whereas the 3′ TRs (~0.3 to ~0.5 kb) lack a poly(A) tail, and both TRs include conserved structural motifs [36–41]. The interactions between flaviviral 5′ and 3′ TRs are also critical for viral replication [6,41–46]. These regions flank a single open reading frame (ORF), which encodes a single polypeptide that is cleaved by a combination of host and viral proteases [47]. Previous work has established that interactions of host proteins with the flaviviral TRs are crucial for viral replication [48–59].

The human DEAD-box family of helicases is comprised of 37 members, each composed of conserved helicase core domains that interact with ATP and RNA [60,61]. The DEAD-box helicases consist of two helicase domains; domain 1 containing motifs Q, I, Ia Ib, Ic, II (DEAD-box), and III; and domain 2 containing motifs IV, IVa, V, Va, and VI [61]. These motifs are involved in either ATP binding/hydrolysis, RNA binding, or couple ATP and RNA binding activities. Although the classical function of DEAD-box helicases is ATP-dependent unwinding of nucleic acids [62], they influence all major aspects of RNA metabolism [63]. DDX3X (X-linked DDX3, 73 kDa, Figure 2.1.1A) is one of the ATP-dependent RNA helicases that plays critical roles in transcription, translation, and mRNA (messenger-RNA) export [59,64,65]. DDX3X unwinds RNA in an ATP-dependent manner, where DDX3X binds to dsRNA (double-stranded RNA) and hydrolyzes ATP to release single-stranded RNA [66]. Apart from playing vital roles in cellular activities, DDX3X was shown to suppress dengue viral infection via interferon activation [67] but promotes WNV infection [68]. Using affinity pull-down and Western blot analysis, it was suggested that DDX3X could interact with 5′ TR of JEV and regulate its replication [50]. Recent studies have suggested that DDX3X inhibitors can suppress WNV replication [68]. Given the magnitude and severity of flaviviral infections, there is a critical need for therapeutics; however, their development is hindered by the limited understanding of the interactions of viral RNAs with the host cellular proteins.

In this study, we followed up Li et al.'s affinity pull-down assays and demonstrated that DDX3X directly interacts with the 5′ TR of JEV [50]. As the 5′ TRs of flaviviruses are hypothesized to be

structurally similar [69,70], we asked if the 5′ TR of ZIKV can also be recognized by DDX3X. Our binding studies demonstrated that DDX3X indeed interacts with the 5′ TR of ZIKV. As DDX3X is an RNA helicase, we performed helicase assays, which suggested that both JEV and ZIKV 5′ TR can be unwound by DDX3X. In summary, our study highlights that DDX3X could serve as an important therapeutic target to inhibit JEV and ZIKV replications.

2.1 Results

2.1.1 Purification of $DDX3X_{132–607}$, JEV 5′ and Zika 5′ TR RNAs

The $DDX3X_{132–607}$ was expressed in Lemo21(DE3) Esherichia coli cells, followed by initial purification using affinity chromatography. Subsequently, affinity-purified $DDX3X_{132–607}$ was subjected to size exclusion chromatography (SEC) purification (see section 4 for additional details). As presented in Figure 2.1.1B, we were able to remove minor aggregation at ~12 mL and ~13 mL elution volumes to obtain homogenous preparation of $DDX3X_{132–607}$ (peak at ~14.5 to 15.5 mL). Subsequently, we analysed the peak fractions using SDS-PAGE, which suggested that $DDX3X_{132–607}$ is devoid of any degradation (Figure 2.1.1C, right lane) and the amino-acid sequence-based molecular weight of 55.3 kDa for $DDX3X_{132–607}$ coincides with the observed band in Figure 2.1.1C.

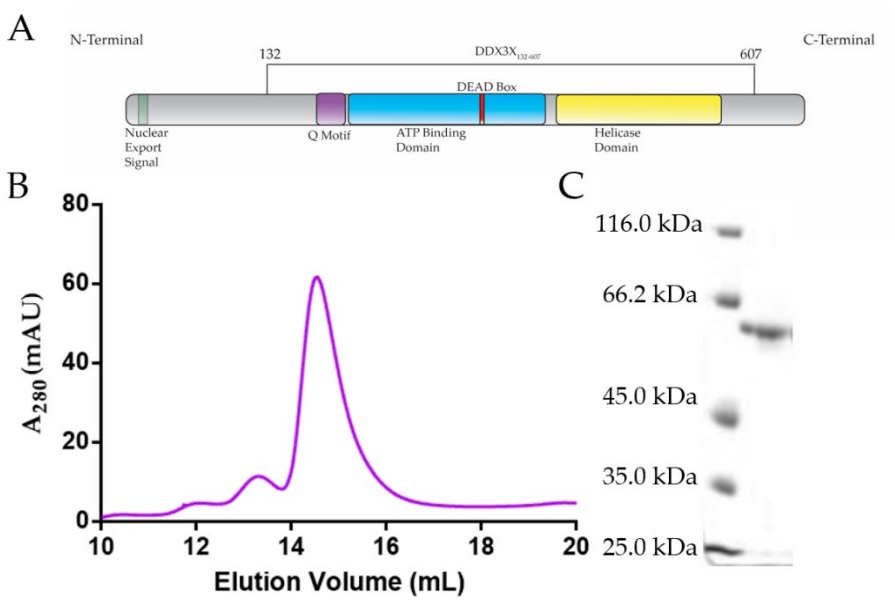

Figure 2.1.1. Purification of recombinant DDX3X$_{132–607}$. (A) Schematic of human DDX3X's domain architecture, indicating that DDX3X$_{132–607}$ consists of all the major domains, except the nuclear export signal sequence. (B) Size exclusion chromatography purification (Superdex 200 Increase GL 10/300) of DDX3X$_{132–607}$ demonstrating that DDX3X$_{132–607}$ can be purified to homogeneity, eluting at ~14.5 mL. Y-axis represents absorbance at 280 nm while the x-axis represents elution volume. (C) SDS-PAGE indicating that the size exclusion chromatography (SEC)-purified DDX3X$_{132–607}$ is monodispersed with the correct molecular weight (55.3 kDa).

The predicted secondary structure of 5′ TRs of JEV and ZIKA (Figure 2.1.2A,B) indicated that both RNAs are composed of a significant amount of double-stranded regions, along with stem-loops. The 5′ TRs for both viruses were in vitro transcribed and natively purified using SEC, similarly to DDX3X$_{132–607}$. The SEC purification indicated that while the ZIKV 5′ TR RNA elutes at approximately 12.5 mL, the JEV 5′ TR elutes at ~13.8 mL (Figure 2.1.2C). In both cases, oligomeric or aggregated species appear to elute around ~10.0 to 11.5 mL. In both SEC profiles, the plasmid DNA that was used as a template elutes around 8 mL, consistent with the column's void volume. Urea-PAGEs confirmed that both RNAs were purified to homogeneity. Monodispersed peak fractions(s) were used in downstream experiments.

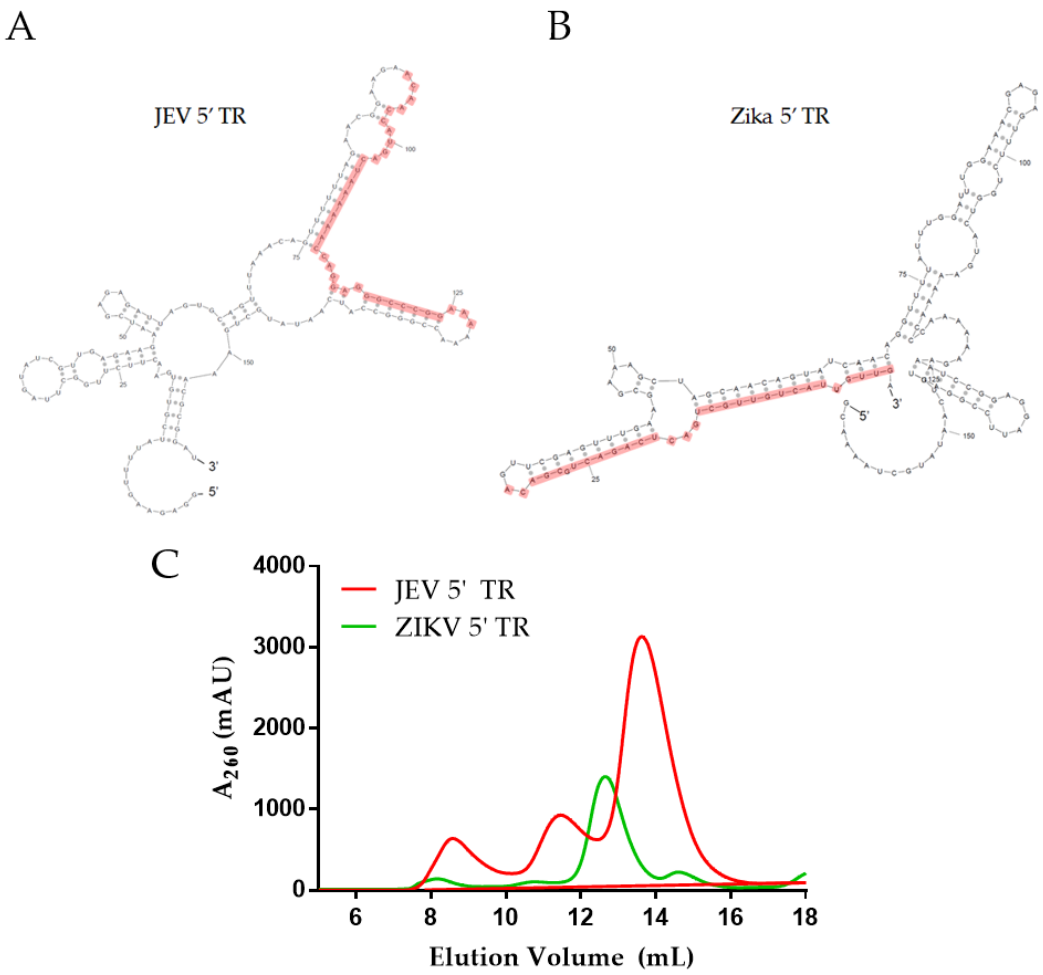

Figure 2.1.2. (A and B) Predicted secondary structure (Sfold v2.2) for the 5′ terminal regions (TRs) of Japanese encephalitis virus (JEV) 5′ and Zika virus (ZIKV), respectively. The regions highlighted in red colour indicate the sequence complementary to the DNA oligo used in the helicase assays. (C) Size exclusion chromatography elution profiles of the 5′ TRs of JEV (red) and ZIKV (green). Arrows indicate peaks that represent monodispersed fractions of RNA, which were used for downstream experiments. Y-axis represents absorbance at 260 nm while the x-axis represents elution volume.

2.1.2 DDX3X$_{132–607}$ Binds to 5′ TRs of JEV and ZIKV

To determine the binding affinity of a previously uncharacterized interaction system containing DDX3X$_{132–607}$ and 5′ TR of JEV, we employed microscale thermophoresis (MST) as performed previously [71,72]. DDX3X$_{132–607}$ was titrated against the constant concentration of the fluorescent ncRNAs (non-coding RNAs) to determine their dissociation constant (Kd). Figure 2.1.3A displays the change in fluorescent migration when the infrared laser affects the samples, where each trace represents a different concentration of DDX3X$_{132–607}$. Additionally, the blue bar indicates the "cold" region, and the red bar

indicates the "hot" region. Figure 2.1.3B and 2.1.3C present the binding curves for 5′ TRs of JEV and ZIKV in red and green, respectively. These experiments suggest that DDX3X$_{132–607}$ has a Kd of 1.66 ± 0.21μM for the 5′ TR of JEV and 7.05 ± 0.75 μM for the 5′ TR of ZIKV.

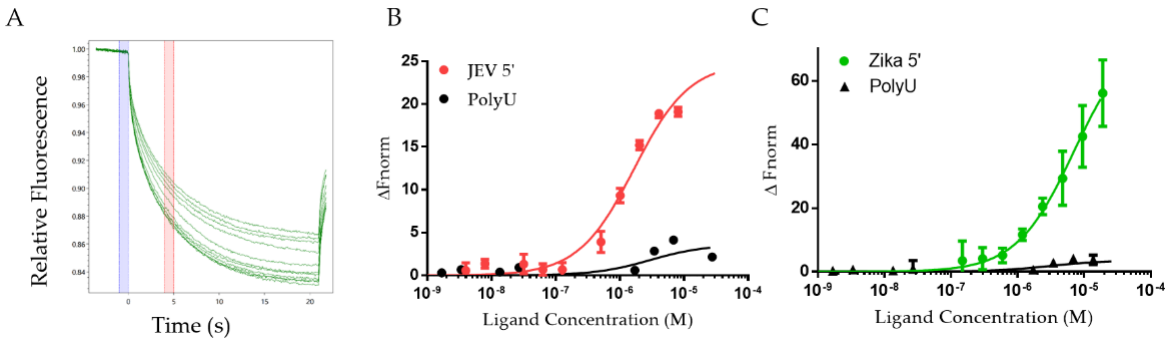

Figure 2.1.3. Interaction studies using microscale thermophoresis (MST). (A) Representative MST traces depicting the change in fluorescent migration of fluorescein-5-thiosemicarbazide (FITC)-JEV 5′ TR due to the excitation with an infra-red laser. Each green trace correlates to a different concentration of DDX3X$_{132–607}$. (B) Binding data for DDX3X$_{132–607}$ with JEV 5′ TR (n = 3). The red curve represents JEV 5′ and has a dissociation constant of 1.66 ± 0.21μM (Std. error of regression = 1.25). The black trace represents that polyU (negative control) does not interact with DDX3X$_{132–607}$. (C) Interaction between DDX3X$_{132–607}$ and ZIKV 5′ TR (n = 3) studied using MST. The green curve represents ZIKV 5′ and has a dissociation constant of 7.05 ± 0.75μM (Std. error of regression = 1.22). PolyU binding data included for reference (black).

2.1.3 DDX3X$_{132–607}$ Unwinds 5′ TRs of JEV and ZIKV

To further investigate if the binding of flaviviral 5′ TRs with DDX3X$_{132–607}$ leads to their unwinding, we designed a helicase assay using MST. We hypothesized that if DDX3X$_{132–607}$ unwinds the 5′ TRs of JEV and ZIKV, the newly formed single-stranded region of viral RNAs could hybridize with their complementary DNA oligos. Therefore, we designed fluorescently-labelled DNA oligos complementary to the region highlighted in red colour in Figures 2.1.2A and B for JEV and ZIKV, respectively. We incubated 5′ TR of JEV (or ZIKV) with DDX3X$_{132–607}$ (or bovine serum albumin (BSA) as a negative control), ATP and complementary oligos, followed by measurements of MST traces. Our MST experiments suggest that in the presence of DDX3X$_{132–607}$, the oligos migrated differently than in the presence of BSA. This indicates that DDX3X$_{132–607}$ is able to unwind the double-stranded region, allowing the oligo to bind. Figure 2.1.4A and B present the unwinding of 5′ TRs of JEV and ZIKV with a signal to noise ratio of 14.8 ± 4.82 and 20.0 ± 5.06, respectively. Note that the signal to noise ratio of 12 or higher indicates the excellent quality of the assay [73]. To achieve the effect of a null mutant DDX3X, which can involve mutating the "DEAD"

region in the ATP-binding domain [74], we compared the ability of $DDX3X_{132–607}$ to unwind ncRNA in the presence and absence of ATP. Figure 2.1.4C shows the change in fluorescent migration as a result of ATP. Adding ATP caused a significant change in the migration of the DNA oligos, indicating that the unwinding activity increased in the presence of ATP.

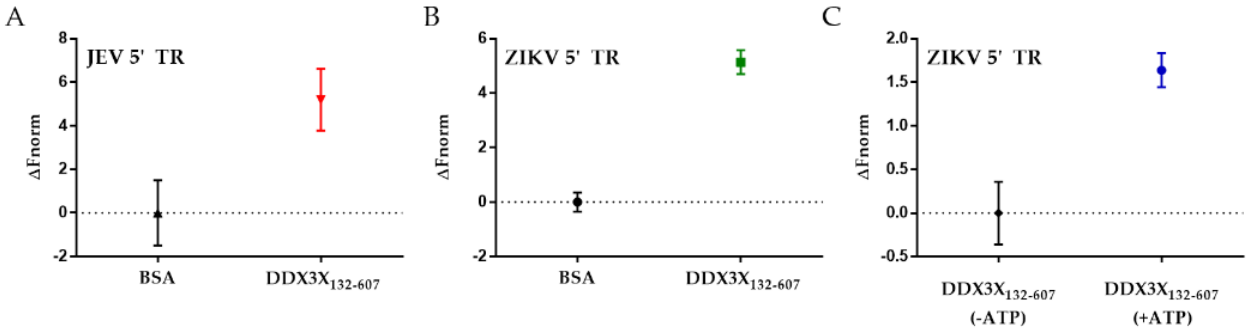

Figure 2.1.4. Helicase assays conducted using microscale thermophoresis (MST). (A) Comparing the change of fluorescent migration of a complementary DNA oligo in the presence of 5′ TR of JEV with ATP and either bovine serum albumin (BSA) or $DDX3X_{132–607}$. The average signal to noise ratio is 14.8 ± 4.82 (n = 3). (B) Comparing the fluorescent migration of a complementary DNA oligo in the presence of ZIKV 5′ TR with ATP and either BSA or $DDX3X_{132–607}$. The average signal to noise is 20.0 ± 5.06 (n = 3). (C) Investigating the role of ATP in $DDX3X_{132–607}$ helicase activity. The average signal to noise ratio is 5.5 ± 0.59 (n = 3), suggesting that ATP is required to unwind RNA.

2.2 Discussion

The purification of $DDX3X_{132–607}$ (55.3 kDa) through SEC resulted in the protein eluting at ~14.5 mL (Figure 2.1.1B), which is consistent with our previous purification of a similar molecular weight human helicase, $DDX17_{135–555}$ (48.5 kDa) [75]. As both helicases are highly similar and belong to the same family of proteins, we are confident that the peak we observe for $DDX3X_{132–607}$ is consistent with a homogenous, monodispersed preparation. Further quality control was performed through SDS-PAGE, which confirms that the peak SEC fractions contain a singular monodispersed species at the correct molecular weight, and are devoid of any degradation (Figure 2.1.1C). The Sfold predicted secondary structures reveal that each RNA adopts a high degree of double-stranded regions (Figure 2.1.2A and B), which is consistent with previous reports of highly structured flaviviral terminal regions [70].

RNA purification was performed immediately after in vitro transcription reaction using SEC. The 5′ TRs of JEV (159 nts) and Zika (163 nts) have sequence molecular weights of 51.5 and 52.3 kDa, respectively. However, they elute at distinctly different positions during SEC purification (Figure 2.1.1C). We believe that the differences in their structures lead to their elution at different positions. For example, based on its predicted structure, it appears that the 5′ TR of JEV could adopt a more compact structure compared to the 5′ TR of ZIKV (Figure 2.1.2A,B). The relatively extended conformation of 5′ TR of ZIKV will have a larger hydrodynamic radius compared to that of JEV, which will cause it to elute earlier in SEC. These results lead us to believe that both RNAs are folded correctly, whereas if the RNA were denatured, we would expect the elution peak to be virtually identical for both RNAs. The MST studies demonstrate that the JEV 5′ TR interacts with high affinity with DDX3X, compared to the ZIKV 5′ TR. As both ncRNAs are of same size but have different conformations, as suggested by SEC elution profiles (Figure 2.1.2C), it could be speculated that DDX3X has high affinity for compact conformation, compared to an extended one. However, the precise mechanisms that determine the specificity and the biological relevance of DDX3X-ZIKV interactions require additional work.

DEAD-box helicase DDX3X has been implicated in many viral systems as a key regulator of viral replication [50,67,68]. However, we lack insights into the affinity of DDX3X for any viral RNA. Moreover, whether DDX3X unwinds viral RNA is also unclear. Therefore, we utilized MST that has emerged as one of the ideal techniques to study biomolecular interactions [76,77]. By assessing the change in fluorescent migration under the influence of an infra-red laser, we are able to quantify the binding affinity between $DDX17_{135–555}$ and 5′ TRs. To our knowledge, this work provides the first evidence of DDX3X directly interacting with in vitro transcribed, natively purified viral terminal regions, as well as the binding affinity of DDX3X with viral RNAs. Figure 2.1.3B and 2.1.3C also highlight how two different viral RNA TRs can have different affinities, despite being highly conserved sequences [70]. The 5′ TR of JEV has over four-times stronger affinity for $DDX3X_{132–607}$ compared to the 5′ TR of ZIKV. Furthermore, DDX3X was identified as an interacting partner for the 5′ TR of JEV in vivo previously [50]. In this study, we also discovered that similar to 5′ TR of JEV, DDX3X also interacts with 5′ TR of ZIKV, albeit with lower affinity. The essential role of DDX3X in the JEV life cycle has already been established [50], but further molecular

virology studies are required to investigate if DDX3X has an impact on ZIKV replication. Figure 2.1.4 suggests that both RNAs can be unwound by DDX3X, potentially indicating that DDX3X may still have a significant role to play, despite the affinity difference, in ZIKV replication. We performed an experiment (presented in Figure 2.1.4C) to simulate a knockout mutant of DDX3X, which lacks the ATP hydrolysis activity [74]. We observed that the amount of fluorescent migration appears to be reduced in the absence of ATP (Figure 2.1.4C), which can be attributed to the fact that $DDX3X_{132–607}$ can unwind RNA but requires ATP for efficient processing of dsRNAs [78].

Previous studies for DDX5, a DDX3X homolog, have suggested that DDX5 interacts with RNA with high affinity in the nanomolar ranges. For example, fluorescence anisotropy experiments have suggested that DDX5 binds to short blunt-ended RNA duplexes with an affinity of ~230 nM [79]. A different group tested DDX5's ability to bind short G-quadruplexes using ELISA and obtained a Kd of 22 nM [80]. Our work was performed using truncated DDX3X (as all our attempts to purify the full-length DDX3X in high amounts were unsuccessful), which could impact the binding specificity and affinity for RNA compared to the full-length DDX3X. Note that a truncated construct, similar to $DDX3X_{132–607}$, was previously described as the minimally active construct [66,81]. Overall, additional work aimed at investigating the role of DDX3X in ZIKV replication could provide critical information towards potential therapeutics for these deadly viruses. In conclusion, our work provides the biochemical basis of the recognition of 5′ TRs of JEV and ZIKV by DDX3X.

2.3 Materials and Methods

2.3.1 Overexpression and Purification of $DDX3X_{132–607}$

The $DDX3X_{132–607}$ cDNA construct was cloned in pET28a, followed by its transformation in Lemo21(DE3) E. coli cells. The cells were allowed to grow in Luria-broth containing kanamycin (50 mg/mL) and chloramphenicol (100 mg/mL) at 37 °C. The next day, the culture was transferred to Terrific broth containing 5% glycerol and grown at 37 °C for 5 h. The temperature was then lowered to 20 °C for 16–18 h. Cells were harvested via centrifugation and resuspended in lysis buffer (50 mM Tris, 500mM NaCl, 10mM imidazole 3mM β-mercaptoethanol, 10 mg/mL lysozyme, 0.1% Tween-20, and 5% glycerol at

pH 8.0). Following 30 min of incubation on ice, the suspension was sonicated and centrifuged at 30,000× g for 45 min. The supernatant was filtered using a 0.45 µm filter for subsequent purification using chromatography methods.

Using the ÄKTA start protein purification system (Global Life Science Solutions USA LLC, Marlborough, MA, USA) equipped with the HisTrap™ High-Performance column, we purified $DDX3X_{132–607}$ via its hexa-histidine tag. Next, we used the ÄKTA pure purification system (Global Life Science Solutions USA LLC, Marlborough, MA, USA) with a Superdex® 200 10/300 GL increase column to further purify affinity-purified protein (in 50 mM Tris, 150 mM NaCl and 3% glycerol at pH 8.0). Peak fractions representing homogenous $DDX3X_{132–607}$ were collected and concentrated using Amicon® Ultra-15 Centrifugal Filter Units (30,000 kDa molecular-wight cut-off) (Millipore Canada Ltd, Etobicoke, ON, Canada). Aliquots were stored at −80 °C. SDS-PAGE (10%) was performed by taking 10 µL of SEC-purified sample and mixed it with 2 µL SDS-loading dye and heated to 95 °C for 5 min. Following heating, samples were loaded into a 1.0 cm well PAGE casting plate (Bio-Rad Laboratories, Mississauga, ON, Canada) and ran for 1 h at 200V in 1× SDS running buffer. A molecular weight ladder was run alongside the purified sample (unstained protein molecular weight marker 116 kDa to 14.4 kDa, Bio Basic Inc., Markham, ON, Canada). Subsequently, the gel was stained with Coomassie brilliant blue (Bio Basic Inc., Markham, ON, Canada) for visualization.

2.3.2 Preparation of Non-Coding RNAs

cDNA sequences were prepared under the control of T7 RNA polymerase, with two additional G nucleotides on the 5′ end with an XbaI restriction enzyme cut site (T^CTAGA) at the 3′ end. Then, 5′ TRs of JEV and Zika construct(s) were designed based on the Genebank sequence of KT957419.1 and KU509998.3, respectively. Underlined regions represent portions to which our fluorescent oligos were designed complementary to, described in a later section. Both RNA constructs used in the experiments are listed as follows:

1. JEV 5′ TR 1-156 (51.5 kDa, 159 nts)

5′GGAGAAGUUUUAUCGUGUGAACUUCUUGGCUUAGUAUCGUUGAGAAGAAUCGAGAGAUUAGUGCAGUUUAAA
CAGUUUUUUAGAACGGAAGAACAACCAUGACUAAAAAACCAGGAGGGCCCGGAAAAAACCGGGCCAUCAAUAUGC
UGAAACGCGGAU3′

2. Zika 5′ TR 1-163 (52.3 kDa, 163 nts)

5′AGUUGUUACUGUUGCUGACUCAGACUGCGACAGUUCGAGUUUGAAGCGAAAGCUAGCAACAGUAUCAACAGGU
UUUAUUUGGAUUUGGAAACGAGAGUUUCUGGUCAUGAAAAACCCAAAAAAGAAAUCCGGAGGAUUCCGGAUUGU
CAAUAUGCUAAAACG3′

Each RNA was prepared through an in vitro transcription reaction using T7 RNA polymerase (purified in-house) followed by size-exclusion chromatography purification in 1× RNA buffer (10 mM Tris pH 7.5, 100 mM NaCl, and 5 mM MgCl2) using a Superdex 200 Increase GL 10/300 (Cytiva) via an ÄKTA pure FPLC (Global Life Science Solutions USA LLC, Marlborough, MA). SEC peak fractions were analyzed via urea-polyacrylamide gel electrophoresis (Urea-PAGE). Then, we mixed 10 µL of each fraction with 2 µL of denaturing RNA loading dye and loaded into a 1.0 cm well PAGE casting plate (Bio-Rad Laboratories, Mississauga, ON, Canada). Urea-PAGE (7.2%) was run at room temperature, 300V, for 25 min in 0.5× TBE (Tris-Borate-EDTA) buffer, followed by staining with Sybr safe (Thermofisher Scientific, Saint-Laurant, QC, Canada) and visualization. Fractions containing a single band were deemed acceptable and used in subsequent experiments.

2.3.3 Fluorescent Labeling of Flaviviral RNA TRs

The 5′ TRs were incubated on ice for 30 min in 0.1 M sodium acetate (pH 5.3) along with 2 mM final concentration potassium periodate. The reaction was quenched through the addition of 10 mM final concentration ethylene glycol followed by incubation on ice for 10 min. Following incubation, we performed two ethanol precipitations and resuspended the RNA in 0.1 M NaOAc and 10 mM fluorescein-5-thiosemicarbazide (FITC) and incubated the mixture in the dark and on ice for 16 h. Following fluorescent

dye incubation, the mixture was phenol extracted (1 vol phenol:1 vol mixture) 5 times until the phenol layer was consistently colourless, indicating all free dye had been removed from the mixture. Finally, the resulting labelled RNA was ethanol precipitated twice and resuspended in RNA buffer.

2.3.4 RNA–Protein Interaction Studies Using Microscale Thermophoresis

A 2-fold serial dilution was performed on $DDX3X_{132–607}$ whereas the highest concentration was 19 µM. Next, a constant amount of fluorescent JEV or Zika 5′ TR was mixed into each serial dilution of $DDX3X_{132–607}$, resulting in a final concentration of 20 nM of RNA. Sample mixtures were incubated at room temperature for 10 min and then placed into Nanotemper Technologies Monolith® NT.115 instrument (Nanotemper Technologies, Munich, Germany) standard capillaries and loaded into the MST. Thermophoresis was measured at room temperature (25 °C) and performed using 20% excitation power (blue filter) for both RNAs and heated using medium MST IR laser power. Fluorescent migration used to determine Kd was measured from 4.0 to 5.0 s and normalized to initial fluorescence (−1.0 to 0 s). Three independent replicates were merged and analyzed using MO.Affinity Analysis software v2.1.3 and fit to the standard Kd fit model describing a molecular interaction with a 1:1 stoichiometry according to the law of mass action. The molarity of polyU RNA could not be determined since the fragment's lengths were variable. We used a final concentration of FITC-labeled polyU of 50 µg/mL in our negative control to achieve a similar magnitude of fluorescence.

2.3.5 Helicase Assay

We input our sequences into Sfold (v2.2) [82] using standard conditions with no maximum distance between paired bases and no additional constraint information. The theoretical secondary structure was used to identify a portion of each RNA molecule that was highly double-stranded. DNA oligos with complementary sequences to the double-stranded region(s) of our RNA(s) were synthesized with a 5′ conjugated FITC fluorophore (Alpha DNA). The region of each RNA molecule to which the oligos hybridize is underlined and described above. The sequences for ZIKV 5′ TR and JEV 5′ TR oligo(s) are: 5′FITC/AACTGTCGCAGTCTGAGTCAGCAACAGTAACAAC and 5′FITC/TTTCCGGGCCCTCCTGGTTTTTTAGTCATGGTTGT, respectively.

If the RNA molecule were unwound by $DDX3X_{132–607}$, it would create an opportunity for the oligos to hybridize to the 5′ TR RNA. The reaction mixture contains 20 nM of FITC-DNA oligos, 1 μM of the RNA, and 4.25 mM of ATP. $DDX3X_{132–607}$ is added to a final concentration of 10 μM. We used BSA at the same concentration as a control for DDX3X. The ATP dependence assay involved comparing 10 μM $DDX3X_{132–607}$ with 20 nM of FITC-DNA oligos and 1 μM of the RNA, but one set of capillaries contained 4.25 mM of ATP and another set did not. An experiment consists of 3 sets of 4 capillaries for each sample, which can then be compared to detect a change in fluorescent migration because of a binding event. Our data represent the normalized magnitude of fluorescent migration differences between two sets of assay conditions. Data were processed using MO.Affinity software, which assesses the signal to noise ratio between a run with and without the protein. Signal to noise is a measure of the response amplitude that is divided by the noise of the environment [83]. If the signal to noise ratio rises above 5, the assay indicates that a binding event has occurred, and the ratio >12 suggests that the assay is considered as desirable [83,84].

2.4 References

1. Chambers, T.J.; Monath, T.P. *The Flaviviruses: Detection*, *Diagnosis and Vaccine Development*; Elsevier: Amsterdam, The Netherlands, 2003.
2. Solomon, T.; Kneen, R.; Dung, N.M.; Khanh, V.C.; Thuy, T.T.N.; Day, N.P.; Nisalak, A.; Vaughn, D.W.; White, N.J. Poliomyelitis-like illness due to Japanese encephalitis virus. *Lancet* **1998**, *351*, 1094–1097.
3. Brasil, P.; Sequeira, P.C.; Freitas, A.D.A.; Zogbi, H.E.; Calvet, G.A.; de Souza, R.V.; Siqueira, A.M.; de Mendonca, M.C.L.; Nogueira, R.M.R.; de Filippis, A.M.B. Guillain-Barré syndrome associated with Zika virus infection. *Lancet* **2016**, *387*, 1482.
4. Pierson, T.C.; Diamond, M.S. The continued threat of emerging flaviviruses. *Nat. Microbiol.* **2020**, *5*, 1–17.
5. Fischer, C.; de Oliveira-Filho, E.F.; Drexler, J.F. Viral emergence and immune interplay in flavivirus vaccines. *Lancet Infect. Dis.* **2020**, *20*, 15–17.
6. Fernandez-Sanles, A.; Rios-Marco, P.; Romero-Lopez, C.; Berzal-Herranz, A. Functional Information Stored in the Conserved Structural RNA Domains of Flavivirus Genomes. *Front. Microbiol.* **2017**, *8*, 546.
7. World Health Organization. *Epidemic Focus—Flavivirus Epidemics*; Geneva, Switzerland, 2020.
8. Huang, Y.-J. S.; Higgs, S.; Horne, K.M.; Vanlandingham, D.L. Flavivirus-mosquito interactions. *Viruses* **2014**, *6*, 4703–4730.
9. Benedict, M.Q.; Levine, R.S.; Hawley, W.A.; Lounibos, L.P. Spread of the tiger: Global risk of invasion by the mosquito Aedes albopictus. *Vector Borne Zoonotic Dis.* **2007**, *7*, 76–85.
10. Reinhold, J.M.; Lazzari, C.R.; Lahondère, C. Effects of the environmental temperature on Aedes aegypti and Aedes albopictus mosquitoes: A review. *Insects* **2018**, *9*, 158.
11. Baig, S.; Fox, K.K.; Jee, Y.; O'Connor, P.; Hombach, J.; Wang, S.A.; Hyde, T.; Fischer, M.; Hills, S.L. Japanese encephalitis surveillance and immunization—Asia and the Western Pacific, 2012. *MMWR Morb. Mortal. Wkly. Rep.* **2013**, *62*, 658.
12. Campbell, G.L.; Hills, S.L.; Fischer, M.; Jacobson, J.A.; Hoke, C.H.; Hombach, J.M.; Marfin, A.A.; Solomon, T.; Tsai, T.F.; Tsu, V.D. Estimated global incidence of Japanese encephalitis: A systematic review. *Bull. World Health Organ.* **2011**, *89*, 766–774.
13. Dubischar, K.L.; Kadlecek, V.; Sablan, B.; Borja-Tabora, C.F.; Gatchalian, S.; Eder-Lingelbach, S.; Kiermayr, S.; Spruth, M.; Westritschnig, K. Immunogenicity of the inactivated Japanese encephalitis virus vaccine IXIARO in children from a Japanese encephalitis virus-endemic region. *Pediatric Infect. Dis. J.* **2017**, *36*, 898–904.
14. Van Gessel, Y.; Klade, C.S.; Putnak, R.; Formica, A.; Krasaesub, S.; Spruth, M.; Cena, B.; Tungtaeng, A.; Gettayacamin, M.; Dewasthaly, S.; Correlation of protection against Japanese encephalitis virus and JE vaccine (IXIARO®) induced neutralizing antibody titers. *Vaccine* **2011**, *29*, 5925–5931.
15. Samarasekera, U.; Triunfol, M. Concern over Zika virus grips the world. *Lancet* **2016**, *387*, 521–524.
16. World Health Organization. *Zika Situation Report*: World Health Organization is based in Geneva, Switzerland, 2016.
17. Carteaux, G.; Maquart, M.; Bedet, A.; Contou, D.; Brugières, P.; Fourati, S.; Cleret de Langavant, L.; de Broucker, T.; Brun-Buisson, C.; Leparc-Goffart, I. Zika virus associated with meningoencephalitis. *N. Engl. J. Med.* **2016**, *374*, 1595–1596.
18. Cauchemez, S.; Besnard, M.; Bompard, P.; Dub, T.; Guillemette-Artur, P.; Eyrolle-Guignot, D.; Salje, H.; Van Kerkhove, M.D.; Abadie, V.; Garel, C. Association between Zika virus and microcephaly in French Polynesia, 2013–2015: A retrospective study. *Lancet* **2016**, *387*, 2125–2132.
19. Gladwyn-Ng, I.; Cordón-Barris, L.; Alfano, C.; Creppe, C.; Couderc, T.; Morelli, G.; Thelen, N.; America, M.; Bessières, B.; Encha-Razavi, F. Stress-induced unfolded protein response contributes to Zika virus–associated microcephaly. *Nat. Neurosci.* **2018**, *21*, 63–71.
20. Mécharles, S.; Herrmann, C.; Poullain, P.; Tran, T.-H.; Deschamps, N.; Mathon, G.; Landais, A.; Breurec, S.; Lannuzel, A. Acute myelitis due to Zika virus infection. *Lancet* **2016**, *387*, 1481.
21. Nascimento, O.J.; da Silva, I.R. Guillain–Barré syndrome and Zika virus outbreaks. *Curr. Opin. Neurol.* **2017**, *30*, 500–507.
22. Oliveira Melo, A.; Malinger, G.; Ximenes, R.; Szejnfeld, P.; Alves Sampaio, S.; Bispo de Filippis, A. Zika virus intrauterine infection causes fetal brain abnormality and microcephaly: Tip of the iceberg? *Ultrasound Obstet. Gynecol.* **2016**, *47*, 6–7.
23. Schwartzmann, P.V.; Ramalho, L.N.; Neder, L.; Vilar, F.C.; Ayub-Ferreira, S.M.; Romeiro, M.F.; Takayanagui, O.M.; Dos Santos, A.C.; Schmidt, A.; Figueiredo, L.T. Zika Virus Meningoencephalitis in

an Immunocompromised Patient. *Mayo Clin. Proc.* **2017**, *92*, 460–466, doi:10.1016/j.mayocp.2016.12.019.
24. Devhare, P.; Meyer, K.; Steele, R.; Ray, R.B.; Ray, R. Zika virus infection dysregulates human neural stem cell growth and inhibits differentiation into neuroprogenitor cells. *Cell Death Dis.* **2017**, 8, e3106–e3106.
25. Broutet, N.; Krauer, F.; Riesen, M.; Khalakdina, A.; Almiron, M.; Aldighieri, S.; Espinal, M.; Low, N.; Dye, C. Zika virus as a cause of neurologic disorders. *New Engl. J. Med.* **2016**, *374*, 1506–1509, doi:10.1056/nejmp1602708.
26. Mlakar, J.; Korva, M.; Tul, N.; Popović, M.; Poljšak-Prijatelj, M.; Mraz, J.; Kolenc, M.; Resman Rus, K.; Vesnaver Vipotnik, T.; Fabjan Vodušek, V. Zika virus associated with microcephaly. *New Engl. J. Med.* **2016**, *374*, 951–958, doi:10.1056/nejmoa1600651.
27. Tang, H.; Hammack, C.; Ogden, S.C.; Wen, Z.; Qian, X.; Li, Y.; Yao, B.; Shin, J.; Zhang, F.; Lee, E.M. Zika virus infects human cortical neural progenitors and attenuates their growth. *Cell Stem Cell* **2016**, *18*, 587–590.
28. Li, C.; Xu, D.; Ye, Q.; Hong, S.; Jiang, Y.; Liu, X.; Zhang, N.; Shi, L.; Qin, C.-F.; Xu, Z. Zika virus disrupts neural progenitor development and leads to microcephaly in mice. *Cell Stem Cell* **2016**, *19*, 120–126.
29. Li, H.; Saucedo-Cuevas, L.; Shresta, S.; Gleeson, J.G. The neurobiology of Zika virus. *Neuron* **2016**, *92*, 949–958.
30. Russo, F.B.; Jungmann, P.; Beltrão-Braga, P.C.B. Zika infection and the development of neurological defects. *Cellular Microbial.* **2017**, *19*, e12744.
31. Barzon, L.; Pacenti, M.; Franchin, E.; Lavezzo, E.; Trevisan, M.; Sgarabotto, D.; Palu, G. Infection dynamics in a traveller with persistent shedding of Zika virus RNA in semen for six months after returning from Haiti to Italy, January 2016. *Eurosurveillance* **2016**, *21*, doi:10.2807/1560-7917.es.2016.21.32.30316.
32. Foy, B.D.; Kobylinski, K.C.; Chilson Foy, J.L.; Blitvich, B.J.; Travassos da Rosa, A.; Haddow, A.D.; Lanciotti, R.S.; Tesh, R.B. Probable non-vector-borne transmission of Zika virus, Colorado, USA. *Emerg. Infect. Dis.* **2011**, *17*, 880–882.
33. Paul, L.M.; Carlin, E.R.; Jenkins, M.M.; Tan, A.L.; Barcellona, C.M.; Nicholson, C.O.; Michael, S.F.; Isern, S. Dengue virus antibodies enhance Zika virus infection. *Clin. Transl. Immunol.* **2016**, *5*, e117.
34. Myers, T.R.; McCarthy, N.L.; Panagiotakopoulos, L.; Omer, S.B. Estimation of the Incidence of Guillain-Barre Syndrome During Pregnancy in the United States. *Open Forum Infect. Dis.* **2019**, *6*, ofz071.
35. Stettler, K.; Beltramello, M.; Espinosa, D.A.; Graham, V.; Cassotta, A.; Bianchi, S.; Vanzetta, F.; Minola, A.; Jaconi, S.; Mele, F.; et al. Specificity, cross-reactivity, and function of antibodies elicited by Zika virus infection. *Science* **2016**, *353*, 823–826.
36. Cleaves, G.R.; Dubin, D.T. Methylation status of intracellular dengue type 2 40 S RNA. *Virology* **1979**, *96*, 159–165.
37. Brinton, M.A.; Fernandez, A.V.; Dispoto, J.H. The 3′-nucleotides of flavivirus genomic RNA form a conserved secondary structure. *Virology* **1986**, *153*, 113–121.
38. Wengler, G.; Wengler, G.; Gross, H.J. Studies on Virus-Specific Nucleic-Acids Synthesized in Vertebrate and Mosquito Cells Infected with Flaviviruses. *Virology* **1978**, *89*, 423–437.
39. Gritsun, T.S.; Gould, E.A. Origin and evolution of 3′UTR of flaviviruses: Long direct repeats as a basis for the formation of secondary structures and their significance for virus transmission. *Adv. Virus Res.* **2007**, *69*, 203–248.
40. Thurner, C.; Witwer, C.; Hofacker, I.L.; Stadler, P.F. Conserved RNA secondary structures in Flaviviridae genomes. *J. Gen. Virol.* **2004**, *85* (Pt 5), 1113–1124.
41. Hahn, C.S.; Hahn, Y.S.; Rice, C.M.; Lee, E.; Dalgarno, L.; Strauss, E.G.; Strauss, J.H. Conserved elements in the 3′ untranslated region of flavivirus RNAs and potential cyclization sequences. *J. Mol. Biol.* **1987**, *198*, 33–41, doi:10.1016/0022-2836(87)90455-4.
42. Alvarez, D.E.; Lodeiro, M.F.; Luduena, S.J.; Pietrasanta, L.I.; Gamarnik, A.V. Long-range RNA-RNA interactions circularize the dengue virus genome. *J. Virol.* **2005**, *79*, 6631–6643.
43. Li, X.D.; Deng, C.L.; Yuan, Z.M.; Ye, H.Q.; Zhang, B. Different Degrees of 5′-to-3′ DAR Interactions Modulate Zika Virus Genome Cyclization and Host-Specific Replication. *J. Virol.* **2020**, *94*, doi:10.1128/JVI.01602-19

44. de Borba, L.; Villordo, S.M.; Iglesias, N.G.; Filomatori, C.V.; Gebhard, L.G.; Gamarnik, A.V. Overlapping local and long-range RNA-RNA interactions modulate dengue virus genome cyclization and replication. *J. Virol.* **2015**, *89*, 3430–3437.
45. Khromykh, A.A.; Meka, H.; Guyatt, K.J.; Westaway, E.G. Essential role of cyclization sequences in flavivirus RNA replication. *J. Virol.* **2001**, *75*, 6719–6728.
46. Friebe, P.; Shi, P.Y.; Harris, E. The 5′ and 3′ downstream AUG region elements are required for mosquito-borne flavivirus RNA replication. *J. Virol.* **2011**, *85*, 1900–1905.
47. Chambers, T.J.; Hahn, C.S.; Galler, R.; Rice, C.M. Flavivirus genome organization, expression, and replication. *Annu. Rev. Microbiol.* **1990**, *44*, 649–688.
48. Tingting, P.; Caiyun, F.; Zhigang, Y.; Pengyuan, Y.; Zhenghong, Y. Subproteomic analysis of the cellular proteins associated with the 3′ untranslated region of the hepatitis C virus genome in human liver cells. *Biochem. Biophys. Res. Commun.* **2006**, *347*, 683–691, doi:10.1016/j.bbrc.2006.06.144.
49. Harris, D.; Zhang, Z.; Chaubey, B.; Pandey, V.N. Identification of cellular factors associated with the 3′-nontranslated region of the hepatitis C virus genome. *Mol. Cell. Proteom.* **2006**, *5*, 1006–1018, doi:10.1074/mcp.m500429-mcp200.
50. Li, C.; Ge, L.L.; Li, P.P.; Wang, Y.; Dai, J.J.; Sun, M.X.; Huang, L.; Shen, Z.Q.; Hu, X.C.; Ishag, H.; et al. Cellular DDX3 regulates Japanese encephalitis virus replication by interacting with viral un-translated regions. *Virology* **2014**, *449*, 70–81.
51. Li, C.; Ge, L.L.; Li, P.P.; Wang, Y.; Sun, M.X.; Huang, L.; Ishag, H.; Di, D.D.; Shen, Z.Q.; Fan, W.X.; et al. The DEAD-box RNA helicase DDX5 acts as a positive regulator of Japanese encephalitis virus replication by binding to viral 3′ UTR. *Antivir. Res.* **2013**, *100*, 487–499.
52. Ward, A.M.; Bidet, K.; Yinglin, A.; Ler, S.G.; Hogue, K.; Blackstock, W.; Gunaratne, J.; Garcia-Blanco, M.A. Quantitative mass spectrometry of DENV-2 RNA-interacting proteins reveals that the DEAD-box RNA helicase DDX6 binds the DB1 and DB2 3′ UTR structures. *RNA Biol.* **2011**, *8*, 1173–1186.
53. Dong, Y.; Yang, J.; Ye, W.; Wang, Y.; Miao, Y.; Ding, T.; Xiang, C.; Lei, Y.; Xu, Z. LSm1 binds to the Dengue virus RNA 3′ UTR and is a positive regulator of Dengue virus replication. *Int. J. Mol. Med.* **2015**, *35*, 1683–1689.
54. Gomila, R.C.; Martin, G.W.; Gehrke, L. NF90 binds the dengue virus RNA 3′ terminus and is a positive regulator of dengue virus replication. *PLoS ONE* **2011**, *6*, e16687.
55. Ward, A.M.; Calvert, M.E.; Read, L.R.; Kang, S.; Levitt, B.E.; Dimopoulos, G.; Bradrick, S.S.; Gunaratne, J.; Garcia-Blanco, M.A. The Golgi associated ERI3 is a Flavivirus host factor. *Sci. Rep.* **2016**, *6*, 34379.
56. Lei, Y.; Huang, Y.; Zhang, H.; Yu, L.; Zhang, M.; Dayton, A. Functional interaction between cellular p100 and the dengue virus 3′ UTR. *J. Gen. Virol.* **2011**, *92* (Pt 4), 796–806.
57. Yu, L.; Nomaguchi, M.; Padmanabhan, R.; Markoff, L. Specific requirements for elements of the 5′ and 3′ terminal regions in flavivirus RNA synthesis and viral replication. *Virology* **2008**, *374*, 170–185.
58. Meier-Stephenson, V.; Mrozowich, T.; Pham, M.; Patel, T.R. DEAD-box helicases: The Yin and Yang roles in viral infections. *Biotechnol. Genet. Eng. Rev.* **2018**, *34*, 3–32.
59. Ng, W.C.; Soto-Acosta, R.; Bradrick, S.S.; Garcia-Blanco, M.A.; Ooi, E.E. The 5′ and 3′ Untranslated Regions of the Flaviviral Genome. *Viruses* **2017**, *9*, 137.
60. Leitao, A.L.; Costa, M.C.; Enguita, F.J. Unzippers, Resolvers and Sensors: A Structural and Functional Biochemistry Tale of RNA Helicases. *Int. J. Mol. Sci.* **2015**, *16*, 2269–2293, doi:10.3390/ijms16022269.
61. Linder, P.; Jankowsky, E. From unwinding to clamping—The DEAD box RNA helicase family. *Nat. Rev. Mol. Cell Biol.* **2011**, *12*, 505–516, doi:10.1038/nrm3154.
62. Pyle, A.M. Translocation and unwinding mechanisms of RNA and DNA helicases. *Annu. Rev. Biophys.* **2008**, *37*, 317–336, doi:10.1146/annurev.biophys.37.032807.125908.
63. Jankowsky, E. RNA helicases at work: Binding and rearranging. *Trends Biochem. Sci.* **2011**, *36*, 19–29.
64. Chao, C.H.; Chen, C.M.; Cheng, P.L.; Shih, J.W.; Tsou, A.P.; Lee, Y.H. DDX3, a DEAD box RNA helicase with tumor growth-suppressive property and transcriptional regulation activity of the p21waf1/cip1 promoter, is a candidate tumor suppressor. *Cancer Res.* **2006**, *66*, 6579–6588.
65. Ariumi, Y.; Kuroki, M.; Abe, K.; Dansako, H.; Ikeda, M.; Wakita, T.; Kato, N. DDX3 DEAD-box RNA helicase is required for hepatitis C virus RNA replication. *J. Virol.* **2007**, *81*, 13922–13926.
66. Song, H.; Ji, X. The mechanism of RNA duplex recognition and unwinding by DEAD-box helicase DDX3X. *Nat. Commun.* **2019**, *10*, 1–8.

67. Li, G.; Feng, T.; Pan, W.; Shi, X.; Dai, J. DEAD-box RNA helicase DDX3X inhibits DENV replication via regulating type one interferon pathway. *Biochem. Biophys. Res. Commun.* **2015**, *456*, 327–332, doi:10.1016/j.bbrc.2014.11.080.
68. Brai, A.; Martelli, F.; Riva, V.; Garbelli, A.; Fazi, R.; Zamperini, C.; Pollutri, A.; Falsitta, L.; Ronzini, S.; Maccari, L. DDX3X helicase inhibitors as a new strategy to fight the West Nile virus infection. *J. Med. Chem.* **2019**, *62*, 2333–2347, doi:10.1021/acs.jmedchem.8b01403.
69. Brinton, M.A. Replication cycle and molecular biology of the West Nile virus. *Viruses* **2013**, *6*, 13–53.
70. Brinton, M.A.; Basu, M. Functions of the 3′ and 5′ genome RNA regions of members of the genus Flavivirus. *Virus Res.* **2015**, *206*, 108–119.
71. Reuten, R.; Patel, T.R.; McDougall, M.; Rama, N.; Nikodemus, D.; Gibert, B.; Delcros, J.-G.; Prein, C.; Meier, M.; Metzger, S. Structural decoding of netrin-4 reveals a regulatory function towards mature basement membranes. *Nat.Commun.* **2016**, *7*, 1–17.
72. Ferens, F.G.; Patel, T.R.; Oriss, G.; Court, D.A.; Stetefeld, J. A Cholesterol Analog Induces an Oligomeric Reorganization of VDAC. *Biophys. J.* **2019**, *116*, 847–859.
73. Wienken, C.J.; Baaske, P.; Rothbauer, U.; Braun, D.; Duhr, S. Protein-binding assays in biological liquids using microscale thermophoresis. *Nat. Commun.* **2010**, *1*, 100.
74. Garbelli, A.; Beermann, S.; Di Cicco, G.; Dietrich, U.; Maga, G. A motif unique to the human DEAD-box protein DDX3 is important for nucleic acid binding, ATP hydrolysis, RNA/DNA unwinding and HIV-1 replication. *PLoS ONE* **2011**, *6*, e19810.
75. Nelson, C.; Mrozowich, T.; Park, S.; D'souza, S.; Henrickson, A.; Vigar, J.; Wieden, H.-J.; Owens, R.; Demeler, B.; Patel, T.R. Human DDX17 unwinds Rift Valley Fever Virus Non-coding RNAs. *Int. J. Mol. Sci.* **2020**, *22*, 54, doi:10.3390/ijms22010054.
76. Jerabek-Willemsen, M.; Wienken, C.J.; Braun, D.; Baaske, P.; Duhr, S. Molecular interaction studies using microscale thermophoresis. *Assay Drug Dev. Technol.* **2011**, *9*, 342–353.
77. Mrozowich, T.; MeierStephenson, V.; Patel, T.R. Microscale thermophoresis: Warming up to a new biomolecular interaction technique. *Biochemist* **2019**, *41*, 8–12.
78. Liu, F.; Putnam, A.; Jankowsky, E. ATP hydrolysis is required for DEAD-box protein recycling but not for duplex unwinding. *Proc. Natl. Acad. Sci. USA* **2008**, *105*, 20209–20214.
79. Xing, Z.; Wang, S.; Tran, E.J. Characterization of the mammalian DEAD-box protein DDX5 reveals functional conservation with S. cerevisiae ortholog Dbp2 in transcriptional control and glucose metabolism. *RNA* **2017**, *23*, 1125–1138.
80. Wu, G.; Xing, Z.; Tran, E.J.; Yang, D. DDX5 helicase resolves G-quadruplex and is involved in MYC gene transcriptional activation. *Proc. Natl. Acad. Sci. USA* **2019**, *116*, 20453–20461.
81. Floor, S.N.; Condon, K.J.; Sharma, D.; Jankowsky, E.; Doudna, J.A. Autoinhibitory interdomain interactions and subfamily-specific extensions redefine the catalytic core of the human DEAD-box protein DDX3. *J. Biol. Chem.* **2016**, *291*, 2412–2421.
82. Ding, Y.; Chan, C.Y.; Lawrence, C.E. S fold web server for statistical folding and rational design of nucleic acids. *Nucleic Acids Res.* **2004**, *32* (Suppl. 2), W135–W141.
83. *User Manual for the Monolith NT.115*; NanoTemper Technologies: Munich, Germany 2018.
84. Seidel, S.A.; Dijkman, P.M.; Lea, W.A.; van den Bogaart, G.; Jerabek-Willemsen, M.; Lazic, A.; Joseph, J.S.; Srinivasan, P.; Baaske, P.; Simeonov, A.; et al. Microscale thermophoresis quantifies biomolecular interactions under previously challenging conditions. *Methods* **2013**, *59*, 301–315.

Chapter 3: Human DDX17 Unwinds Rift Valley Fever Virus Non-Coding RNAs[a]

3.0 Introduction

Rift Valley fever virus (RVFV) is part of the *Bunyaviridae* family and the genus *Phlebovirus*. The virus was first identified in the early 1930s during a large outbreak on a sheep farm in the Rift Valley of Kenya [1]. Since then, the virus transmission has been reported in several countries located within Sub-Saharan Africa and the Arabian Peninsula due to infected livestock trade. Transmission of this virus is through competent mosquito vector hosts, Aedes and Culex, to animals and humans. Infection is currently untreatable and primarily affects domesticated animals such as camels, goats, sheep, and cattle, but can also affect humans [2]. Infections in animals mainly occur through mosquito bites, and terminal human hosts can be infected by infected mosquitos and direct contact with infected ruminant blood and bodily fluids. Symptoms of RVFV infection in humans can include acute febrile illness followed by hemorrhagic fever, encephalitis, or ocular disease [2]. These mosquito vectors can also transmit a variety of flaviviral diseases such as Zika, yellow fever, and chikungunya. Additionally, its presence on every continent except for Antarctica makes this virus a severe threat to global health and food security [3]. There is currently an inactivated vaccine (MP-12) that has been shown to confer long-term immunity in humans with a single dose. This vaccine is also effective in animals; however, it is not currently commercially available [4].

According to the World Health Organization (WHO), RVFV infection is one of the top eight emerging diseases likely to cause significant epidemics that currently have no medical countermeasures [5]. RVFV is maintained in the environment via vertical transmission from the mosquito vector to offspring during high rainfall periods, which amplifies mosquito breeding [6]. Infectious outbreaks occur after long intervals of dormancy, between 5–15 years, but can cause detrimental economic losses due to livestock

---

[a] Reprinted with permission from Nelson, C., Mrozowich, T., and Patel, T. R. (2021). Human DDX17 Unwinds Rift Valley Fever Virus Non-Coding RNAs. *International Journal of Molecular Sciences*, *22*(1), 54.

infection, which causes mortality rates of 10–30% and >90% abortion rates. Moreover, these epizootic outbreaks have resulted in a total death toll of over 100,000 sheep, over half a million livestock abortions, and more than 2300 human deaths [1,7].

RVFV is an enveloped virus that contains a linear, tripartite, ssRNA ambisense genome [8]. The total tripartite genome size for RVFV is 10.4 kb and encompasses three different viral RNA components which are replicated in the host cell cytoplasm: L (large, 6.4 kb) and M (medium, 2.3 kb), which are both negative sense, and S (small, 1.7 kb) which is ambisense [9]. The L-segment encodes the RNA-dependent RNA polymerase, while the M-segment encodes two envelope glycoproteins, Gn and Gc, and two accessory proteins. The S-segment (S2) ambisense RNA encodes a positive-sense RNA template of the non-structural protein (NS) and a negative-sense RNA for the viral nucleoprotein (N) [10,11]. The S-segment contains two notable noncoding regions; the 5′ noncoding region (NCR), responsible for transcription and translation initiation of the NS segment, and the intergenic region (IGR), responsible for transcription termination on both the NSs and N mRNA [12]. These two regions have been demonstrated to form hairpin-like structures, which are recognized by host cellular machinery. The human protein, DDX17, which is a DEAD-box helicase, has been shown to interact with the 5′ noncoding S-segment (RVFV NCR) and the noncoding sequence between N and NSs (RVFV IGR) [11]. The knockdown of DDX17, but not its paralog DDX5, led to unrestricted viral replication of RVFV in U2OS cells [11].

DEAD-box helicases have been described as ATP-dependent chaperones that reconfigure RNA by disrupting secondary and tertiary RNA–RNA or RNA–protein interactions [13,14]. The DDX17 helicase has roles in transcription, splicing, mRNA decay, rRNA biogenesis, and miRNA processing as well as antiviral defense [15,16]. The target motifs on the viral RNA S-segment are two hairpin structures, which are unique to the *Bunyaviridae* family [10]. CLIP-seq data indicate that DDX17 interacts with both the IGR and 5′ NCR of the RVFV S-segment. We wanted to examine these interactions in vitro to determine if DDX17 is capable of functioning independently or whether it requires additional binding partners, as described previously [17]. Additionally, we would like to investigate the structural differences between the noncoding RNAs (ncRNAs) and how this could affect their interactions with DDX17.

Therefore, by utilizing multiple biophysical techniques, we have characterized the interaction between RVFV noncoding RNA (ncRNA) and $DDX17_{135–555}$ to determine that not only does $DDX17_{135–555}$ directly interact with RVFV ncRNA, it also unwinds the ncRNA in the presence of ATP. This work supports previous observations of direct anti-viral effects of DDX17 [11] while providing a new, easy approach to investigate the helicase activity of a protein.

3.1 Results

3.1.1 Purification of $DDX17_{135–555}$, RVFV S-segment IGR, and 5′ NCR

$DDX17_{135–555}$ was overexpressed in *Escherichia coli* (Lemo21) and purified using affinity and size exclusion chromatography (SEC), as detailed in the Materials and Methods section. Figure 3.1.1A shows the schematics of full-length DDX17 and the truncated $DDX17_{135–555}$ that was used in this study, as we were unable to express sufficient amounts of full-length DDX17. As presented in Figure 3.1.1B, the peak fractions (15 mL to 17 mL), devoid of any contamination or aggregation, were collected, followed by the purity check using SDS-PAGE. As presented in the inset to Figure 3.1.1B, the final preparation does not contain any degraded material, and it corresponds to the correct molecular weight of ~50 kDa. To further study the homogeneity of $DDX17_{135–555}$ in solution, the SEC-purified preparation that presented a single band in SDS-PAGE was used to perform an analytical ultracentrifugation sedimentation velocity experiment (SV-AUC). The SV-AUC results suggest that $DDX17_{135–555}$ is mainly homogenous with a sedimentation coefficient of 3.16 S (Figure 3.1.1C) and a diffusion coefficient of 5.22×10^{-7} cm^2/s (Table 1).

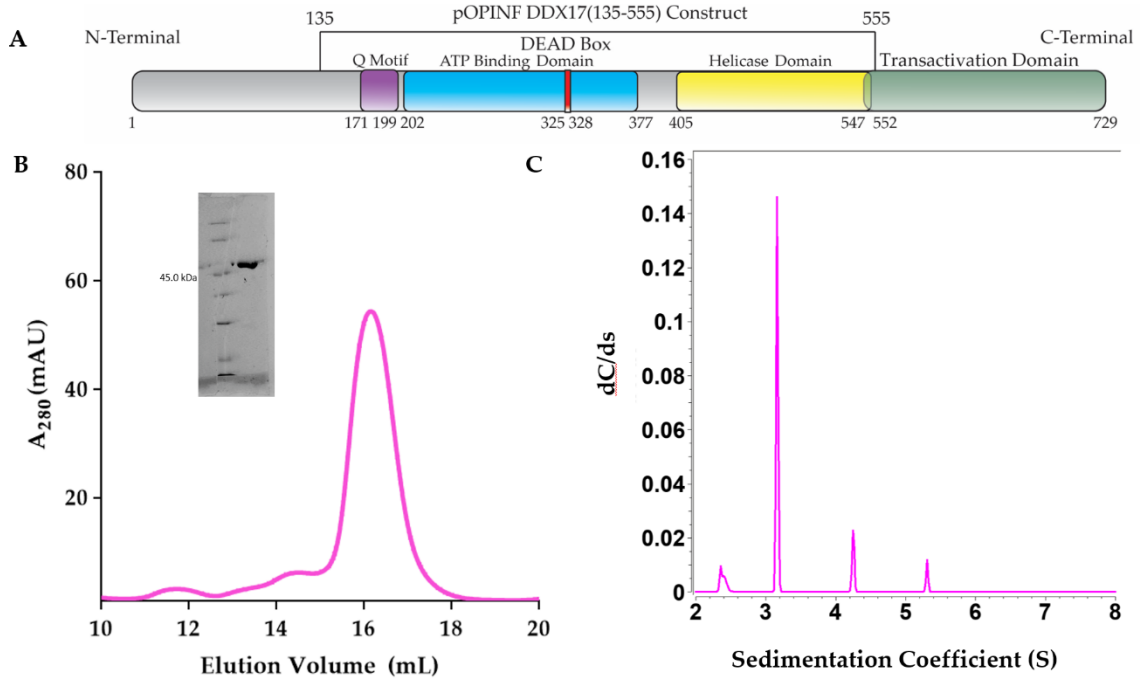

Figure 3.1.1. Purification of RNA Helicase DDX17 (**A**) Schematic representation of DDX17 highlighting individual domains. $DDX17_{135–555}$, which contains the Q motif, ATP binding domain, DEAD-box, and the helicase domain, was used in downstream studies. (**B**) The chromatogram from the size exclusion purification (Superdex 200 Increase gl 10/300) of $DDX17_{135–555}$, suggesting that $DDX17_{(135–555)}$ can be purified to ~68% homogeneity (~16 mL). The y-axis represents absorbance at 260 nm while the x-axis represents elution volume. We collected peak fractions from 15.5 to 16.5 mL for subsequent analysis. The inset to Figure 3.1.1B represents the SDS-PAGE analysis of $DDX17_{135–555}$ (48.45 kDa) following size exclusion chromatography. **C)** Sedimentation coefficient distribution of $DDX17_{135–555}$ obtained from analytical ultracentrifugation sedimentation velocity (SV-AUC) experiment. The peak at ~3.16S represents monodispersed $DDX17_{135–555}$. Sedimentation coefficient values are corrected to standard solvent conditions (20 °C in water).

The in vitro transcribed RVFV IGR and 5′ NCR RNAs were purified using SEC, similar to $DDX17_{135–555}$ (Figure 3.1.2A). The IGR eluted at approximately ~14 mL, while the 5′ NCR eluted at ~14.5 mL. Peak fractions were collected and analyzed by urea-PAGE, which displayed a single band (Figure 3.1.2A inset). Next, we utilized SV-AUC to determine the purity of SEC-purified RVFV ncRNA. Our SV-AUC analysis suggested that monomeric IGR and 5′ NCR have sedimentation coefficients of 4.07 S and 4.18 S, respectively. The SV-AUC analysis also yielded diffusion coefficients of 7.62×10^{-7} cm^2/s and 6.58×10^{-7} cm^2/s, respectively. Overall, both ncRNAs appear to be relatively pure (Figure 3.1.2B).

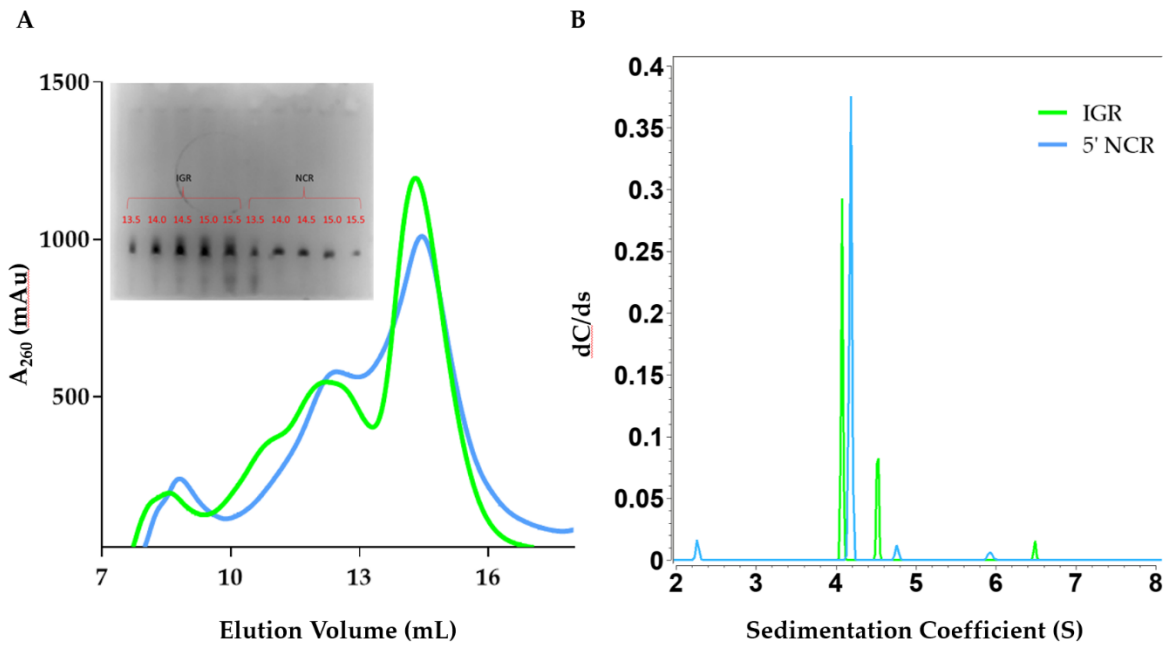

Figure 3.1.2. Purification and hydrodynamic characterization of in vitro transcribed Rift Valley fever virus RNA. (**A**) Size exclusion chromatogram of the elution profile of both Rift Valley fever virus (RVFV) 5′ intergenic region (IGR) and RVFV 5′ noncoding region (NCR). The y-axis represents absorbance at 260 nm while the x-axis represents elution volume. An inset to Figure 3.1.2A represents the urea-PAGE (7.5%) analysis of RVFV IGR and 5′ NCR after size exclusion chromatography. Each well represents 10 µL of a 500 µL elution fraction from size exclusion chromatography. The gel was run for 25 min, at 300 V in 0.5× TBE (Tris-Borate-EDTA) running buffer and was visualized using Sybr Safe dye. (**B**) Sedimentation coefficient distribution profiles for RVFV 5′ IGR (green) and RVFV 5′ NCR (blue) from SV-AUC. The primary SV peaks for each RNA are 4.07 S and 4.18 S for IGR and 5′ NCR, respectively, and represent the monomeric form. Sedimentation coefficient values were corrected to standard conditions (20 °C in water).

3.1.2 Solution Conformation of DDX17$_{135–555}$, RVFV S-Segment IGR, and 5′NCR

SAXS analysis allows for low-resolution structural determination of biomolecules in solution. The instrumentation provided at the B21 Beamline (Diamond Light Source, UK) allows for the employment of HPLC connected in-line to SAXS detection to maintain confidence in the monodispersity of samples, keeping them free of aggregates and degradation [18–20]. SEC-SAXS data for the merged datasets are presented in Figure 3.1.3A. The merged data were further processed using Guinier analysis (plot of (I(q)) vs. (q^2)) to detect the purity and for the determination of the R_g (average root mean squared radius from the center of mass for the biomolecule) from the low-q region [21]. Figure 3.1.3B represents the Guinier plots for IGR, 5′ NCR, and DDX17$_{135–555}$, whereas the linearity of the low-q region indicates that all three

biomolecules were monodisperse. R_g values of 36.42 ± 0.10, 50.44 ± 0.88, and 24.78 ± 0.36 for IGR, 5′ NCR, and $DDX17_{135–555}$, respectively, were obtained from Guinier analysis (see Table 1). After we confirmed monodispersity from Guinier analysis, we further processed the SAXS scattering data from Figure 3.1.3A to obtain dimensionless Kratky plots [19,22] which allowed for analysis of the foldedness of the biomolecules (Figure 3.1.3C). In general, globular biomolecules in solution show a well-defined maximum value of 1.1 at $q*R_g = 1.73$ [23]. The dimensionless Kratky plots for the two ncRNAs suggested that both are well folded and extended in solution, whereas $DDX17_{135–555}$ is relatively more compact.

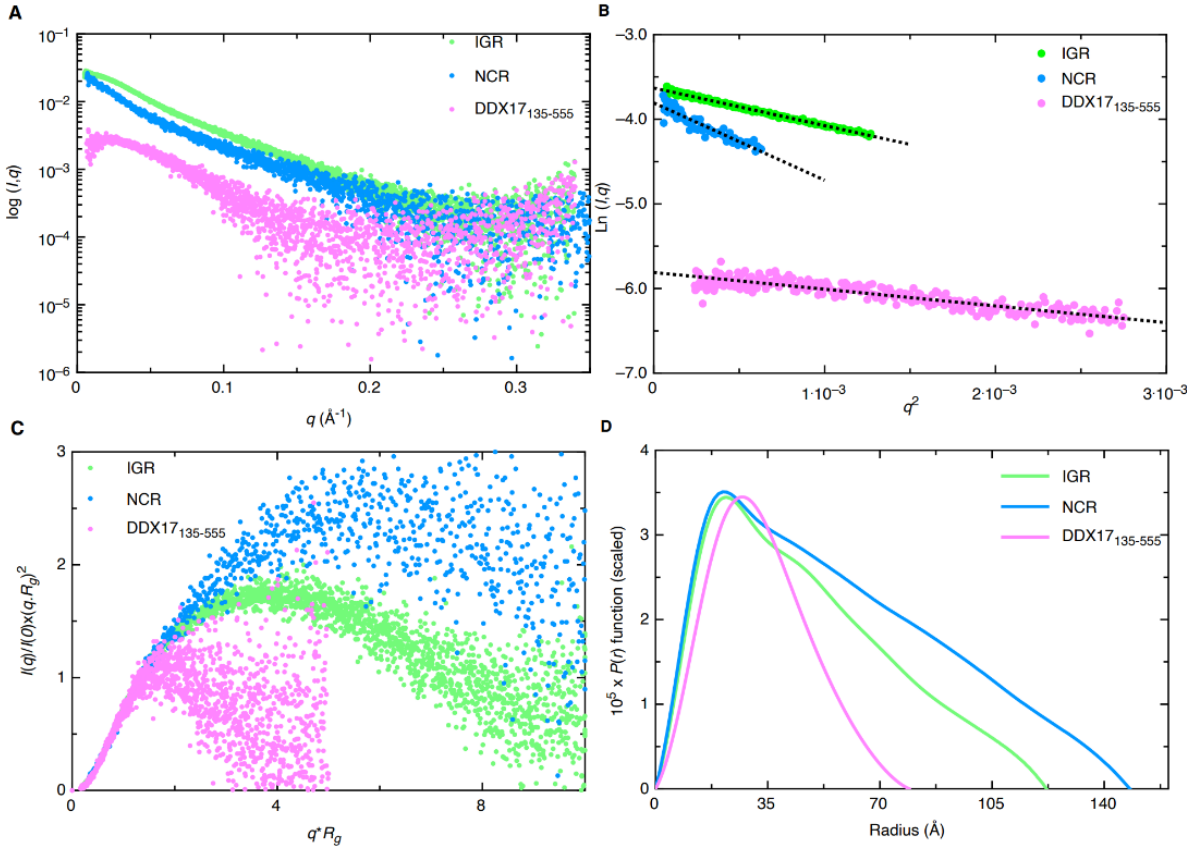

Figure 3.1.3. Small-angle X-ray scattering (SAXS) characterization of RVFV RNA (IGR and NCR) and $DDX17_{135–555}$. (**A**) Merged scattering data of RVFV RNA and $DDX17_{135–555}$ showing scattering intensity (log I(q)) vs. scattering angle ($q = 4\pi\sin\theta/\lambda$). (**B**) Guinier plots allowing for the determination of R_g from low-angle region data and representing the homogeneity of samples. (**C**) Dimensionless Kratky plots ($I(q)/I(0)*(q*R_g)^2$ vs. $q*R_g$) of RVFV RNA and $DDX17_{135–555}$, demonstrating extended structures for RVFV RNA and a more compact structure for $DDX17_{135–555}$. (**D**) Pair distance distribution (P(r)) plots for RVFV RNA and $DDX17_{135–555}$ which allow for the determination of R_g from the entire SAXS dataset, and maximal particle dimension (D_{max}).

Next, indirect Fourier transformations on each dataset were performed to convert the reciprocal-space information of data presented in Figure 3.1.3A to real-space electron pair distance distribution functions (P(r)) plots, which are presented in Figure 3.1.3D using the GNOM [24] program. Using the P(r) plots, the R_g was obtained along with the D_{max} (maximal particle dimension) for all three biomolecules. Importantly, compared to Guinier analysis, which provides R_g from the low-q region, the P(r) analysis utilizes a larger range of the dataset which adds to the reliable determination of the R_g and D_{max}. Table 1 contains all values calculated from the P(r) analysis; we obtained a D_{max} of ~120 Å, 145 Å, and 80 Å for IGR, 5′ NCR, and $DDX17_{135–555}$, respectively. Additionally, we obtained P(r) R_g values of 38.00 ± 0.08, 46.66 ± 0.34, and 25.46 ± 0.27 Å for IGR, 5′ NCR, and $DDX17_{135–555}$, respectively. These values correlate very well to those obtained from prior Guinier analysis, indicating these data are suitable to proceed with low-resolution structure determination. The P(r) plot is also indicative of a biomolecules' relative solution conformation; a more globular-shaped biomolecule will adopt a bell-shaped P(r) distribution with a maximum at $D_{max}/2$ [25], and a more extended molecule will adopt a bell-shaped curve with an extended tail, suggesting an elongated structure [20]. The P(r) plot for $DDX17_{135–555}$ adopts a typical bell-shaped curve, which suggests that this protein is more globular relative to the ncRNAs (Figure 3.1.3D).

Next, we employed DAMMIN [26] to obtain low-resolution structures for each biomolecule, which involves a simulated annealing protocol allowing for the incorporation of P(r) data (D_{max} and R_g as constraints). Twelve models were calculated for all three biomolecules and all models have excellent agreement (X^2) between the experimentally obtained scattering data and the calculated scattering data (Table 1). Following DAMMIN, we employed DAMAVER [27] for the alignment and rotation of all 12 models to gain an averaged filtered structure for each biomolecule, which represents averaged structural features from individual models (Figures 2.1.4 and 2.1.5A) [27]. For each case, the overlap function, the normalized spatial discrepancy (NSD), was estimated to provide a measure of the goodness of fit of the superimposition of each model. Table 3.1.1 presents the NSD values for the 12 models calculated for each biomolecule, and the low values suggest that the models in each case are highly similar to each other. The models presented in Figures 3.1.4 and 3.1.5A are the averaged filtered structures for NCR, 5′ IGR,

and DDX17$_{135–555}$, which indicate that both ncRNAs adopt extended structures in solution, while DDX17$_{135–555}$ has a nearly globular conformation.

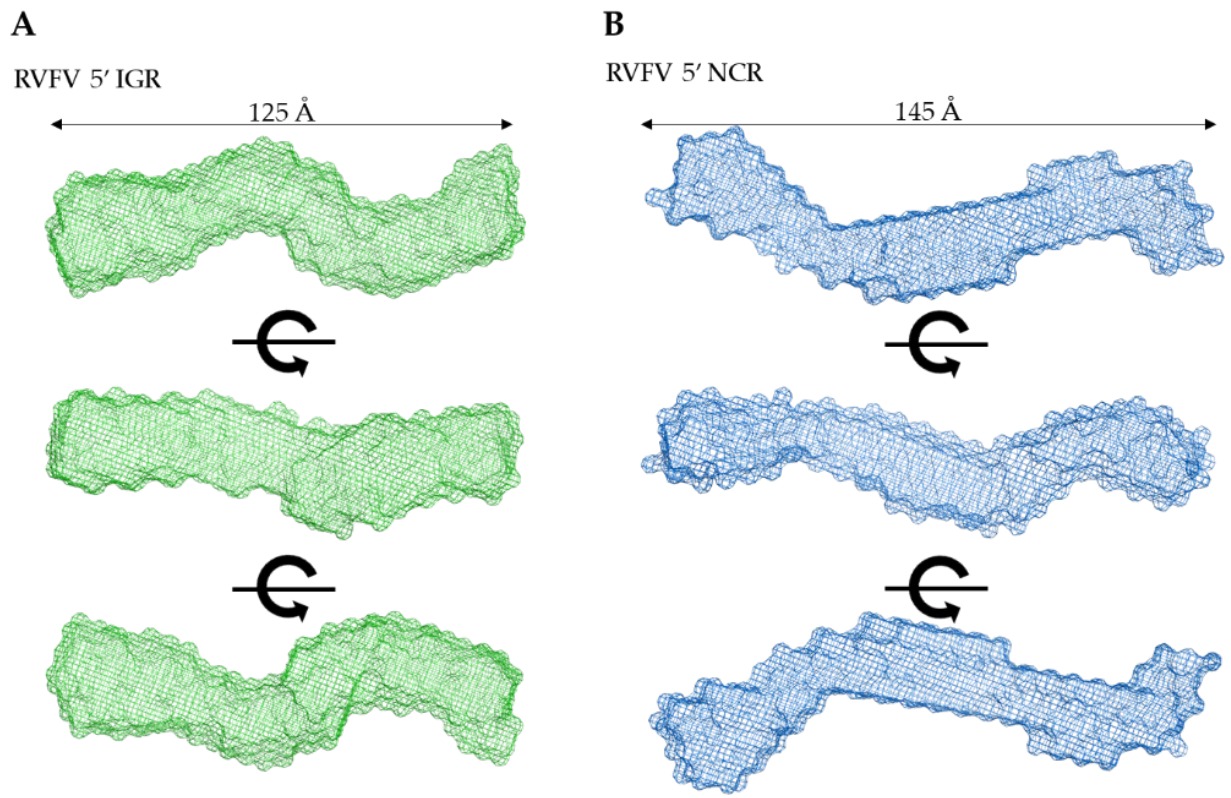

Figure 3.1.4. Low-resolution structure determination via SAXS for RVFV 5′ NCR and RVFV 5′ IGR, indicating that these RNA molecules adopt an extended solution structure. (**A**,**B**) Three structures representing sequential 90° rotational angles from the top panel structure. Dimensions represent the D_{max} obtained from P(r) analysis.

Table 3.1.1. Solution properties of $DDX17_{135–555}$, IGR, and 5′ NCR.

Sample	**$DDX17_{135\_555}$**	**IGR**	**5′ NCR**
M_w (kDa, sequence)	48.45	23.82	24.70
Sedimentation coefficient, S (10^{-13} s) ▽	3.16	4.07	4.18
Diffusion coefficient D (10^{-7} cm^2/s) ▽	5.22	7.62	6.58
R_h (Å) ▽	41.06	28.11	32.64
I(0) #	0.003 ± 2.5 × 10^{-5}	0.026 ± 4.4 × 10^{-5}	0.022 ± 2.6 × 10^{-4}
q.Rg range #	0.39–1.30	0.26–1.29	0.40–1.29
R_g (Å) #	24.78 ± 0.36	36.42 ± 0.10	50.44 ± 0.88
I(0) Δ	0.003 ± 2.3 × 10^{-5}	0.026 ± 4.3 × 10^{-5}	0.019 ± 1.7 × 10^{-4}
R_g (Å) Δ	25.46 ± 0.27	38.00 ± 0.08	46.66 ± 0.34
D_{max} (Å)Δ	79.21	122	148
$\mathbf{X}^2$ *	~1.00	~1.10	~1.30
NSD *	0.52 ± 0.02	0.73 ± 0.02	0.58 ± 0.01

The M_w values were calculated using nucleotide sequences. ▽—determined using SV-AUC analysis and UltraScan-III package [28]. Sedimentation coefficients obtained following genetic algorithm–Monte Carlo analysis. #—obtained from Guinier analysis [21]. Δ—determined using $P(r)$ analysis using the GNOM program [24]. *—values derived from DAMMIN [26] and DAMAVER [27] analysis.

Recently, a high-resolution structure of DDX17 containing the ATP-binding and helicase domains (6UV0) was determined using X-ray crystallography [29]. We noticed a flexible linker between the ATP-binding and helicase domains, which could not be resolved in the high-resolution crystal structure. Therefore, we sought to use the scattering data of $DDX17_{135–555}$ to perform high-resolution modeling using the program CORAL, as described elsewhere [30]. Using the crystal structure's high-resolution information of the ATP-binding domain (155aa-382) and the helicase domain (389aa-555), we calculated 12 separate models and assessed their quality by comparing model-derived SAXS data with experimentally collected SAXS data. Each of the 12 models we calculated has X^2 values of ~1.2, suggesting they are a good fit for the original data. This led us to believe that the helicase domain can adopt multiple different orientations in solutions, consistent with our initial low-resolution SAXS structure presented in Figure 3.1.5A. Figure

3.1.5B presents the CORAL-derived representative models, which highlight the relative orientations of the helicase domain due to the presence of a linker. Figure 3.1.5C demonstrates the overlay of the CORAL-derived model with the $DDX17_{135–555}$ low-resolution structure, indicating an overall agreement between both approaches.

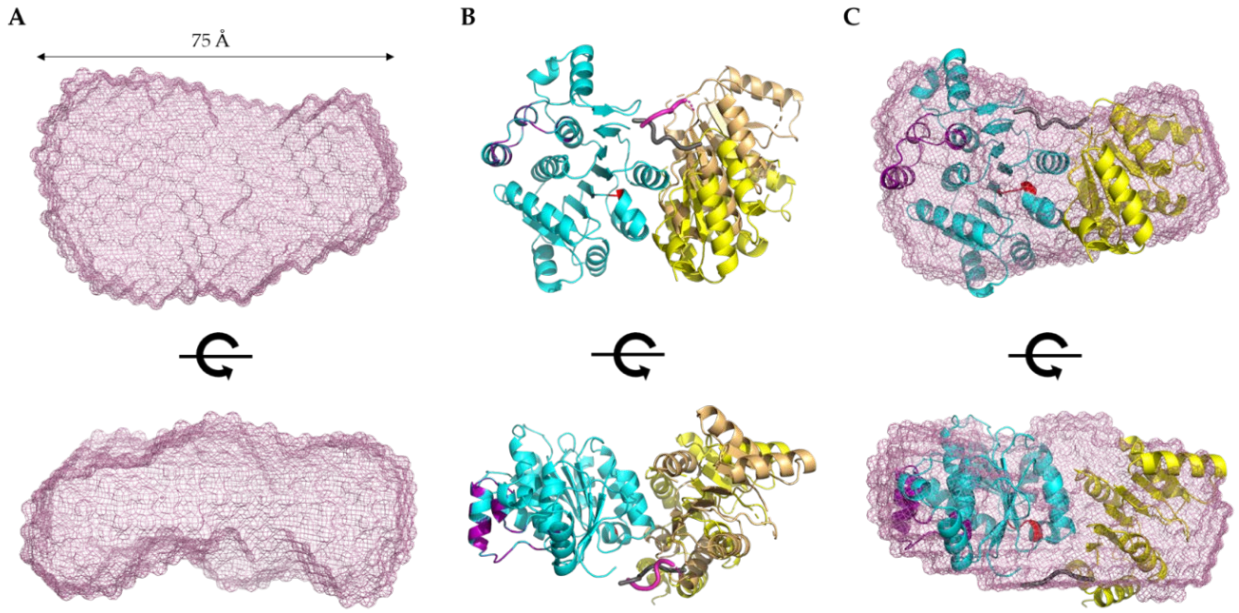

Figure 3.1.5. Structural modeling of $DDX17_{135–555}$. (**A**) Low-resolution SAXS structure indicating that $DDX17_{135–555}$ adopts an extended globular conformation in solution. The bottom panel represents a 90° rotation of the x-axis from the top panel. Dimensions represent the D_{max} from P(r) analysis. (**B**) CORAL-derived models of $DDX17_{135–555}$ (6UV0), suggesting a linker (purple/gray chain) between the ATP-binding domain (blue ribbon), and the helicase domain (yellow/brown ribbon), allowing them to adopt different orientations. (**C**) SAXS envelope overlayed with the CORAL-derived representative model highlighting an agreement between high- and low-resolution models.

3.1.3 DDX17 Binds to the IGR and 5'NCR Non-Coding RNAs

After analyzing the homogeneity of $DDX17_{135–555}$, RVFV S-segment IGR, and 5' NCR, we determined the affinity of DDX17 for both ncRNAs using microscale thermophoresis (MST). MST is a powerful technique that allows for rapid interaction analysis by measuring the change in fluorescent migration as the molecules are excited via infrared laser [31,32]. $DDX17_{135–555}$ was titrated against the fluorescently labeled RVFV RNAs. The addition of $DDX17_{135–555}$ (the ligand) to the fluorescent RNA molecules (the target) causes them to migrate at a rate different than when $DDX17_{135–555}$ is absent. A dissociation constant is determined by relating the change in fluorescent migration of the target to the

concentration of the added ligand [33]. Figure 3.1.6A represents MST traces, where the blue highlight represents the "cold" region which is used to normalize the change of fluorescence measured in red, representing the "hot" region. Our MST studies demonstrate that DDX17$_{135–555}$ interacts with IGR and 5′ NCR with dissociation constants of 5.77 ± 0.15 μM and 9.85 ± 0.11 μM, respectively (Figure 3.1.6B).

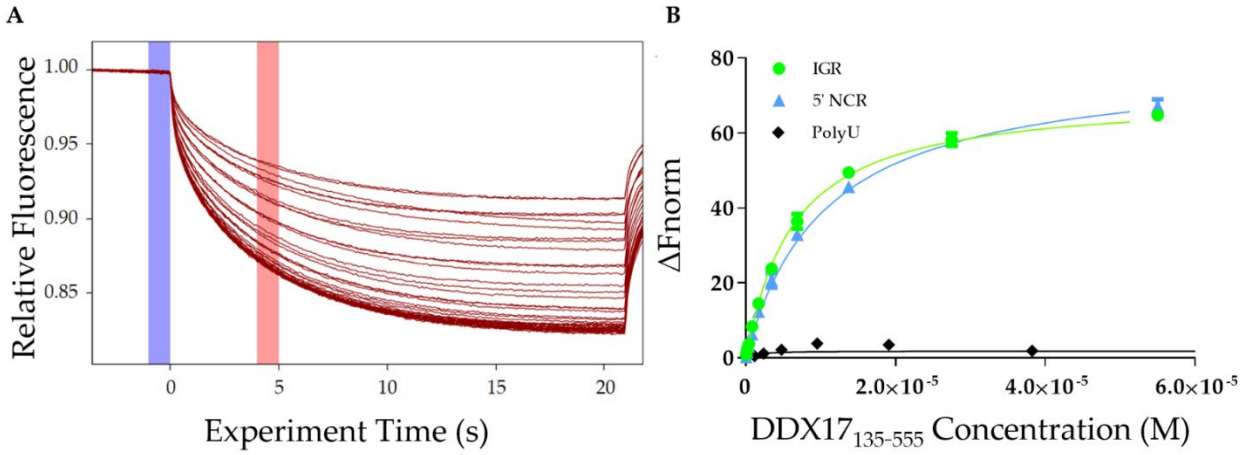

Figure 3.1.6. Interaction studies of DDX17$_{135–555}$ with IGR and 5′ NCR. (**A**) Microscale thermophoresis (MST) traces indicating the change in fluorescence when exposed to the infrared laser. Each trace represents a different concentration of DDX17$_{135–555}$ and is used to assess how the change in concentration affects the fluorescently labeled RNA migration. The blue highlight is the "cold" region and the red highlight is the "hot" region. The difference between these regions is used to calculate the ΔF_{norm}. (**B**) The MST binding curves for the IGR and 5′ NCR RVFV RNAs (n = 3). RNA was used at a concentration of 40 nM while DDX17$_{135–555}$ was titrated up to a maximum concentration of 55μM. The y-axis ΔF_{norm} is the change in fluorescent migration normalized to 0. The dissociation constant for DDX17$_{135–555}$ and the IGR was determined to be 5.78 ± 0.15 μM (reduced X^2 = 0.967, Std. error of regression = 0.702) while for DDX17$_{135–555}$ and the 5′ NCR was determined to be 9.85 ± 0.11 μM (reduced X^2 = 0.996, Std. error of regression = 0.351). We used polyU RNA as a negative control (black diamonds) that did not bind to DDX17$_{135–555}$.

3.1.4 DDX17 Unwinds RVFV RNA in an ATP-Dependent Fashion

Since we confirmed that DDX17$_{135–555}$ binds to both ncRNAs, we wanted to evaluate DDX17's ability to unwind the RNAs. Figure 3.1.7A is a schematic representation of the experimental design which describes the overall approach of utilizing MST to perform a helicase assay. The signal to noise ratio, which is a measure of significance that uses the response amplitude of the MST traces, is indicated in Figure 3.1.7B. To assess statistical significance, we used unpaired *t*-tests. We determined that the fluorescent migration did not experience a significant change (p = 0.9350, signal to noise = 0.750) in the presence of bovine serum albumin (BSA) with the reaction mixture (RNA + fluorescent oligo + ATP),

suggesting that BSA cannot unwind RNA, which makes it a suitable control for the subsequent experiments. Next, we compared the BSA reaction mixture to the reaction mixture with $DDX17_{135–555}$. The results suggest that the addition of DDX17 with either IGR or 5′ NCR causes a significant change in the migration of fluorescence ($p < 0.0001$ for both, signal to noise = 12.5 and 9.17, respectively), indicating a binding event occurred upon the addition of DDX17. Collectively, our analysis demonstrates that $DDX17_{135–555}$ can unwind the RNA, allowing the hybridization of the DNA oligo to the RNA(s). To determine the effect of ATP on the helicase activity of DDX17, we compared the reaction mix with and without ATP (gray bar). We observed that the presence of ATP resulted in a significant difference in fluorescence migration compared to without ATP ($p = 0.0059$, signal to noise = 8.70).

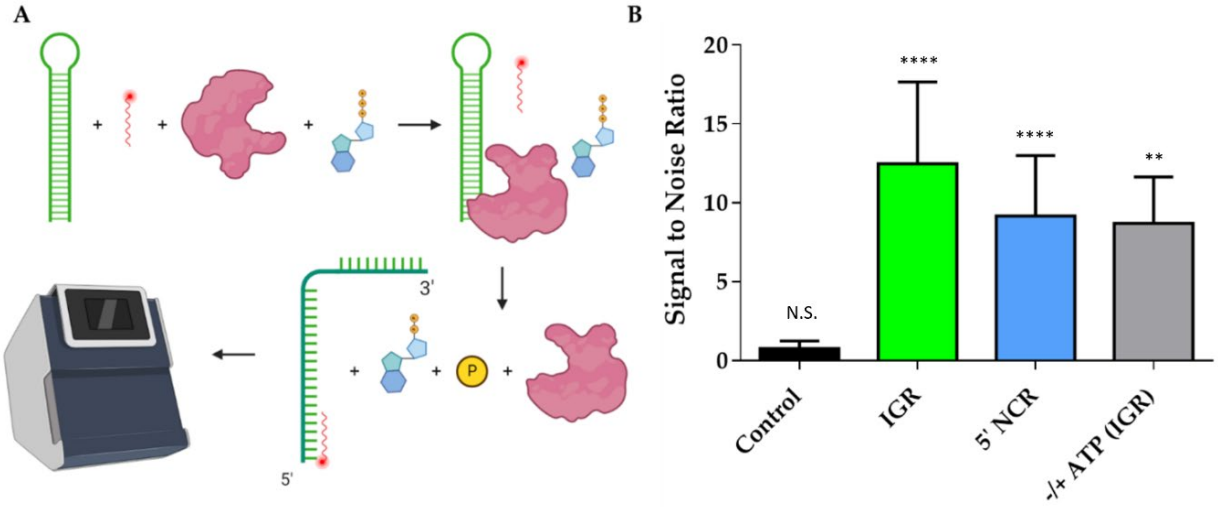

Figure 3.1.7. $DDX17_{135–555}$ helicase assays performed using MST. (**A**) Representation of helicase assay using MST. The helicase assay was performed by combining the RNAs, fluorescently labeled DNA oligo, $DDX17_{135–555}$, and ATP. $DDX17_{135–555}$ hydrolyzes the ATP and unwinds the RNA, giving the oligo access to the newly opened complimentary site. The fluorescently labeled DNA oligo hybridized to the RNA can be measured in the MST by detecting the change in migration. This is compared to a control that uses bovine serum albumin (BSA) instead of $DDX17_{135–555}$, and a change in the migration indicates that the RNA has been unwound by DDX17. (**B**) Signal to noise ratios of different comparative assays (n = 3). Control compared a reaction mix without protein to BSA, signal to noise did not meet the threshold of 5 and was not significant, unpaired *t*-test ($p = 0.9350$, N.S.). $DDX17_{135–555}$ caused a significant change in the IGR ($p < 0.0001$, ****), with the signal to noise ratio reaching 12.5. The 5′ NCR also experienced a significant shift in the presence of $DDX17_{135–555}$ ($p < 0.0001$, ****), having a signal to noise ratio of 9.17. Gray bar represents including ATP vs. not including ATP in the reaction mixture, showing ATP causes a significant change in fluorescent migration, having a signal to noise of 8.70 ($p = 0.0059$, **).

3.2 Discussion

The study performed by Moy et al. in 2014 [11] concluded, in vivo, that U2OS human cells infected with RVFV cause activation of DDX17 to restrict RVFV replication through an interferon-independent pathway. CLIP-seq analysis determined that DDX17 binds to two essential stem-loop regions on the RVFV S-segment RNA: IGR and 5′ NCR [11]. We, therefore, sought to characterize this interaction in vitro to substantiate that DDX17 is an interacting partner of RVFV ncRNAs.

We expressed and purified a construct that contains both the ATP-binding domain and the helicase domain, $DDX17_{135–555}$ (Figure 3.1.1). Next, we transcribed, purified, and characterized the RVFV IGR and 5′ NCR ncRNAs in vitro. As AUC is a reliable and widely accepted technique to assess the solution state of biomolecules [34–36], we performed the SV-AUC experiments. The SV-AUC data suggested that both ncRNAs are relatively pure, with the presence of dimer and tetrameric assemblies (Figure 3.1.2B), which is similar to our prior study on Murrey Valley and Powassan virus ncRNAs where we also observed the presence of oligomeric species [20]. Similarly, SV-AUC studies also indicated that $DDX17_{135–555}$ is mainly monomeric at the examined concentration. We also obtained the diffusion coefficients and the Stokes radii for $DDX17_{135–555}$, IGR, and 5′ NCR (Table 1).

SAXS excels at being a complementary structural biophysical method by enabling solution structure studies of virtually all biomolecules, and their biomolecular complexes [18,22,30,37–40]. While SAXS structures are low resolution in comparison to high-resolution structures determined using X-ray crystallography or NMR, oftentimes obtaining high-quality crystals for crystallography or biomolecular labeling for NMR is challenging [18,38,40–43]. By employing HPLC-SAXS for data collection instead of traditional SAXS, we ensure that our collected scattering data will be monodispersed. These monodispersed preparations were confirmed by the linearity of fit in the low-q region using the Guinier analysis (Figure 3.1.3B). Using Guinier analysis, we also calculated R_g values for all three biomolecules (based on low-q region) (Figure 3.1.3B) and compared them to those calculated through P(r) analysis (Figure 3.1.3D). The R_g values for both analyses were highly similar (Table 1), which confirms that our data are reliable and it is worth proceeding with more analysis. Dimensionless Kratky analysis suggested

that the IGR and 5′ NCR adopt an elongated structure (Figure 3.1.3C). Finally, the P(r) distribution (Figure 3.1.3D) reveals that both ncRNAs quickly increase to the maxima, and then steadily decrease, which suggests an elongated structure, as observed earlier [20,38]. Comparatively, the P(r) distribution of $DDX17_{135–555}$ displays a skewed Gaussian distribution, suggesting that it adopts a more compact conformation compared to the ncRNAs (Figure 3.1.3D). We observe that both ncRNAs have different D_{max} (110 vs. 145 Å), despite having a similar length. The 5′ NCR, based on its D_{max}, likely contains extended amounts of single-stranded regions (Figure 3.1.4A), whereas IGR could have a higher content of double-stranded structures (Figure 3.1.4B). IGR and 5′ NCR (Figure 3.1.4A,B) confirm that both RNAs adopt an elongated structure, as indicated by initial dimensionless Kratky analysis. The ratio of R_g to R_h is a good indicator of the solution conformation of biomolecules. Compact spherical biomolecules typically have an R_g/R_h ratio of ~0.70. This ratio increases as the shape of the molecule changes from globular to extended conformation [44,45]. For IGR and 5′ NCR, the R_g/R_h values are 1.35 and 1.43, suggesting that both ncRNAs have extended conformations. For $DDX17_{135–555}$, we obtained an R_g/R_h of 0.62, indicating that it is more globular than the ncRNAs.

The low-resolution structural modeling of DDX17 confirmed its extended globular nature (Figure 3.1.4A). A secondary strength of SAXS is the ability to combine high-resolution structures or homology models of individual domains, or computational studies with low-resolution SAXS models [18,30,38,41,42]. The crystal structure of DDX17 containing the ATP-binding and helicase domain (6UV0) was determined [29], allowing us to compare their high-resolution data to our low-resolution models to evaluate the validity of our models. Since the flexible linker between the ATP-binding and helicase domains was not resolved, we performed structural modeling using CORAL, which suggested that relative to the ATPase domain, the helicase domain exhibits conformational flexibility in solution (Figure 3.1.5C).

To establish the direct interaction between $DDX17_{135–555}$ and both IGR and 5′ NCR ncRNAs, we performed MST assays as described previously [30,46,47]. Our analysis indicated that both RNAs interact with $DDX17_{135–555}$. However, despite having relatively similar nucleotide length, IGR binds with a comparatively higher affinity to 5′ NCR (5.77 μM for the IGR vs. 9.85 μM for the 5′ NCR) (Figure 3.1.6B).

Compared to the observations made for DDX5 (a DDX17 homolog), our results suggest that the DDX17 interacts with RVFV RNAs weakly (in μM range) [48,49]. However, an important distinction between previous studies and our work is that we have used considerably longer ncRNAs, and the minimalistic DDX17 construct. This could result in differences in specificity, nonetheless, we have demonstrated that our construct is specific to the RVFV RNAs and binds with them with different affinities. Considering how compact the IGR is, based on scattering analysis, it may indicate that DDX17 has tighter binding to double-stranded RNA regions. Although DDX17 is primarily located in the nucleus, its presence in the cytoplasm and ability to interact with RNAs, including the RVFV ncRNAs, suggests that DDX17 may act as a sensor for these viral RNAs within the cytoplasm [50,51], similar to other helicases and host proteins, like DDX3X and Protein Kinase R (PKR) [52,53]. Since DDX17 is a known helicase, we wanted to perform helicase assays to determine if $DDX17_{135–555}$ can unwind RVFV ncRNA. Helicase assays are often conducted by using radioactivity or fluorescent resonance energy transfer (FRET)based analysis [54,55]. However, our endeavor to develop a time and cost-effective alternative led us to design a unique experiment using MST. MST is ideal for our experiment because of its sensitivity for binding events, the low concentrations of samples required, and the availability of the reaction components, other than fluorescently labeled DNA oligos [56,57]. Using this simple assay, we demonstrated that $DDX17_{135–555}$ was able to unwind both RNAs and in a manner that is ATP dependent (Figure 3.1.7B). Currently, it is speculated that the ATP-binding domain hydrolyzes ATP to drive the helicase activity [58] which is consistent with our results. In conclusion, we have demonstrated that $DDX17_{135–555}$ is capable of directly binding and unwinding the noncoding regions of the S-segment genome of Rift Valley fever virus. This suggests that it could be critical for recognizing noncoding regions from other viral RNA.

3.3 Materials and Methods

3.3.1 Protein Expression and Purification of $DDX17_{135–555}$

The $DDX17_{135–555}$ cDNA construct in the pOPINF vector was designed with the help from the Oxford Protein Production Facility (OPPF, Harwell Oxford, Didcot, UK). $DDX17_{135–555}$ was expressed using Lemo21(DE3) *E. coli* cells. The culture was grown in Luria broth containing kanamycin (50 mg/mL) and

chloramphenicol (100 mg/mL) antibiotics. The culture was then transferred to Terrific broth containing 5% glycerol, and the cells were grown at 37 °C in an orbital shaker for 5 h, followed by a reduction in temperature to 20 °C for 16–18 h, harvested by centrifugation, and resuspended in lysis buffer (50 mM Tris, 500 mM NaCl, 10 mM imidazole 3 mM 2-Mercaptoethanol, 10mg/mL Lysozyme, 0.1% Tween-20, and 5% glycerol). The resulting cell suspension was sonicated and centrifuged at 30,000× *g*. The supernatant was filtered through a 0.45 µm syringe filter to prepare for chromatography.

Nickel affinity purification was performed using the ÄKTA start protein purification system (Global Life Science Solutions USA LLC, Marlborough, MA) with the HisTrap™ High-Performance column (Global Life Science Solutions USA LLC, Marlborough, MA) via the hexahistidine tag on $DDX17_{135–555}$. Protein was eluted in 2mL fractions using an imidazole gradient up to 500 mM. Further purification and buffer exchange were performed using an ÄKTA pure purification system (Global Life Science Solutions USA LLC, Marlborough, MA) using Superdex® 200 10/300 GL (Global Life Science Solutions USA LLC, Marlborough, MA). $DDX17_{135–555}$ was eluted in 50 mM Tris, 150 mM NaCl, and 3% glycerol. Elutions containing $DDX17_{135–555}$ were pooled and concentrated using Amicon® Ultra-15 Centrifugal Filter Units (30,000 MWCO, Millipore Canada Ltd, Etobicoke, ON). The 110µM $DDX17_{135–555}$ stocks were aliquoted and frozen in liquid nitrogen before being stored at −80 °C.

3.3.2 Preparation of Rift Valley Fever Virus Non-Coding RNAs

The cDNA sequences were prepared under T7 RNA polymerase control, with two additional G nucleotides on the 5′ end followed by an XbaI restriction enzyme cut site (T^CTAGA) on the 3′ end. Both RVRV constructs were designed based on the Genebank sequence of EU312119.1. The underlined regions are the complimentary regions to our fluorescent oligos described in a later section. Both RNA constructs used in the experiments are listed as follows:

1. RVFV NCR S Segment 812–886

5′GGAUUUGUUGAGGUUGAUUAGAGGUUAAGGCUGCCCCACCCCCCACCCCCUAAUCCCGACCGUAACCCCAACU
CCU3′

2. RVFV IGR S Segment 25–100

5′GGCAAGUAUAUCAUGGAUUACUUUCCUGUGAUAUCUGUUGAUUUGCAGAGUGGUCGUCGUGUUGUGUCAGUG
GAGUACAU3′

Each RNA was prepared using an in vitro transcription reaction using T7 RNA polymerase (made in-house) followed by purification using a Superdex® 200 10/300 GL via an ÄKTA pure system (Global Life Science Solutions USA LLC, Marlborough, MA). Fractions were analyzed using urea-polyacrylamide gel electrophoresis (urea-PAGE): 10 µL of each fraction were mixed with 2 µL of RNA loading dye and loaded into a 1.0 cm well PAGE (Bio-Rad Laboratories (Mississauga, ON). The urea-PAGE (7.5%) was then developed at 300 V, room temperature for 25 min in 0.5× TBE, followed by staining and visualization with Sybr Safe (Thermofisher Scientific, Saint-Laurant, QC, Canada). Fractions containing a single band were used for further experimentation. Fractions containing the purified RNA of interest were concentrated by ethanol precipitation, and each pellet was resuspended in RNA buffer (10 mM Tris pH 7.5, 100 mM NaCl, and 5 mM $MgCl_2$).

3.3.3 Fluorescent Labeling of RNA

RNAs were incubated on ice for 30 min in 0.1M sodium acetate (pH 5.3) and 2 mM potassium periodate. Following incubation, the reaction was stopped by adding ethylene glycol to a concentration of 10 mM and incubated again on ice for 10 min. We then performed two ethanol precipitations, resuspended the RNA in water, along with 0.1 M NaOAc and 10 mM fluorescein-5-thiosemicarbazide (FITC), and incubated the mixture on ice and in the dark for 16 h. Following incubation with the fluorescent dye, the mixture was phenol extracted (1 vol phenol:1 vol mixture) 5 times until the phenol layer no longer changed color, indicating all free dye had been removed from the RNA mixture. We then ethanol precipitated the resulting labeled RNA twice, followed by resuspension in RNA buffer.

3.3.4 Analytical Ultracentrifugation (AUC)

We collected SV-AUC data for FPLC-purified RNA and protein using a Beckman Optima AUC centrifuge with an AN60-Ti rotor at 20 °C. Each sample was loaded into Epon-2 channel centerpieces and was measured at 0.5 OD_{260} for RNA (680 nM) and 0.5 OD_{280} for protein (10.2 µM). For SV-AUC experiments, we used 10 mM Tris and 500 mM NaCl with 5 mM $mgCl_2$ buffer at pH 7.5 for RNA and 50 mM Tris, 150 mM NaCl, and 5% glycerol buffer at pH 8 for protein. Intensity scans were collected at 20 s intervals at 40,000 revolutions per minute, measuring at 20 °C. All data were analyzed using UltraScan-III [59] according to the workflow described elsewhere [60]. Finite element fits were processed on the Lonestar5 (Texas Advanced Computing Center, Austin, TX, USA) and Comet (San Diego Supercomputing Center, San Diego, CA, USA) supercomputers. The collected SV-AUC data were analyzed using two-dimensional spectrum analysis (2DSA) to subtract time and radially invariant noise components and to fit the meniscus and bottom positions [61], followed by genetic algorithm analysis combined with Monte Carlo analysis [62]. The buffer density and viscosity corrections were calculated with UltraScan (1.0030 g/cm^3 and 1.0100 cP, respectively, for the RNA buffer and 1.017 g/cm^3 and 1.152 cP for the protein buffer). Partial specific volumes of 0.55 mL/g [20] and 0.732 mL/g [63] were assumed for RNAs and protein, respectively. All reported hydrodynamic parameters are corrected to standard conditions (20 °C and water), as implemented in UltraScan [59].

3.3.5 Microscale Thermophoresis RNA and Protein Binding Studies

A two-fold serial dilution was performed on $DDX17_{135–555}$ where the highest concentration was 55 µM (as presented in Figure 3.1.6B). A constant amount of FITC-labeled RVFV NCR, or 5′ IGR, was added to each serial dilution of $DDX17_{135–555}$, resulting in a final concentration of 40 nM. The final concentration of polyU (negative control, Sigma-Aldrich Canada) in each assay was 50 µg/mL, and the initial fluorescence was similar to the ncRNA experiments. Samples were incubated together at room temperature for 10 min and then added to Nanotemper Technologies Monolith® NT.115 instrument (Munich, Germany) hydrophobic capillaries and loaded onto the MST block. Thermophoresis was measured at an ambient room temperature of 25 °C and performed using 20% excitation power for RVFV

NCR and 40% for 5′ IGR (blue filter) and medium MST IR-laser power. Fluorescent migration used to determine K_d was measured from 4.0 to 5.0s and then normalized to initial fluorescence (−1.0 to 0s). The data from three independent replicates were analyzed using MO Affinity Analysis software v2.1.3 and fit to the standard K_d fit model, which describes a molecular interaction with a 1:1 stoichiometry according to the law of mass action. K_d is estimated by fitting Equation (1), where $F(c)$ is the fraction bound at a given ligand concentration c; Unbound is the F_{norm} signal of the target alone; $Bound$ is the F_{norm} signal of the complex; K_d is the dissociation constant; and c_{target} is the final concentration of the target in the assay.

$$F(c) = Unbound + (Bound - Unbound) \times \frac{c + c_{target} + K_d - \sqrt{\left(c + c_{target} + K_d\right)^2 - 4cc_{target}}}{2c_{target}}$$

3.3.6 Helicase Assay

Firstly, we input our sequences into sfold (v2.2) [64] to determine the theoretical secondary structure and identified a portion of each RNA molecule that was double stranded. Oligos with complementary sequences to the double-stranded region(s) of the RNA(s) analyzed here were synthesized with a 5′ conjugated Cy5 fluorophore. The region of each RNA molecule which the oligos hybridize to is underlined, as described above (4.3). The sequences for RVFV 5′ IGR and RVFV 5′ NCR oligo(s) are: 5′Cy5/CAACTCCAACTAATCTCCA3′ and 5′Cy5/AGACAACTAAACGTCTCAC3′, respectively.

Using Monolith® NT.115 that assesses the change in fluorescence migration, we were able to determine if the RNA molecules were unwound, thus allowing the oligo to bind to the now exposed complementary RNA. The reaction mixture contains 40nM of Cy5-DNA oligos, 1 μM of the RNA, and 4.25 mM of ATP. To test the helicase activity of $DDX17_{135–555}$, we added the enzyme to a final concentration of 20 μM. As a control, we compared the unwinding activity of bovine serum albumin (BSA) with the activity observed in the absence of any protein (black bar). For the BSA control, the same concentration was used as for DDX17 (green and blue bars). Additionally, to assess the importance of ATP in unwinding activity, we compared $DDX17_{135–555}$ without ATP to DDX17 with ATP (gray bar). Each run uses 4 capillaries, and we performed 3 runs for each condition before using the MO.Affinity Analysis (v2.1.3) software to analyze the data. The analysis software assesses the signal to noise ratio between a run with and without the

protein. Signal to noise is a measure of the response amplitude that is divided by the noise of the environment, and Equation (2) represents how this can be calculated [65]. If the signal to noise ratio rises above 5, the assay indicates that a binding event has occurred. To further analyze the helicase assay, unpaired *t*-tests were performed

3.3.7 Small-Angle X-ray Scattering

Small-angle X-ray scattering was performed by utilizing the B21 BioSAXS beamline at Diamond Light Source (Didcot, Oxfordshire, UK) to collect high-performance liquid chromatography SAXS (HPLC-SAXS) data which can be found described previously [66]. Using a specialized flow cell connected to an in-line Agilent 1200 (Agilent Technologies, Stockport, UK) HPLC, 50µL of each purified sample (protein or RNA) were injected onto a Shodex KW403-4F (Showa Denko America Inc., New York, NY, USA) size exclusion column pre-equilibrated with buffer, at a flow rate of 0.160 mL per minute. X-rays were exposed to each frame for 3 s. The peak region for each sample was buffer subtracted using baseline measurements and merged using Primus [67] or ScAtter [68], as previously described. The merged data were analyzed initially by Guinier approximation [21] to obtain the radius of gyration (R_g) and evaluate homogeneity. Dimensionless Kratky analysis [23] was performed on all samples to evaluate the folding extend of the biomolecules of interest, which is reviewed in detail elsewhere [22]. Following Kratky analysis, we performed a pair distance distribution (P(r)) analysis using GNOM [24] to additionally provide the R_g and the maximum particle dimension (Dmax). Using the information from the P(r) plot, we generated models using DAMMIN [26], without enforced symmetry, which can be found previously described [30]. Finally, the resulting models were averaged and filtered to generate a single representative averaged model using DAMAVER [27,43,69].

Recently, a crystal structure of DDX17 containing the ATP and helicase domain (6UV0) was published [29]. We used the scattering data of $DDX17_{135–555}$ and performed high-resolution modeling, using the crystal structure and CORAL program, as described earlier [30]. Briefly, the high-resolution structure information of the ATP domain (155aa–382) and helicase domain (389aa–555) was provided as input data along with the raw scattering data, and the residues 383–388 were used as a flexible linker.

Using this approach, we initially calculated 12 models and the quality of the models was assessed using X^2 values.

3.4 References

1. Findlay, G.; Daubney, R. The Virus of Rift Valley Fever or Enzootic Hepatitis. *Lancet* **1931**, *25*, 229–248.
2. Balkhy, H.H.; Memish, Z.A., Rift Valley fever: An uninvited zoonosis in the Arabian peninsula. *Int. J. Antimicrob. Agents* **2003**, *21*, 153–157.
3. Bird, B.H.; Ksiazek, T.G.; Nichol, S.T.; MacLachlan, N.J. Rift Valley fever virus. *J. Am. Vet. Med. Assoc.* **2009**, *234*, 883–893.
4. Ikegami, T. Rift Valley fever vaccines: An overview of the safety and efficacy of the live-attenuated MP-12 vaccine candidate. *Expert Rev. Vaccines* **2017**, *16*, 601–611.
5. World Health Organization. *Rift Valley Fever Virus*; WHO: Geneva, Switzerland, 2020.
6. Linthicum, K.; Davies, F.; Kairo, A.; Bailey, C. Rift Valley fever virus (family Bunyaviridae, genus Phlebovirus). Isolations from Diptera collected during an inter-epizootic period in Kenya. *Epidemiol. Infect.* **1985**, *95*, 197–209.
7. Nanyingi, M.O.; Munyua, P.; Kiama, S.G.; Muchemi, G.M.; Thumbi, S.M.; Bitek, A.O.; Bett, B.; Muriithi, R.M.; Njenga, M.K. A systematic review of Rift Valley Fever epidemiology 1931–2014. *Infect. Ecol. Epidemiol.* **2015**, *5*, 28024.
8. Terasaki, K.; Murakami, S.; Lokugamage, K.G.; Makino, S. Mechanism of tripartite RNA genome packaging in Rift Valley fever virus. *Proc. Natl. Acad. Sci. USA* **2011**, *108*, 804–809.
9. Pepin, M.; Bouloy, M.; Bird, B.H.; Kemp, A.; Paweska, J. Rift Valley fever virus (Bunyaviridae: Phlebovirus): An update on pathogenesis, molecular epidemiology, vectors, diagnostics and prevention. *Vet. Res.* **2010**, *41*, 61.
10. Ikegami, T.; Makino, S. The pathogenesis of Rift Valley fever. *Viruses* **2011**, *3*, 493–519.
11. Moy, R.H.; Cole, B.S.; Yasunaga, A.; Gold, B.; Shankarling, G.; Varble, A.; Molleston, J.M.; Lynch, K.W.; Cherry, S. Stem-loop recognition by DDX17 facilitates miRNA processing and antiviral defense. *Cell* **2014**, *158*, 764–777.
12. Gauliard, N.; Billecocq, A.; Flick, R.; Bouloy, M. Rift Valley fever virus noncoding regions of L, M and S segments regulate RNA synthesis. *Virology* **2006**, *351*, 170–179.
13. Byrd, A.K.; Raney, K.D. Superfamily 2 helicases. *Front. Biosci. (Landmark Ed.)* **2012**, *17*, 2070.
14. Meier-Stephenson, V.; Mrozowich, T.; Pham, M.; Patel, T.R. DEAD-box helicases: The Yin and Yang roles in viral infections. *Biotechnol. Genet. Eng. Rev.* **2018**, *34*, 3–32.
15. Linder, P.; Jankowsky, E. From unwinding to clamping—the DEAD box RNA helicase family. *Nat. Rev. Mol. Cell Biol.* **2011**, *12*, 505–516.
16. Fuller-Pace, F.V. The DEAD box proteins DDX5 (p68) and DDX17 (p72): Multi-tasking transcriptional regulators. *Biochim. Biophys. Acta (BBA)-Gene Regul. Mech.* **2013**, *1829*, 756–763.
17. Rozen, F.; Edery, I.; Meerovitch, K.; Dever, T.E.; Merrick, W.C.; Sonenberg, N. Bidirectional RNA helicase activity of eucaryotic translation initiation factors 4A and 4F. *Mol. Cell Biol.* **1990**, *10*, 1134–1144.
18. Brosey, C.A.; Tainer, J.A. Evolving SAXS versatility: Solution X-ray scattering for macromolecular architecture, functional landscapes, and integrative structural biology. *Curr. Opin. Struct. Biol.* **2019**, *58*, 197–213.
19. Pérez, J.; Vachette, P. *A Successful Combination: Coupling SE-HPLC with SAXS. Biological Small Angle Scattering: Techniques, Strategies and Tips*; Springer: Berlin/Heidelberg, Germany, 2017; pp 183–199.
20. Mrozowich, T.; Henrickson, A.; Demeler, B.; Patel, T.R. Nanoscale Structure Determination of Murray Valley Encephalitis and Powassan Virus Non-Coding RNAs. *Viruses* **2020**, *12*, 190.
21. Guinier, A.; Fournet, G.; Yudowitch, K.L. Small-angle scattering of X-rays. **1955**, *19*, 594.
22. Patel, T.R.; Chojnowski, G.; Koul, A.; McKenna, S.A.; Bujnicki, J.M. Structural studies of RNA-protein complexes: A hybrid approach involving hydrodynamics, scattering, and computational methods. *Methods* **2017**, *118*, 146–162.

23. Durand, D.; Vivès, C.; Cannella, D.; Pérez, J.; Pebay-Peyroula, E.; Vachette, P.; Fieschi, F. NADPH oxidase activator p67phox behaves in solution as a multidomain protein with semi-flexible linkers. *J. Struct. Biol.* **2010**, *169*, 45–53.
24. Svergun, D. Determination of the regularization parameter in indirect-transform methods using perceptual criteria. *J. Appl. Crystallogr.* **1992**, *25*, 495–503.
25. Svergun, D.I.; Koch, M.H. Small-angle scattering studies of biological macromolecules in solution. *Rep. Prog. Phys.* **2003**, *66*, 1735.
26. Svergun, D.I. Restoring low resolution structure of biological macromolecules from solution scattering using simulated annealing. *Biophys. J.* **1999**, *76*, 2879–2886.
27. Volkov, V.V.; Svergun, D.I. Uniqueness of ab initio shape determination in small-angle scattering. *J. Appl. Crystallogr.* **2003**, *36*, 860–864.
28. Demeler, B. UltraScan: A comprehensive data analysis software package for analytical ultracentrifugation experiments. *Mod. Anal. Ultracentrifugation Tech. Methods* **2005**, doi:10.1039/9781847552617-00210.
29. Ngo, T.D.; Partin, A.C.; Nam, Y. RNA specificity and autoregulation of ddx17, a modulator of microRNA biogenesis. *Cell Rep.* **2019**, *29*, 4024–4035. e5.
30. Reuten, R.; Patel, T.R.; McDougall, M.; Rama, N.; Nikodemus, D.; Gibert, B.; Delcros, J.-G.; Prein, C.; Meier, M.; Metzger, S. Structural decoding of netrin-4 reveals a regulatory function towards mature basement membranes. *Nat. Commun.* **2016**, *7*, 1–17.
31. Jerabek-Willemsen, M.; Wienken, C.J.; Braun, D.; Baaske, P.; Duhr, S. Molecular interaction studies using microscale thermophoresis. *Assay Drug Dev. Technol.* **2011**, *9*, 342–353.
32. Mrozowich, T.; MeierStephenson, V.; Patel, T.R. Microscale thermophoresis: Warming up to a new biomolecular interaction technique. *Biochemist* **2019**, *41*, 8–12.
33. Jerabek-Willemsen, M.; André, T.; Wanner, R.; Roth, H.M.; Duhr, S.; Baaske, P.; Breitsprecher, D. MicroScale Thermophoresis: Interaction analysis and beyond. *J. Mol. Struct.* **2014**, *1077*, 101–113.
34. Schuck, P.; Perugini, M.A.; Gonzales, N.R.; Howlett, G.J.; Schubert, D. Size-distribution analysis of proteins by analytical ultracentrifugation: Strategies and application to model systems. *Biophys. J.* **2002**, *82*, 1096–1111.
35. Chillón, I.; Marcia, M.; Legiewicz, M.; Liu, F.; Somarowthu, S.; Pyle, A.M. *Native Purification and Analysis of Long RNAs. Methods in Enzymology*; Elsevier: Amsterdam, The Netherlands, 2015; Volume 558, pp. 3–37.
36. Patel, T.R.; Winzor, D.J.; Scott, D.J. Analytical ultracentrifugation: A versatile tool for the characterisation of macromolecular complexes in solution. *Methods* **2016**, *95*, 55–61.
37. Chen, Y.; Pollack, L. SAXS studies of RNA: Structures, dynamics, and interactions with partners. *Wiley Interdiscip. Rev. RNA* **2016**, *7*, 512–526.
38. Kim, D.N.; Thiel, B.C.; Mrozowich, T.; Hennelly, S.P.; Hofacker, I.L.; Patel, T.R.; Sanbonmatsu, K.Y. Zinc-finger protein CNBP alters the 3-D structure of lncRNA Braveheart in solution. *Nat. Commun.* **2020**, *11*, 1–13.
39. Patel, T.R.; Meier, M.; Li, J.; Morris, G.; Rowe, A.J.; Stetefeld, J. T-shaped arrangement of the recombinant agrin G3–IgG Fc protein. *Protein Sci.* **2011**, *20*, 931–940.
40. Krahn, N.; Meier, M.; To, V.; Booy, E.P.; McEleney, K.; O'Neil, J.D.; McKenna, S.A.; Patel, T.R.; Stetefeld, J. Nanoscale assembly of high-mobility group AT-Hook 2 protein with DNA replication fork. *Biophys. J.* **2017**, *113*, 2609–2620.
41. Deo, S.; Patel, T.R.; Chojnowski, G.; Koul, A.; Dzananovic, E.; McEleney, K.; Bujnicki, J.M.; McKenna, S.A. Characterization of the termini of the West Nile virus genome and their interactions with the small isoform of the 2′ 5′-oligoadenylate synthetase family. *J. Struct. Biol.* **2015**, *190*, 236–249.
42. Dzananovic, E.; Chojnowski, G.; Deo, S.; Booy, E.P.; Padilla-Meier, P.; McEleney, K.; Bujnicki, J.M.; Patel, T.R.; McKenna, S.A. Impact of the structural integrity of the three-way junction of adenovirus VAI RNA on PKR inhibition. *PLoS ONE* **2017**, *12*, e0186849.

43. Dzananovic, E.; Patel, T.R.; Chojnowski, G.; Boniecki, M.J.; Deo, S.; McEleney, K.; Harding, S.E.; Bujnicki, J.M.; McKenna, S.A. Solution conformation of adenovirus virus associated RNA-I and its interaction with PKR. *J. Struct. Biol.* **2014**, *185*, 48–57.
44. Burchard, W. Static and dynamic light scattering approaches to structure determination of biopolymers. *Laser Light Scatt. Biochem.* **1982**, *48*, doi:10.1007/3-540-12030-0_1.
45. Stetefeld, J.; McKenna, S.A.; Patel, T.R. Dynamic light scattering: A practical guide and applications in biomedical sciences. *Biophys. Rev.* **2016**, *8*, 409–427.
46. Ferens, F.G.; Patel, T.R.; Oriss, G.; Court, D.A.; Stetefeld, J. A Cholesterol Analog Induces an Oligomeric Reorganization of VDAC. *Biophys. J.* **2019**, *116*, 847–859.
47. Moon, M.H.; Hilimire, T.A.; Sanders, A.M.; Schneekloth Jr.,J.S. Measuring RNA–ligand interactions with microscale thermophoresis. *Biochemistry* **2018**, *57*, 4638–4643.
48. Xing, Z.; Wang, S.; Tran, E.J. Characterization of the mammalian DEAD-box protein DDX5 reveals functional conservation with S. cerevisiae ortholog Dbp2 in transcriptional control and glucose metabolism. *RNA* **2017**, *23*, 1125–1138.
49. Wu, G.; Xing, Z.; Tran, E.J.; Yang, D. DDX5 helicase resolves G-quadruplex and is involved in MYC gene transcriptional activation. *Proc. Natl. Acad. Sci. USA* **2019**, *116*, 20453–20461.
50. Moy, R.H.; Cole, B.S.; Yasunaga, A.; Gold, B.; Shankarling, G.; Varble, A.; Molleston, J.M.; tenOever, B.R.; Lynch, K.W.; Cherry, S. Stem-loop recognition by DDX17 facilitates miRNA processing and antiviral defense. *Cell* **2014**, *158*, 764–777.
51. Moy, R.H.; Cherry, S. DDX17: Structured RNA recognition drives diverse outputs. *Cell Cycle* **2014**, *13*, 3467–3468.
52. Song, H.; Ji, X. The mechanism of RNA duplex recognition and unwinding by DEAD-box helicase DDX3X. *Nat. Commun.* **2019**, *10*, 1–8.
53. Dzananovic, E.; Patel, T.R.; Deo, S.; McEleney, K.; Stetefeld, J.; McKenna, S.A. Recognition of viral RNA stem–loops by the tandem double-stranded RNA binding domains of PKR. *RNA* **2013**, *19*, 333–344.
54. Mendoza, O.; Gueddouda, N.M.; Boulé, J.-B.; Bourdoncle, A.; Mergny, J.-L. A fluorescence-based helicase assay: Application to the screening of G-quadruplex ligands. *Nucleic Acids Res.* **2015**, *43*, e71.
55. Mojumdar, A.; Deka, J. *Assaying the Activity of Helicases: An Overview. Helicases from All Domains of Life*; Elsevier: Amsterdam, The Netherlands, 2019; pp 235–246.
56. Cordin, O.; Tanner, N.K.; Doere, M.; Linder, P.; Banroques, J. The newly discovered Q motif of DEAD-box RNA helicases regulates RNA-binding and helicase activity. *EMBO J.* **2004**, *23*, 2478–2487.
57. Tani, H.; Akimitsu, N.; Fujita, O.; Matsuda, Y.; Miyata, R.; Tsuneda, S.; Igarashi, M.; Sekiguchi, Y.; Noda, N. High-throughput screening assay of hepatitis C virus helicase inhibitors using fluorescence-quenching phenomenon. *Biochem. Biophys. Res. Commun.* **2009**, *379*, 1054–1059.
58. Lamm, G.M.; Nicol, S.M.; Fuller-Pace, F.V.; Lamond, A.I. P72: A human nuclear DEAD box protein highly related to p68. *Nucleic Acids Res.* **1996**, *24*, 3739–3747.
59. Demeler, B.; Gorbet, G.E. *Analytical Ultracentrifugation Data Analysis with UltraScan-III. Analytical Ultracentrifugation*; Springer: Berlin/Heidelberg, Germany, 2016; pp 119–143.
60. Demeler, B. Methods for the design and analysis of sedimentation velocity and sedimentation equilibrium experiments with proteins. *Curr. Protoc. Protein Sci.* **2010**, *60*, 7.13.1–7.13.24.
61. Brookes, E.; Cao, W.; Demeler, B. A two-dimensional spectrum analysis for sedimentation velocity experiments of mixtures with heterogeneity in molecular weight and shape. *Eur. Biophys. J.* **2010**, *39*, 405–414.
62. Brookes, E.H.; Demeler, B. Parsimonious Regularization Using Genetic Algorithms Applied to the Analysis of Analytical Ultracentrifugation Experiments. In Proceedings of the 9th Annual Conference on Genetic and Evolutionary Computation, London, UK, 7–11 July 2007; pp. 361–368.
63. Durchschlag, H. *Specific Volumes of Biological Macromolecules and Some Other Molecules of Biological Interest. Thermodynamic Data for Biochemistry and Biotechnology*; Springer: Berlin/Heidelberg, Germany, 1986; pp 45–128.

64. Ding, Y.; Chan, C.Y.; Lawrence, C.E. S fold web server for statistical folding and rational design of nucleic acids. *Nucleic Acids Res.* **2004**, *32* (Suppl. 2), W135–W141.
65. Seidel, S.A.; Dijkman, P.M.; Lea, W.A.; van den Bogaart, G.; Jerabek-Willemsen, M.; Lazic, A.; Joseph, J.S.; Srinivasan, P.; Baaske, P.; Simeonov, A.; et al. Microscale thermophoresis quantifies biomolecular interactions under previously challenging conditions. *Methods* **2013**, *59*, 301–315.
66. Meier, M.; Moya-Torres, A.; Krahn, N.J.; McDougall, M.D.; Orriss, G.L.; McRae, E.K.S.; Booy, E.P.; McEleney, K.; Patel, T.R.; McKenna, S.A. Structure and hydrodynamics of a DNA G-quadruplex with a cytosine bulge. *Nucleic Acids Res.* **2018**, *46*, 5319–5331.
67. Konarev, P.V.; Volkov, V.V.; Sokolova, A.V.; Koch, M.H.; Svergun, D.I., PRIMUS: A Windows PC-based system for small-angle scattering data analysis. *J. Appl. Crystallogr.* **2003**, *36*, 1277–1282.
68. Rambo, R.; ScÅtter, a JAVA-based application for basic analysis of SAXS datasets. **2017**.
69. Patel, T.R.; Bernards, C.; Meier, M.; McEleney, K.; Winzor, D.J.; Koch, M.; Stetefeld, J. Structural elucidation of full-length nidogen and the laminin–nidogen complex in solution. *Matrix Biol.* **2014**, *33*, 60–67.

Chapter 4: Development Towards a Baculovirus Proteins Expression System

4.0 Introduction

Insect cells have been available for laboratory use since the middle of the twentieth century, but it was not until the 1980s that their popularity rose to prominence [1]. The most widely available insect cells come from some Lepidopteran species, SF9 cells being the most common, sourced from the Fall Army Worm (*Spodoptera frugiperda*). The largest factor behind the increased popularity came from modifications made to a natural virus. Genetically engineered baculovirus made it possible to express recombinant proteins with insect cells as a powerful tool that provides alternatives to protein expression within mammalian cells. Deletions made to the polyhedrin coding portion of the *Autographa californica* nuclear polyhedrosis virus, a Baculovirus, allowed researchers to screen for viral genomes that had exchanged genetic information, allowing for the virus's exploitation [2].

Baculoviruses have seen implementation to control insect populations [3] but are more often used to express foreign proteins in a eukaryotic system. The main benefit of baculovirus protein expression is the eukaryotic post-translation modifications that would not be present in a prokaryotic expression system [1]. The safety risks of mammalian cell culture are also significantly reduced when using insect viruses, all while being more cost-effective.

Expression of recombinant protein is achieved when the virus enters the latter stages of replication, the polyhedrin protein that would typically begin expression has been replaced by a protein of interest [4]. Designing the viral construct containing the recombinant protein can be achieved in several ways, for example, cloning directly into the viral genome [5], yeast recombination [6] or using transposons in bacteria [7]. However, the simplest method involves linearizing the genome, forcing the cut viruses' recombination with the desired protein's genetic information to restore the viral function [8]. There are also lethal knockout genes included in the viral construct that prevent viral replication unless recombination occurs to ensure that no wild-type virus survives [9].

Eukaryotic proteins that are difficult to express in bacterial hosts can be a significant constraint for labs, especially biophysics labs that require high quantities of full-length proteins for research work. Insect cells are known to express large quantities of eukaryotic proteins with post-translational modifications [9]. Therefore, I opted to express the full-length dead-box helicases (DDX3X) in insect cells following successive failed attempts using bacterial systems.

4.1 Methods

4.1.1 Insect Cell Culturing

SF9 cells (Thermofisher Scientific, Saint-Laurant, QC, Canada) were seeded to a density of ~$5x10^5$ cells/mL in SF900III Serum-Free Media (SFM) media (Thermofisher Scientific) in shake flasks at 27°C with shaking set to 120rpm. Cells were grown to a density of $6x10^6$ cells/mL before being passaged back to the initial density of $5x10^5$ cells/mL. SF9 cells can tolerate 30 passages or three months before a fresh aliquot should be thawed.

High Five cells (Thermofisher Scientific) were grown via adherent culture but can adapt to suspension cultures to allow for higher cell densities. Cells were seeded at a density of $2x10^4$-$5x10^4$ cells/cm^2. Once confluency reaches 90%, the cells are passaged and returned to $2x10^4$–$5x10^4$ cells/cm^2. Adapting cells to suspension means that heparin is added to the media to prevent cell aggregation. Ten units of heparin per mL of media are added until the cells reach 95% viability in suspension. Heparin can then be weaned from the cells as they are now considered adapted to suspension. Once cell density reaches $2x10^6$, the cells need to be passaged back to $3x10^5$.

4.1.2 Baculovirus DNA Purification

E. coli (HS996) containing the Baculovirus genome are grown in Luria's Broth (LB) at 37°C overnight, or until the cell density reaches OD_{600}. The DNA is extracted using the FosmidMax DNA Purification Kit (Lucigen, Middleton, WI, USA). To start, cells are spun at 15,000xg for 2 minutes. The pellet is resuspended in 200µL of chilled Solution 1. Next, 400µL of Solution 2 is added; this begins the lysis reaction for no greater than 5 minutes. At this point, the DNA should be treated cautiously; too great

of mechanical force could lead to sheared DNA. 300µL of Solution 3 is added to stop the reaction, and at this point, a white precipitate will form. Following incubation on ice for 15 minutes, the sample is centrifuged for 15 minutes at 4°C and 15,000xg. The supernatant is collected and mixed with 540µL of isopropanol before being centrifuged once again for 15 minutes at 4°C and 15,000xg. The isopropanol layer is removed, and the pellet is dried for 3-5 minutes. Caution should be used, as an over-dry pellet will not resuspend easily. The pellet is resuspended in 250µL of TE buffer, then mixed with 250µL of chilled solution 4 and incubated on ice for 15 minutes. The sample is centrifuged for 15 minutes at 4°C and 15,000xg. The supernatant is collected and transferred to a clean microcentrifuge tube. Next, we add 1 mL of ethanol and centrifuge for 15 minutes at 4°C and 15,000xg. The pellet is dried and resuspended in 25µL of TE buffer.

4.1.3 Restriction Digest of Baculovirus

Baculovirus DNA is set to 100ng/mL. Next, we add the 10x cut smart buffer to a final concentration of 1x. For each µg of DNA, 1µL of the restriction enzyme Bsu36I (New England BioLabs, Whitby, ON, Canada) is added. The reaction runs for 2 hours, at 37°C, then the same amount of Bsu36I was added once again, followed by another 2-hour incubation at 37°C. To stop the reaction, the sample is heated to 72°C. To ensure the DNA was digested, a 0.5% agarose gel was run for 35 minutes at 100V.

4.1.4 Transfection of Insect Cells with Recombinant Virus

SF9 cells are prepared by adding 2mL of cells at $5x10^5$ cells/mL to a 6 well plate. The cells need to attach to the plate, which requires 1 hour at room temperature. A transfection mix is made using 200µL of media (SF900III), 750ng of the linearized bacmid, 1.5µg of the vector DNA and 4µL of Insect Gene Juice® transfection reagent (Sigma-Aldrich, Oakville, ON, Canada) The mixture needs to incubate for 30 minutes, then is added to the plated SF9 cells. The plate is incubated at 27°C for 6-7 days. Parafilm is used to wrap and seal the interface between the plate and its lid, preventing the wells from drying up.

4.1.5 Viral Amplification

Generating higher viral titres for protein expression requires multiple infection steps. 2 mL of cells at $1x10^6$ cells/mL are added to a 6 well plate, then 20µL of the P0 viral stock is added. Incubate at 27°C for 6-7 days, then harvest the supernatant, also known as the P1 viral stock.

50mL of Sf9 at $1x10^6$ cells/mL is transfected using 400µL of the P1 viral stock. The cells are incubated for 6-7 days at 27°C and 120rpm. Next, they are pelleted by centrifugation at 1000xg for 10 minutes. The supernatant is collected and stored in a tin-foil wrapped falcon tube to protect from light at 4°C. This is the P2 viral stock.

4.1.6 Recombinant Protein Expression

The initial cell density should be around $1x10^6$ cells/mL, using 500mL of culture in a 2L flask. Next, we add 15mL of the P2 stock. The cells are incubated at 27°C and rotate at 120rpm for 3 days. The cells are harvested by centrifugation at 6000xg for 15 minutes.

4.1.7 Recombinant Protein Purification

Next, the cells are resuspended in lysis buffer (50mM Tris, 300mM NaCl, 1% Triton X-100, 10mM Imidazole, 3mM BME, 5% Glycerol, 1mM PMSF and DNase). The sample is incubated on ice for 30 minutes prior to sonication for 10 minutes. Cellular debris is pelleted by centrifugation at 30,000xg for 45 minutes. The remaining supernatant is syringe filtered through a 0.45µm filter to remove any remaining debris. The sample is loaded into the ÄKTA start protein purification system (Global Life Science Solutions USA LLC, Marlborough, MA, USA) with a HisTrap™ High-Performance column. The sample is washed with a mixture of 93% binding buffer (50mM Tris, 300mM NaCl, 0.1% Triton X-100, 5% Glycerol, 10mM Imidazole and 3mM BME) and 7% Elution buffer (50mM Tris, 300mM NaCl, 0.1% Triton X-100, 5% Glycerol, 500mM Imidazole and 3mM BME). Following the wash, the elution buffer percentage increases until it reaches 100% throughout a 20mL elution volume.

Elution fractions with a peak at 280nm are collected for further purification using size exclusion chromatography (SEC). We used the ÄKTA pure purification system (Global Life Science Solutions USA

LLC) with a Superdex® 200 10/300 GL increase column to buffer exchange and purify our recombinant protein samples. The size exclusion buffer consists of 300mM NaCl, 50mM Tris, 5% glycerol and 5mM EDTA. The final check is done using SDS-PAGE to verify the sample and its purity. 10µL of sample is mixed with 2µL of dye, then loaded on a 10% SDS-PAGE, which runs for 60 minutes at 200V. The gel is subsequently stained with Coomassie brilliant blue (Bio Basic Inc., Markham, ON, Canada).

4.1.8 Analytical Ultracentrifugation

AUC data was collected using the Beckman Optima AUC centrifuge with an AN60-Ti rotor at 20°C. 500µL of protein sample in the size exclusion buffer was run at 0.5 OD_{280}. Intensity scans were taken every 40 seconds at 35,000 rpm. The data was processed using Ultrascan-III, two-dimensional spectrum analysis (2DSA) is used to remove time and radially invariant noise while also accounting for the meniscus and bottom of the cell.

4.2 Results

4.2.1 Transfection of SF9 Cells with Baculovirus

Initial transfection attempts were performed with baculovirus given to us by Dr. Ian Jones from the University of Reading (UK). A 0.5% agarose gel was run to ensure that the baculovirus DNA was purified and digested correctly. The agarose gel in figure 4.2.1 shows that the baculovirus genome is a relatively large DNA construct.

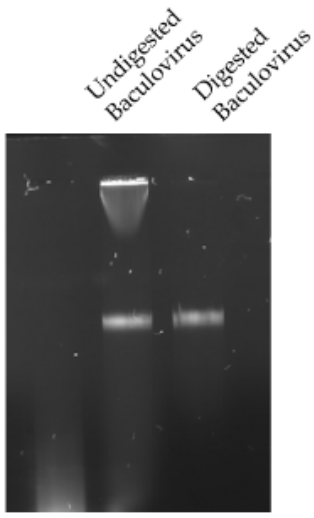

Figure 4.2.1. 0.5% agarose gel run at 100V for 35 minutes. From left to right, DNA Ladder ranging from 1 to 1000 base pairs, undigested baculovirus DNA and, Baculovirus DNA double digested with Bsu36I. Each well was loaded with 10µL of sample and 2µL of DNA loading dye.

We can be confident the genome was isolated as it is typical for the intact genome to be stuck in the well of the agarose, as observed in the middle lane of figure 4.2.1. Upon digestion with Bsu36I, the band caught in the well is no longer present, indicating that the digestion was successful, leaving the cleaved fragment prepared to be recombined. The band in the middle lane below the baculovirus genome may be baculovirus genome that was damaged during preparation, large DNA constructs must be prepared cautiously because of this.

For the first transfection, DDX3X in pOPINF was used with our linearized baculovirus. After two days in the incubator, the media evaporated. To improve retention of the media, parafilm was used to seal the six-well plates. Comparing the size of virally infected cells could be used to determine transfection efficiency [10]. However, this can be challenging. To overcome this challenge, we obtained a baculovirus that expresses mCherry, a red spectrum fluorescent protein that can be detected visually and can provide a relative measure of transfection, from Dr. Arnaud Poterszman of the Institut de Génétique et de Biologie Moléculaire et Cellulaire (France). The mCherry provides a visible pink tint to the SF9 culture, confirming

that transfection has occured [11]. To test for protein expression, we used a full-length DDX3X with a GFP tag.

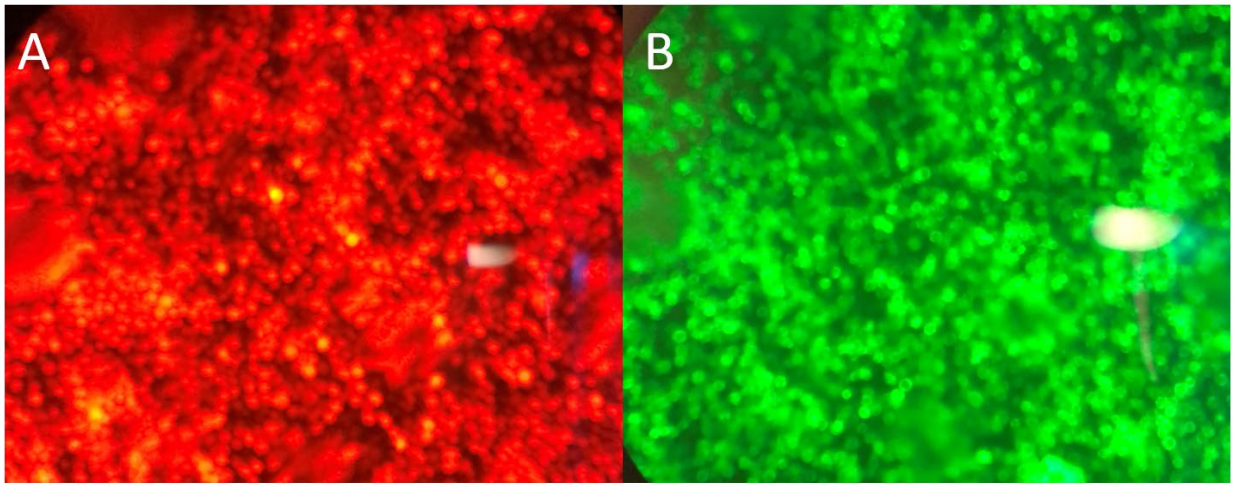

Figure 4.2.2. SF9 cells transfected with DDX3X-GFP examined using fluorescence microscopy. A) SF9 cells examined using the green filter at 100X, confirming the expression of mCherry and positive transfection. B) Same SF9 cells were examined using the blue filter at 100X, indicating expression of GFP-tagged DDX3X.

Initial transfections using the mCherry-expressing virus appeared pink following the 1-week incubation. Figure 4.2.2A confirms transfection using fluorescent microscopy, while figure 4.2.2B confirms the expression of DDX3X-GFP. The next step is to increase the viral titer to optimize the expression of the recombinant protein. Adding the virally infected media from the initial transfection to new SF9 cells in shaking flasks allows for higher titre viral stocks.

4.2.2 Expression of Full-Length DDX3X

Expression of DDX3X full-length began by using 500mL of $1x10^6$ Sf9 cells/mL with 15mL of P2 viral stocks. Figure 4.2.3A shows the SF9 culture following 3-days of incubation, and the culture is now a deep pink colour, indicating successful upregulation of the virus. Allowing the virus to incubate past three days leads to cell lysis, reducing the protein yield [12, 13]. After lysing the cells and sonicating, mCherry is released from the cells and can be used as a crude measurement of cell lysis, as shown in figure 4.2.3C.

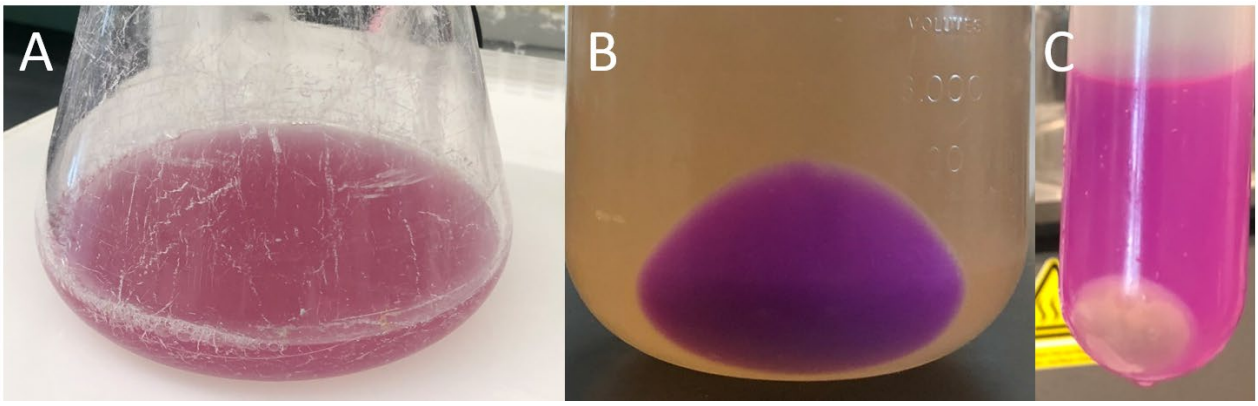

Figure 4.2.3. Stages of SF9 protein purifications. A) 500mL of SF9 cells following three days of incubation with baculovirus in a 2L shake flask, indicating expression of mCherry and viral replication. B) Pelleted SF9 culture immediately following centrifugation, showing that the SF9 cells are intact and the mCherry is contained within the cells. C) Pelleted cell debris following cell lysis by sonication and centrifugation, indicating successful lysis of the cells.

The chromatogram in figure 4.2.4A shows a peak at 280nm, the absorbance indicating a relatively large amount of protein being present in the samples collected from 11.5mL to 16mL. These samples were collected, pooled and run on the SEC. Figure 4.2.4B is the SEC chromatogram, showing peaks around 8.29mL and 12.7mL. Finally, assessing the quality of the protein should be done by SDS-PAGE. The full-length DDX3X is approximately 73.0 kDa. Figure 4.2.5 shows that DDX3X full-length appears to be present in our sample, eluting at ~10 mL, but there is a band at the top of the gel in multiple lanes, indicating contamination or an aggregate unable to be denatured by SDS.

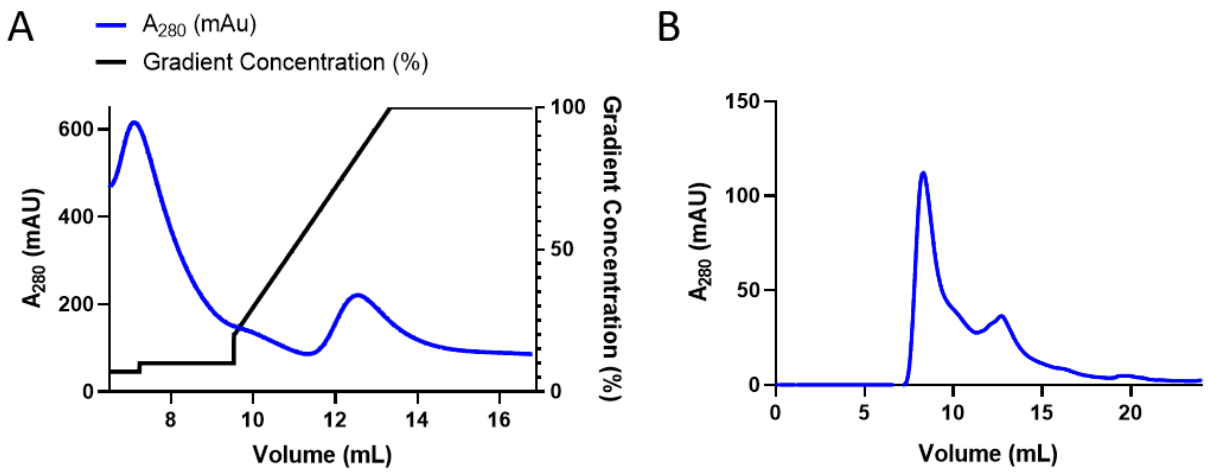

Figure 4.2.4. Full-Length DDX3X Purification Chromatograms A) Nickel affinity purification chromatogram. The blue line represents 280nm absorbance, and the black line represents the percentage of elution buffer mixed with binding buffer. Elutions from 11.5mL to 16mL were collected and processed on the size exclusion. B) Size-exclusion purification chromatogram. The blue line represents the absorbance at 280nm. Fractions were collected in 1 mL volumes.

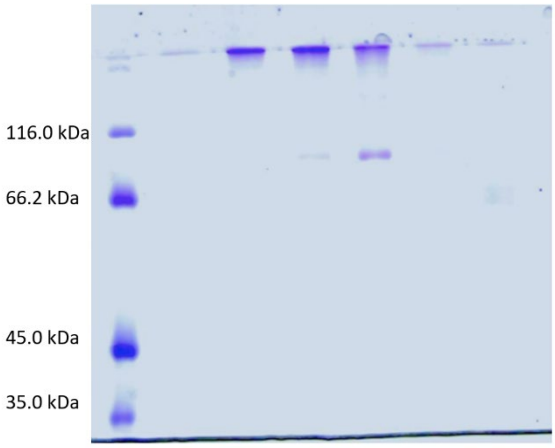

Figure 4.2.5. Full-Length DDX3X SDS-PAGE. 10% SDS-PAGE ran for 60 minutes at 200V. Samples run from left to right include the protein ladder, 1 mL fractions from 8 mL to 10mL, and the 13 mL and 14 mL fractions.

4.2.3 Analytical Ultracentrifugation of DDX3X

The final quality check performed is analytical ultracentrifugation (AUC). AUC is an ideal technique for assessing the quality of protein in solution and elucidates its hydrodynamic properties. The DDX3X was concentrated from the 10 mL fraction, the lane from figure 4.2.5 that showed the highest concentration of DDX3X. Using 500 µL of DDX3X at an A_{280} of 0.5, the sample is spun at 40,000 rpm, with wavelength scans occurring every 20 seconds. Figure 4.2.6 shows the results of AUC following 2DSA analysis, which reflects the SDS-PAGE observations. The AUC results show two predominant species, one peak in the range of ~7S (figure 4.2.6B) and a much larger component around ~400S. Ultrascan 4 can infer each species' molecular weights using the hydrodynamic properties and predicted partial specific volume. The predicted molecular weight of the 7S peak is 104.5kDa, larger than the 73.0kDa molecular weight of DDX3X.

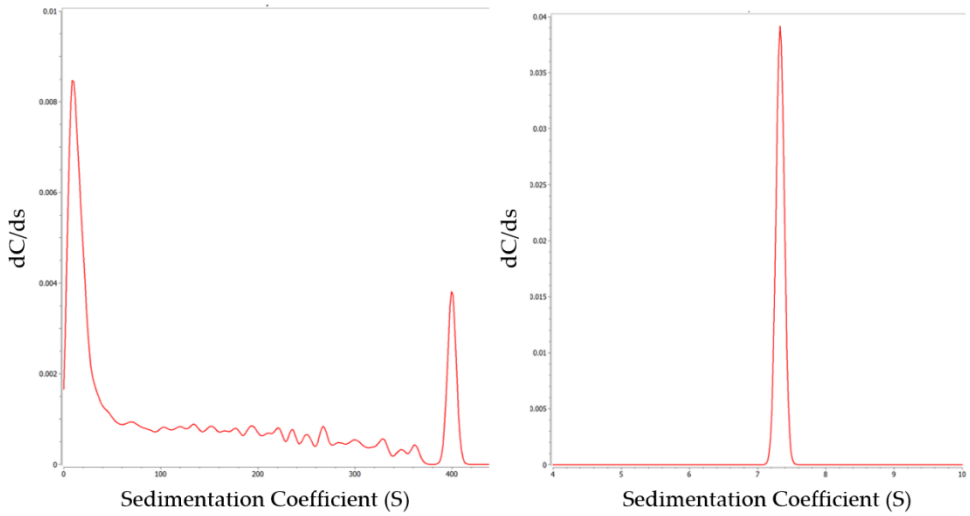

Figure 4.2.6. Analytical ultracentrifugation of DDX3X purified from insect cells. A) Overall sedimentation coefficient distribution of DDX3X. Multiple species present, with two predominant species at ~7S and ~400S. Sedimentation coefficient values are corrected to standard solvent conditions (20°C in water). B) Sediment coefficient distribution from A, reformatted to highlight S values between 4 and 10.

4.3 Discussion

Our previous attempts to express full-length DDX3X in *E. coli* systems had never been successful, but the same constructs in insect cells have shown expression. Although the length of time until protein

expression is significantly increased relative to bacterial expression, it does appear that baculovirus expression is more consistent, potentially reducing the number of troubleshooting steps required [9]. Baculovirus is also a common choice in expressing multi-unit complexes and hard to express viral nonstructural proteins [14-16].

The baculovirus containing mCherry and the 1629 KO we were provided from France simplifies the transfection protocol compared to other commonly used systems such as "Bac-to-bac" or "Flashbac" [17, 18]. Using the 1629 KO also has the added benefit of allowing us to use the pOPIN DNA constructs, of which we have an extensive library of proteins contained therein. The cells transfected with a DDX3X-GFP in figure 4.2.2 show the benefit of the mCherry expressing baculovirus in conjunction with a fluorescent protein. The ability to ascertain both transfection and expression separately using fluorescence is robust, providing immediate confidence in our transfected culture's ability to express the desired proteins.

The experiments proceeded using a non-GFP variant because the full-length DDX3X without GFP appeared to be achieving higher viral titers. The DDX3X construct affinity purification gives a reasonable yield (figure 4.2.4A), albeit slightly less than what is typical of purification in *E. coli*. This exact construct, however, typically yields no protein in *E. coli*. The size exclusion chromatogram (figure 4.2.4B) indicates that the protein begins eluting at ~8.3 mL, which is the void volume of the column, suggesting that whatever is being eluted here is likely too large to be pure DDX3X.

A 73 kDa protein would be expected to elute at ~13 mL, but our SDS-PAGE (figure 4.2.5) revealed no protein at the 13 mL position. Interestingly, the gel shows a probable 73 kDa protein that was eluted at the 10 mL volume. The single band may be a part of an aggregate that the SDS denatured, but that would not explain how the protein's monomer was detected in the AUC. The next steps will involve finding ways to prevent aggregation. 2-Mercaptoethanol (BME) is present in the affinity buffer but is removed during SEC. Maintaining a reducing agent's presence may be essential to prevent the formation of disulfide bonds, potentially reducing the aggregation. The terminal ends of DDX3X are notoriously unstable [19, 20]; changing the buffer compositions could yield improved stability for DDX3X.

Many Baculovirus-expressed proteins are purified under denaturing conditions [21]. Although refolding proteins is not ideal, it may significantly improve the yield of DDX3X when expressed via insect cells.

AUC data predicted the molecular weight of DDX3X to be 104.5kDa, larger than the estimated 73.0kDa based on the amino acid sequence. The difference could be explained as a result of post-translation modifications. Insect cells, like mammalian cells, have several modifications that are made to proteins that do not otherwise happen in bacterial cells [22]. Glycosylation is a common modification in proteins that can significantly impact the function and stability of a protein. Insect cells carry out O- and N- glycosylation but potentially lack some metabolic pathways as mammals concerning the modifications [23]. This is to say that the insect cells may not be precisely equivalent to the mammalian system but provide some attractive benefits despite it. Some proteins receive protection from proteolysis due to glycosylation and benefit from modifications when carrying out their enzymatic functions [24, 25].

The baculovirus system still requires fine-tuning to optimize protein production but has demonstrated the ability to produce proteins that are notoriously difficult to express in *E. coli*. On top of that, human proteins will be more biologically relevant when produced in baculovirus systems than their *E. coli* expressed counterparts. Insect cell culturing for protein production is a middle ground for a system that offers host-like expression while being more affordable.

4.4 References

1. Luckow, V. A.; Summers, M. D., Trends in the development of baculovirus expression vectors. *Bio/technology* **1988,** 6, (1), 47-55.
2. Smith, G. E.; Fraser, M.; Summers, M. D., Molecular engineering of the Autographa californica nuclear polyhedrosis virus genome: deletion mutations within the polyhedrin gene. *Journal of virology* **1983,** 46, (2), 584-593.
3. Lacey, L. A.; Unruh, T. R., Biological control of codling moth (Cydia pomonella, Lepidoptera: Tortricidae) and its role in integrated pest management, with emphasis on entomopathogens. *Vedalia* **2005,** 12, (1), 33-60.
4. O'Reilly, D.; Miller, L.; Luckow, V., Baculovirus expression vectors: a laboratory manual. *Baculovirus expression vectors: a laboratory manual.* **1994**.
5. Ernst, W. J.; Grabherr, R. M.; Katinger, H., Direct cloning into the Autographa californica nuclear polyhedrosis virus for generation of recombinant baculoviruses. *Nucleic acids research* **1994,** 22, (14), 2855.
6. Patel, G.; Nasmyth, K.; Jones, N., A new method for the isolation of recombinant baculovirus. *Nucleic acids research* **1992,** 20, (1), 97-104.
7. Luckow, V. A.; Lee, S.; Barry, G.; Olins, P., Efficient generation of infectious recombinant baculoviruses by site-specific transposon-mediated insertion of foreign genes into a baculovirus genome propagated in Escherichia coli. *Journal of virology* **1993,** 67, (8), 4566-4579.
8. Kitts, P. A.; Possee, R., A method for producing recombinant baculovirus expression vectors at high frequency. *Biotechniques* **1993,** 14, (5), 810-817.
9. Osz-Papai, J.; Radu, L.; Abdulrahman, W.; Kolb-Cheynel, I.; Troffer-Charlier, N.; Birck, C.; Poterszman, A., Insect cells–baculovirus system for the production of difficult to express proteins. *Insoluble Proteins* **2015**, 181-205.
10. Rosinski, M.; Reid, S.; Nielsen, L. K., Osmolarity effects on observed insect cell size after baculovirus infection are avoided using growth medium for sample dilution. *Biotechnology progress* **2000,** 16, (5), 782-785.
11. Shaner, N. C.; Campbell, R. E.; Steinbach, P. A.; Giepmans, B. N.; Palmer, A. E.; Tsien, R. Y., Improved monomeric red, orange and yellow fluorescent proteins derived from Discosoma sp. red fluorescent protein. *Nature biotechnology* **2004,** 22, (12), 1567-1572.
12. Blissard, G. W.; Rohrmann, G. F., Baculovirus diversity and molecular biology. *Annual review of entomology* **1990,** 35, (1), 127-155.
13. Steele, K. H.; Stone, B. J.; Franklin, K. M.; Fath-Goodin, A.; Zhang, X.; Jiang, H.; Webb, B. A.; Geisler, C., Improving the baculovirus expression vector system with vankyrin-enhanced technology. *Biotechnology progress* **2017,** 33, (6), 1496-1507.
14. Trowitzsch, S.; Bieniossek, C.; Nie, Y.; Garzoni, F.; Berger, I., New baculovirus expression tools for recombinant protein complex production. *Journal of structural biology* **2010,** 172, (1), 45-54.
15. Bieniossek, C.; Richmond, T. J.; Berger, I., MultiBac: multigene baculovirus-based eukaryotic protein complex production. *Current protocols in protein science* **2008,** 51, (1), 5.20. 1-5.20. 26.
16. Jones, L. D.; Williams, T.; Bishop, D.; Roy, P., Baculovirus-expressed nonstructural protein NS2 of bluetongue virus induces a cytotoxic T-cell response in mice which affords partial protection. *Clinical and diagnostic laboratory immunology* **1997,** 4, (3), 297-301.
17. Xiang, X.; Yang, R.; Yu, S.; Cao, C.; Guo, A.; Chen, L.; Wu, X.; Cui, W.; Cenis, J., Construction of a BmNPV polyhedrin-plus Bac-to-Bac baculovirus expression system for application in silkworm, Bombyx mori. *Applied microbiology and biotechnology* **2010,** 87, (1), 289-295.
18. Hitchman, R. B.; Locanto, E.; Possee, R. D.; King, L. A., Optimizing the baculovirus expression vector system. *Methods* **2011,** 55, (1), 52-57.
19. Meier-Stephenson, V.; Mrozowich, T.; Pham, M.; Patel, T. R., DEAD-box helicases: the Yin and Yang roles in viral infections. *Biotechnology and Genetic Engineering Reviews* **2018,** 34, (1), 3-32.
20. Linder, P.; Jankowsky, E., From unwinding to clamping—the DEAD box RNA helicase family. *Nature reviews Molecular cell biology* **2011,** 12, (8), 505-516.

21. Urban, S.; Hildt, E.; Eckerskorn, C.; Sirma, H.; Kekule, A.; Hofschneider, P. H., Isolation and molecular characterization of hepatitis B virus X-protein from a baculovirus expression system. *Hepatology* **1997,** 26, (4), 1045-1053.
22. Ailor, E.; Betenbaugh, M. J., Modifying secretion and post-translational processing in insect cells. *Current opinion in biotechnology* **1999,** 10, (2), 142-145.
23. Marchal, I.; Jarvis, D. L.; Cacan, R.; Verbert, A., Glycoproteins from insect cells: sialylated or not? *Biological chemistry* **2001,** 382, (2), 151.
24. Takashi, Y.; Kosako, H.; Sawatsubashi, S.; Kinoshita, Y.; Ito, N.; Tsoumpra, M. K.; Nangaku, M.; Abe, M.; Matsuhisa, M.; Kato, S., Activation of unliganded FGF receptor by extracellular phosphate potentiates proteolytic protection of FGF23 by its O-glycosylation. *Proceedings of the National Academy of Sciences* **2019,** 116, (23), 11418-11427.
25. Goettig, P., Effects of glycosylation on the enzymatic activity and mechanisms of proteases. *International journal of molecular sciences* **2016,** 17, (12), 1969.

Chapter 5: Conclusions

5.1 Overview

Characterizing the interactions between the viral non-coding RNAs and host factors allows us to obtain mechanistic insights into host-viral interactions, which ultimately could aid the elucidation of novel antiviral therapies. The work presented in this thesis focused on two human RNA helicases that have been implicated in many viral replication pathways [1-3]. Previous studies have highlighted that DDX3X is dispensable concerning cell viability [4, 5], and DDX3X inhibitors could effectively treat some flavivirus infections, such as West Nile Virus, where DDX3X inhibitors are currently being explored [6]. Expanding the potential use of pre-existing therapeutics is the best case scenario, saving time and expenses by reducing the number of trials it would need to clear.

DDX3X is required to promote JEV replication [1], meaning antivirals should seek to ablate the helicase's function. In Chapter 2, we demonstrated that DDX3X binds to the JEV 5' TR independently, making it an excellent druggable target. Additionally, DDX3X is primarily located in the cytoplasm [7, 8], unlike DDX17, which depends on nuclear export [9]. Having the target in the cytoplasm simplifies drug design since the nucleus restricts imports [10]. DDX3X downregulates DENV via cell signalling function, independent of its helicase activity [3]. The helicase assay performed with the JEV 5' revealed that it was capable of unwinding the RNA in the presence of ATP.

Although the interaction was previously undocumented, ZIKV was selected to juxtapose JEV because of the similarities proposed in 5' TRs of flaviviruses [11, 12]. We wanted to test how specifically DDX3X interacts with the different terminal regions between the flaviviruses. The 5' of ZIKV was also bound by DDX3X, albeit with a weaker affinity. It is unclear if the interaction between the Zika 5' TR and DDX3X has any implications in the viral life cycle, but DDX3X can recognize and unwind ZIKV 5' TR, as confirmed via helicase assay.

The terminal regions of all flaviviruses are highly conserved [11], making it likely that DDX3X interacts with a number of them. In the future, investigations to identify other biologically relevant

flavivirus terminal region interactions with DDX3X could have a significant impact. Finding commonalities among viruses may enable broad-spectrum treatment options to be developed. *In vitro* techniques allow us to examine the system quantitatively, but the living world is rarely as simple as it may seem *in vitro*. As other studies have shown, DDX3X will not provide the universal flavivirus treatment [3], but there may be several members that DDX3X inhibitors are effective against [6].

The ability of DDX17 to bind to both the 5' NCR and IGR was demonstrated *in vitro*, following up previous observations made *in vivo* [2]. Since binding occurred in isolation, it suggests that DDX17 can act on the S segment independent of cofactors. DDX17 has been observed as a Drosha component, assisting in the generation of siRNAs. DDX17's role with the RNA silencing pathway is critical to suppress RVFV infection [2, 13]. Our work also found that DDX17 was able to unwind both non-coding RNAs in an ATP-dependent manner. DDX17 is an integral part of the innate antiviral response against RVFV [2], meaning antiviral therapies should seek to promote DDX17 activity.

Demonstrating that both DDX3X and DDX17 bind and unwind their respective viral RNA targets provides a foundation to understand the mechanism of the interactions between hosts and pathogen. Using full-length protein will further our understanding by comparing the protein against its truncates, indicating the more and less significant regions. Therapeutic peptides could be designed to out-compete the natural binding partners to ablate the viral replication function in the case of DDX3X or artificially enhance Drosha activity through a DDX17 mimic. Peptide therapeutics are emerging as attractive candidates because they are less immunogenic, having fewer off-target side effects and promising efficacies [14, 15]. There are currently peptide therapeutics in development for DENV that obstructs the virus' non-structural protein interactions [16].

To conclude, my work presents the interactions between the helicase cores of both DDX3X and DDX17 with multiple viral binding partners. A novel helicase assay determined that both helicases are capable of unwinding their targets. Characterizing the interactions is one step towards finding ways to treat deadly viral infections that infect thousands of people every year, leading to numerous sequelae and deaths [17-20].

5.2 Future Perspectives

As discussed previously, it is critical to determine the specific locus of interaction between the viral RNA and RNA helicases. The most straightforward approach would be to mix and match both the protein and RNA's truncates and utilize MST to analyze the interactions. Alternatively, a biophysical method, like cryo-EM or SAXS, would provide a more precise answer. Both methods will depend on the production of currently troublesome proteins, so continued work on the baculovirus expression system is critical.

It is pertinent to determine whether DDX3X is significant in ZIKV infections and other flaviviruses. One approach would be to use a replicon system to simulate viral infection. Replicons are effectively non-infectious versions of viruses that can be exploited for drug screening [21]. Often they are selected due to the improved safety over infectious viruses. Systems for JEV and ZiKV are already being explored [22, 23]. Using a ZIKV replicon in a human cell line could reveal the potential role DDX3X plays in viral replication. Additionally, replicon systems are a powerful tool for finding antivirals, potentially allowing us to develop antivirals based on the RNA helicases examined in this thesis.

Emerging flaviviruses, like Powassan, which has origins in North America [24], should be studied as quickly as possible to allow for the development of therapies that could prove instrumental should an outbreak occur. The methods we used to characterize DDX3X and DDX17's viral RNA interactions are a powerful set of tools that we can utilize to quickly and accurately quantify host-pathogen interactions. Our work will look to characterize even more viral interactions using techniques like MST and SAXS in the hopes of finding new interactions that can be exploited towards the development of antivirals.

5.3 References

1. Li, C.; Ge, L.-l.; Li, P.-p.; Wang, Y.; Dai, J.-j.; Sun, M.-x.; Huang, L.; Shen, Z.-q.; Hu, X.-c.; Ishag, H., Cellular DDX3 regulates Japanese encephalitis virus replication by interacting with viral un-translated regions. *Virology* **2014,** 449, 70-81.
2. Moy, R. H.; Cole, B. S.; Yasunaga, A.; Gold, B.; Shankarling, G.; Varble, A.; Molleston, J. M.; Lynch, K. W.; Cherry, S., Stem-loop recognition by DDX17 facilitates miRNA processing and antiviral defense. *Cell* **2014,** 158, (4), 764-777.
3. Li, G.; Feng, T.; Pan, W.; Shi, X.; Dai, J., DEAD-box RNA helicase DDX3X inhibits DENV replication via regulating type one interferon pathway. *Biochemical and biophysical research communications* **2015,** 456, (1), 327-332.
4. Kondaskar, A.; Kondaskar, S.; Fishbein, J. C.; Carter-Cooper, B. A.; Lapidus, R. G.; Sadowska, M.; Edelman, M. J.; Hosmane, R. S., Structure-based drug design and potent anti-cancer activity of tricyclic 5: 7: 5-fused diimidazo [4, 5-d: 4′, 5′-f][1, 3] diazepines. *Bioorganic & medicinal chemistry* **2013,** 21, (3), 618-631.
5. Bol, G. M.; Vesuna, F.; Xie, M.; Zeng, J.; Aziz, K.; Gandhi, N.; Levine, A.; Irving, A.; Korz, D.; Tantravedi, S., Targeting DDX 3 with a small molecule inhibitor for lung cancer therapy. *EMBO molecular medicine* **2015,** 7, (5), 648-669.
6. Brai, A.; Martelli, F.; Riva, V.; Garbelli, A.; Fazi, R.; Zamperini, C.; Pollutri, A.; Falsitta, L.; Ronzini, S.; Maccari, L., DDX3X helicase inhibitors as a new strategy to fight the West Nile virus infection. *Journal of medicinal chemistry* **2019,** 62, (5), 2333-2347.
7. Choi, Y. J.; Lee, S. G., The DEAD-box RNA helicase DDX3 interacts with DDX5, co-localizes with it in the cytoplasm during the G2/M phase of the cycle, and affects its shuttling during mRNP export. *Journal of cellular biochemistry* **2012,** 113, (3), 985-996.
8. Lai, M.-C.; Lee, Y.-H. W.; Tarn, W.-Y., The DEAD-box RNA helicase DDX3 associates with export messenger ribonucleoproteins as well astip-associated protein and participates in translational control. *Molecular biology of the cell* **2008,** 19, (9), 3847-3858.
9. Li, K.; Mo, C.; Gong, D.; Chen, Y.; Huang, Z.; Li, Y.; Zhang, J.; Huang, L.; Li, Y.; Fuller-Pace, F. V., DDX17 nucleocytoplasmic shuttling promotes acquired gefitinib resistance in non-small cell lung cancer cells via activation of β-catenin. *Cancer letters* **2017,** 400, 194-202.
10. Deepthi, A.; Raju, S.; Kalyani, A.; Kiran, U. M.; Vanaja, A., Targeted drug delivery to the nucleus and its potential role in cancer chemotherapy. *Journal of Pharmaceutical Sciences and Research* **2013,** 5, (2), 48.
11. Brinton, M. A.; Basu, M., Functions of the 3′ and 5′ genome RNA regions of members of the genus Flavivirus. *Virus research* **2015,** 206, 108-119.
12. Brinton, M. A.; Dispoto, J. H., Sequence and secondary structure analysis of the 5′-terminal region of flavivirus genome RNA. *Virology* **1988,** 162, (2), 290-299.
13. Fukuda, T.; Yamagata, K.; Fujiyama, S.; Matsumoto, T.; Koshida, I.; Yoshimura, K.; Mihara, M.; Naitou, M.; Endoh, H.; Nakamura, T., DEAD-box RNA helicase subunits of the Drosha complex are required for processing of rRNA and a subset of microRNAs. *Nature cell biology* **2007,** 9, (5), 604-611.
14. Fosgerau, K.; Hoffmann, T., Peptide therapeutics: current status and future directions. *Drug discovery today* **2015,** 20, (1), 122-128.
15. Tsomaia, N., Peptide therapeutics: targeting the undruggable space. *European journal of medicinal chemistry* **2015,** 94, 459-470.
16. Rothan, H. A.; Mohamed, Z.; Suhaeb, A. M.; Rahman, N. A.; Yusof, R., Antiviral cationic peptides as a strategy for innovation in global health therapeutics for dengue virus: high yield production

of the biologically active recombinant plectasin peptide. *Omics: a journal of integrative biology* **2013,** 17, (11), 560-567.
17. World Health Organization, Japanese Encephalitis. https://www.who.int/en/news-room/fact-sheets/detail/japanese-encephalitis
18. Bird, B. H.; Ksiazek, T. G.; Nichol, S. T.; MacLachlan, N. J., Rift Valley fever virus. *Journal of the American Veterinary Medical Association* **2009,** 234, (7), 883-893.
19. Cauchemez, S.; Besnard, M.; Bompard, P.; Dub, T.; Guillemette-Artur, P.; Eyrolle-Guignot, D.; Salje, H.; Van Kerkhove, M. D.; Abadie, V.; Garel, C., Association between Zika virus and microcephaly in French Polynesia, 2013–15: a retrospective study. *The Lancet* **2016,** 387, (10033), 2125-2132.
20. Cao-Lormeau, V.-M.; Blake, A.; Mons, S.; Lastère, S.; Roche, C.; Vanhomwegen, J.; Dub, T.; Baudouin, L.; Teissier, A.; Larre, P., Guillain-Barré Syndrome outbreak associated with Zika virus infection in French Polynesia: a case-control study. *The Lancet* **2016,** 387, (10027), 1531-1539.
21. Hannemann, H., Viral replicons as valuable tools for drug discovery. *Drug discovery today* **2020,** 25, (6), 1026-1033.
22. Zhang, Q.-Y.; Li, X.-D.; Liu, S.-Q.; Deng, C.-L.; Zhang, B.; Ye, H.-Q., Development of a stable Japanese encephalitis virus replicon cell line for antiviral screening. *Archives of virology* **2017,** 162, (11), 3417-3423.
23. Mutso, M.; Saul, S.; Rausalu, K.; Susova, O.; Žusinaite, E.; Mahalingam, S.; Merits, A., Reverse genetic system, genetically stable reporter viruses and packaged subgenomic replicon based on a Brazilian Zika virus isolate. *Journal of General Virology* **2017,** 98, (11), 2712-2724.
24. Ebel, G. D., Update on Powassan virus: emergence of a North American tick-borne flavivirus. *Annual review of entomology* **2010,** 55, 95-110.